

ETD Archive

2019

A Reticulation of Skin-Applied Strain Sensors for Motion Capture

Christopher A. Schroeck
Cleveland State University

Follow this and additional works at: <https://engagedscholarship.csuohio.edu/etdarchive>



Part of the [Mechanical Engineering Commons](#)

How does access to this work benefit you? Let us know!

Recommended Citation

Schroeck, Christopher A., "A Reticulation of Skin-Applied Strain Sensors for Motion Capture" (2019). *ETD Archive*. 1148.

<https://engagedscholarship.csuohio.edu/etdarchive/1148>

This Thesis is brought to you for free and open access by EngagedScholarship@CSU. It has been accepted for inclusion in ETD Archive by an authorized administrator of EngagedScholarship@CSU. For more information, please contact library.es@csuohio.edu.

A RETICULATION OF SKIN-APPLIED STRAIN SENSORS FOR MOTION
CAPTURE

CHRISTOPHER SCHROECK

Bachelor of Science in Mechanical Engineering

Cleveland State University

May 2017

submitted in partial fulfillment of requirements for the degree

MASTER OF SCIENCE IN MECHANICAL ENGINEERING

at the

CLEVELAND STATE UNIVERSITY

May 2019

© COPYRIGHT BY CHRISTOPHER SCHROECK 2019

We hereby approve this thesis for

CHRISTOPHER SCHROECK

Candidate for the Master of Science in Mechanical Engineering degree

for the Department of Mechanical Engineering

And

CLEVELAND STATE UNIVERSITY'S

College of Graduate Studies by

Antonie J van den Bogert, Committee Chairperson
Department of Mechanical Engineering

Date

Eric Schearer, Committee Member
Department of Mechanical Engineering

Date

Douglas A Wajda, Committee Member
Department of Health and Human Performance

Date

Student's Date of Defense: May 2, 2019

Dedicated to Sarah Mok; your turn.

ACKNOWLEDGMENT

I would like to acknowledge the efforts and interest of the individuals who helped make this work possible, to whom I am indebted to, indescribably:

Dr. Antonie van den Bogert, Huawei Wang, Katherine Florik, Nattawat Sunpituksaree, Michael Hanson, Russel Donda, Anne Koelewijn, Dr. Eric Schearer, Derek Wolf, Professor Michael Gallagher, Gianfranco Travato, Brianna McKinney, Gautam Mankaney, Michael Wilson, Justin & Robert Meinecke, Jacob Baier, Marcus Bowers, Daoning Zhou

& A Special Thank You To:

Cleveland State University, Washkewicz College of Engineering, the Mechanical Engineering Department Faculty and Staff thereof, CSU's Technical Transfer Office, the Human Motion and Controls Laboratory and its members, Parker Hannifin, the Monte Ahuja College of Business, the Staff and Mentors of Startup Vikes & the Weston Ideation Lab, StartMart, FlashStart

“It takes a village to raise a child and a committee to deny his master’s degree.”

~proverb... amended

A RETICULATION OF SKIN-APPLIED STRAIN SENSORS FOR MOTION
CAPTURE

CHRISTOPHER SCHROECK

ABSTRACT

The purpose of this research is to develop a system of motion capture based on skin-applied strain sensors. These elastic sensors are of interest because they can be applied to the body without restricting motion and are well suited to operate in more practical environments, such as sports fields, gymnasiums, and outdoor areas. This combination is currently not available in the field of motion capture. The current issues with strain sensor motion capture technology is the accurate is not sufficient for motion analysis and axial rotation monitoring of joints is not available. This project will build and test a sensor arrangement designed to measure axial joint rotation and a calibration that compensates for crosstalk from other joint motions.

An arrangement of four strain sensors was created to capture hip and knee motion indirectly through a geometric relationship. Sensors were arranged around the hip and knee with compression pants that emulate the pressure sensation of kinesiology tape. This pressure is desirable for high level athletes are comfortable with this feeling, meaning most wearers would likely agree. This prototype was tested on six participants of varying height with Institutional Review Board approval and was referenced against a passive marker, visual motion capture system with ten cameras.

The test results show the geometric calibration with crosstalk compensation is the most successful general calibration. The overall root-mean-square error of the hip flexion, hip abduction, hip rotation, and knee flexion measurements were $4.6 \pm 1.2^\circ$ ($p = 0.95$),

$4.7 \pm 1.5^\circ$ ($\rho = 0.82$), $6.7 \pm 2.0^\circ$ ($\rho = 0.89$), and $6.2 \pm 1.3^\circ$ ($\rho = 0.96$) respectively, compared to a commercial xSens system with $5.7 \pm 2.1^\circ$ ($\rho = 0.99$), $4.1 \pm 2.0^\circ$ ($\rho = 0.91$), $6.5 \pm 2.8^\circ$ ($\rho = 0.68$), and $4.4 \pm 2.0^\circ$ ($\rho = 0.99$). The geometric calibration without crosstalk compensation tends to miss the relation of the data but may be sufficient for small ranges of motion. Specifically, axial rotation sensing capacity was shown to be important for the accuracy of other sensor's angle readings. The gaussian processes regression (GPR) tended to overfit the calibration data. In conclusion, the geometric calibration with crosstalk compensation created the most successful, stable, and general calibration. This testing was performed with a \$200 prototype and produced results comparable to a \$20,000 commercial system.

TABLE OF CONTENTS

	Page
ABSTRACT.....	vi
LIST OF TABLES	xii
LIST OF FIGURES	xiv
CHAPTER	
I. PREFACE.....	1
A. Background	1
1) Optical Systems:	2
2) Inertial Systems:	7
3) Magnetic Systems:.....	10
4) Acoustic Systems:.....	11
5) Mechanical Systems:	11
B. Analysis & Problem Identification.....	12
C. Solution Proposal	14
II. MECHANICAL SYSTEM DESIGN.....	17
A. Design Concept	17
B. Existing Eap Technologies.....	18
C. Work Thus Far	20
D. Physical Design.....	26
1) Anchors:.....	27

2) Straps:	31
a) Clothing:	31
b) Kinesiology Tape:.....	32
E. Present Development.....	33
F. Future Work.....	35
1) Mass-Producible Work:	35
2) Expansion Work:	37
a) Everywhere Excluding the Back:	38
b) The Back:.....	40
III. CALIBRATION METHOD	50
A. Introduction.....	50
1) Work Thus Far:.....	51
2) Analyzing the Mechanical System:	53
B. Method Concepts.....	53
1) Geometric Calibration:	54
2) Gaussian Process Regression:	55
3) Method Comparison:	57
C. Method Theory.....	57
1) Flexion Sensor Geometry:	58
2) Rotation Sensor Geometry:	61
3) Gaussian Process Regression:	67

4) Signal Crosstalk:.....	69
D. Programing.....	69
1) Geometric Equation Code:	70
2) Gaussian Process Regression Code:	75
E. Future Work.....	75
IV. TESTING & DATA PROCESSING	79
A. Protocol Planning.....	79
B. Range of Motion Tests	80
1) Test Modification:	81
C. Finalized Protocol	82
D. Testing.....	82
1) Processing Visual Motion Capture Data:	83
2) Initial Test:.....	84
a) Protocol Amendments:	85
b) Initial Conclusion:	85
3) Statistical Testing:	87
a) Geometric Results with Crosstalk Compensation:	89
b) Geometric Results with No Crosstalk:	91
c) Gaussian Process Regression Results:	93
d. Protocol Amendments:.....	95
E. Data Analysis.....	95

1) Observations of the Initial Test:	96
2) Observations of the Statistical Testing:	96
V. SUMMARY & CONCLUSION	99
A. System Summary	99
B. Test Result Summary	100
C. Implications & Conclusion.....	106
D. Personal Annotations	107
REFERENCES	111
APPENDICES	
A. MatLab Program leg_main.mat	117
B. MatLab Program leg_solve.mat	123
C. MatLab Program leg_fk.mat	126
D. MatLab Program CalibrationTestCode.mat.....	128
E. MatLab Program CaliCurve.mat	138
F. MatLab Program gaitgraph.mat.....	139
G. IRB-Approved Test Protocol Document.....	140
H. Permission from Katherine Florek.....	143

LIST OF TABLES

Table	Page
1. xSens Walking Gait Data [35]	87
2. Relevant Participant Information	87
3. Total Error of the GC model	89
4. Normal Walking Gait Error of the GC model	89
5. Toes-Out Walking Gait Error of the GC model.....	90
6. Toes-In Walking Gait Error of the GC model	90
7. ROM Stability Comparison of the GC model.....	90
8. Total Error of the GNC model	91
9. Normal Walking Gait Error of the GNC model.....	91
10. Toes-Out Walking Gait Error of the GNC model.....	92
11. Toes-In Walking Gait Error of the GNC model	92
12. ROM Stability Comparison of the GNC model.....	92
13. Total Error of the GPR Model	94
14. Normal Walking Gait Error of the GPR Model.....	94
15. Toes-Out Walking Gait Error of the GPR Model.....	94
16. Toes-In Walking Gait Error of the GPR Model.....	95
17. ROM Stability Comparison of the GPR Model	95

18. Normal Walking Gait Error Averages	101
19. P-Values of Model Comparison to xSens in Normal Gait.....	101
20. Toes-Out Walking Gait Error Averages	102
21. Toes-In Walking Gait Error Averages	102
22. Total Error Averages.....	102
23. P-Values of GNC and GRP models vs GC.....	103
24. Stability Comparison	103
25. Pearson Correlation Quality [36]	105
26. Pearson Correlation Coefficients	105

LIST OF FIGURES

Figure	Page
1. Example of a capture volume being formed by a surrounding Vicon camera and data processing system [5] (Pictures from Vicon.com).	3
2. Comparison between passive (left, Wikipedia.org) and active (right, Berkeley.edu) marker suits.	5
3. Kinect’s 3D imaging abilities using specialized light patterns (Pictures from yting.com).	6
4. Example of a seventeen-sensor inertial motion capture system (left), standard IMU (top right), and waterproof, metal IMU (bottom right) (Pictures from YostLabs.com).	8
5. Xsens 22 sensor suit (left) and system layout (right) (Pictures from Xsens.com).	10
6. An example of a magnetic motion capture system (from source [13]).	11
7. The Gypsy 6 mechanical motion capture suit. The Gypsy 7 has a resolution of 0.125 degrees [22] (Pictures from Pinterest.co.uk).	12
8. An example of a dielectric, electroactive polymer strain sensor, one-dimensional. (Pictures from Parker Hannifin at Parker.com).	18
9. An example of a research, EAP, motion tracking suit (right, image from source [24]). Bend system (left, image from source [23]) claims to monitor knee flexion and glute “involvement,” which may mean sensing topical distortion caused by flexing gluts. The wearable soft sensing suit is a two-dimensional monitor, which still has linear calibration issues, possibly due to the participants’ inabilities to restrict themselves to pure planar motion.	19
10. The resulting locations of the leg’s flexion (blue) and rotation (green) sensors.	21
11. The resulting system of flexion (blue) and rotation (green) sensors integrated into compression pants.	25
12. A comparison of a calibration equation’s effects on the calibration data (top) and a dataset from a different test of the same participant (bottom) (graphs and calibration created by Katherine Florek: permission in APPENDIX H)	26

13. An infinitely long strap modelled and analyzed in Solidworks, based on the dimensions of the anchor material (1.5” standard nylon strapping). “Infinitely long” in this context means the stress/strain flow becomes perfectly distributed before the geometry ends.	28
14. A shortened, yet still infinitely long, strap. Because the perfect distribution of strain just develops at the end of this length, any longer straps will have excess material that does not provide any benefits.	28
15. A blank strap with unnecessary material removed.	29
16. An increase of the attachment perimeter.	29
17. An almost uniform stress (left) and strain (right) distribution of the final anchor geometry.	30
18. The current system being used (modified from the systems from the previous project). The hip rotation and knee flexion sensors are unchanged (left), while the hip abduction and hip flexion sensors were added.	35
19. The relevant DoF of the body (left) and possible sensor locations (right). In this diagram, ‘flexion’ refers to the flexion sensor arrangement, which can be used for both flexion and abduction motions. Note to scapula/clavicle complex of the shoulder is assumed to have only two degrees of freedom. This assumption is used to describe the resulting motions possible of the glenohumeral cup and does not look to describe the orientation of the scapula. This assumption may need to be changes, especially if muscle forces need to be solved for.	38
20. The anatomical orientation of an array of strain sensors used to measure the degrees of freedom of the back (image edited from cec-animation.com).	42
21. An alternative orientation of an array of strain sensors used to measure the degrees of freedom of the back (image edited from cec-animation.com).	43
22. A three-sensor array of strain sensors used to measure the degrees of freedom of the back (image edited from cec-animation.com).	44
23. An image defining the anatomical planes (image from TeachMeAnatomy.info).	45
24. Transverse section of the torso. The spine (grey) is for directional reference.	46

25. Sensor deformation corresponding to a forward (left) and backward (right) bend (green describes a strain sensor length increase; blue, decrease).....	46
26. Sensor deformation corresponding to a leftward (left) and rightward (right) bend (green describes a strain sensor length increase; blue, decrease).....	46
27. Sensor deformation corresponding to a clockwise (left) and counter-clockwise (right) rotation (green describes a strain sensor length increase; blue, decrease).	47
28. Resulting sensor deformation corresponding to a combine backward and rightward bend (green describes a strain sensor length increase; blue, decrease; yellow, combination of increase and decrease).	48
29. The resulting sensor deformation corresponding to a combine backward bend and counter clockwise rotation (green describes a strain increase; blue, decrease; yellow, combination of increase and decrease).	48
30. Resulting sensor deformation corresponding to a combine backward bend, counter clockwise rotation, and right bend (green describes a strain increase; blue, decrease; yellow, combination of increase and decrease; pink and orange are not equal in magnitude, but are related by their component motions).	49
31. An example of correct (middle) and incorrect (outer left and right) fit possibilities of machine learning-based trendlines. (Pictures from BogoToBogo.com).	56
32. The geometric model of the flexion sensor arrangement. The green area represents the area of skin around the joint that displays significant motion relative to the long bones that make up the joint, while the black areas are comparatively static. Note this makes anatomical flexion/extension a direct measurement.	58
33. The dynamic area is not the only source of pollution, but it must be encompassed by the anchors to fully capture the magnitude of the joint motion. While it is not shown in this nor the previous figure, other dynamic areas will exist around the joint due to muscles flexing/relaxing and excess skin motions cause by nearby joint motions.	61
34. The geometric model of a rotation sensor arrangement on the thigh, relating arclength changes due to internal/external rotation (left) in the cross section to the sensor arrangement on the surface of the thigh. Note that this arrangement makes anatomical rotation an indirect measurement.	61

35. A planar model of a correct, single rigid body, rotation sensor arrangement (left) with one known (green) and one unknown (red), compared to the multiple unknowns that develop from multiple rigid bodies (right) (The hip is used as an example).....	62
36. An example of unaligned visual (black) and strain (red) datasets. The offset can be estimated to be about 0.6 seconds. Because the visual data's sampling rate is 0.01 seconds, the maximum resolution that makes sense is half that value, or 0.005 seconds. This limiting factor is important so that alignment is taken far enough, but not too far. For example, the offset was estimated to by 0.6 seconds. To make this value a final solution, it would need to be 0.600 seconds, meaning 0.595 and 0.605 seconds were shown to not lower the RMS error.	71
37. An example of a calibration data set plot.....	73
38. An example of a total hip flexion data set plot.....	74
39. An example of the gait graphs. This example displays normal or toes-forward gait.....	74
40. An example of a stability check plot.	75
41. A planar model of a correct, multi-bodied rotation sensor setup with one unknown (red), which uses corresponding sensor data to determine variable angle φ (The hip is used as an example, meaning angle φ is a multi-dimensional vector).	76
42. A planar model of a correct, multi-bodied rotation sensor setup with one unknown (red), which uses corresponding sensor data to determine variable angles φ and θ (The hip is used as an example, meaning angle φ is a multi-dimensional vector). Angle θ can have more than one degree of freedom, so long as none produce axial rotation.	77
43. An examples of active versions of hip flexion with knee straight test (upper left), hip flexion with knee flexed test (upper right), internal and external hip rotation test (lower left), and hip abduction and adduction test (lower right) (left-most picture, from Joint Range of Motion and Muscle Length Testing: Third Edition), and the double leg squat test (right-most picture, from FourFourTwo.com).....	81
44. An example of the GPR calibration model overfitting a calibration set and fitting to error.	104
45. An example of the GNC model failing to emulate the trend of the line. Due to the data's low range, the RMS error was 6.45°	104

CHAPTER I

PREFACE

A. Background

The current state of the art in the human motion capture field is the technology is divided into five main, basic methods of motion detection: optical, inertial, mechanical, magnetic, and acoustical [1]. Each method has associated strengths and weaknesses, accuracy potentials, and constraints on participant movement freedom. Often, hybrid systems are used to combine the strengths of multiple method types in a way that most effectively counteracts their shortcomings. For example, inertial sensor systems have no way to identify their global position in an environment or their position relative to other test participants, while magnetic systems tend to be very sensitive to their environment's electromagnetic properties. Inertial sensors are often paired with magnetic positioning systems, giving them global positioning in a defined environment. Since there are many magnetic sensors making the same measurement in these applications, they are less vulnerable to minor environmental fluctuations than a purely magnetic system. This is not to say that every system has an equal potential to perform well, nor that the right combination of systems will compensate for every issue, nor that every situation currently

has a good solution. There are clearly dominant methods for motion capture, and there exist certain situations which do not have good motion capture options available, presently. A short summary of each technology will be presented, and their respective strengths and weaknesses will be discussed to yield a better understanding of which methods have advantages in which environments and which environments have no practical, reliable systems of motion capture.

1) *Optical Systems*: Optical motion capture systems come in several subcategories. The most general division is between systems which use markers and ones that don't. Either case have the same basic working principle that a light (usually non-visible) is emitted and then detected. At some point, the light interacts with the participant being monitored [2]. However, when this interaction happens and what the nature of that interaction is differs from method to method. Once the light interacts with the target, it is sent to a receiver, which may or may not record the intensity, but always logs the specific spatial and temporal coordinates. The method of region selection is done in varying ways and is method specific as well. Data processing is usually performed to enhance accuracy. This means optical systems traditionally did not provide real-time feedback [1], but now are capable of doing so [3]. By definition, all optical systems use light to make their measurements, which mean a clear line of sight must be maintained between the receiver, emitter, and reflection point (if applicable) for every optical method. Multiple emitters and receivers are often placed at various distances and orientations from each other to reduce blind spots. This will form a region which is optimal for the system to accurately collect motions called a capture volume. Capture volumes are often custom designed for individual rooms or customer needs [4] [5]. Due to the nature of the equipment used to

observe this volume and the need for the equipment's relative geometry to stay constant for accurate measurements, these systems are almost never mobile and often confined to a single room for their useful lifetime. The capture volumes can be much greater for movie special effects or videogame controls than for biomechanical research for the entertainment industry is mostly concerned with the general motion where research may need to have near exact records to observe nuanced movements or changes in posture.

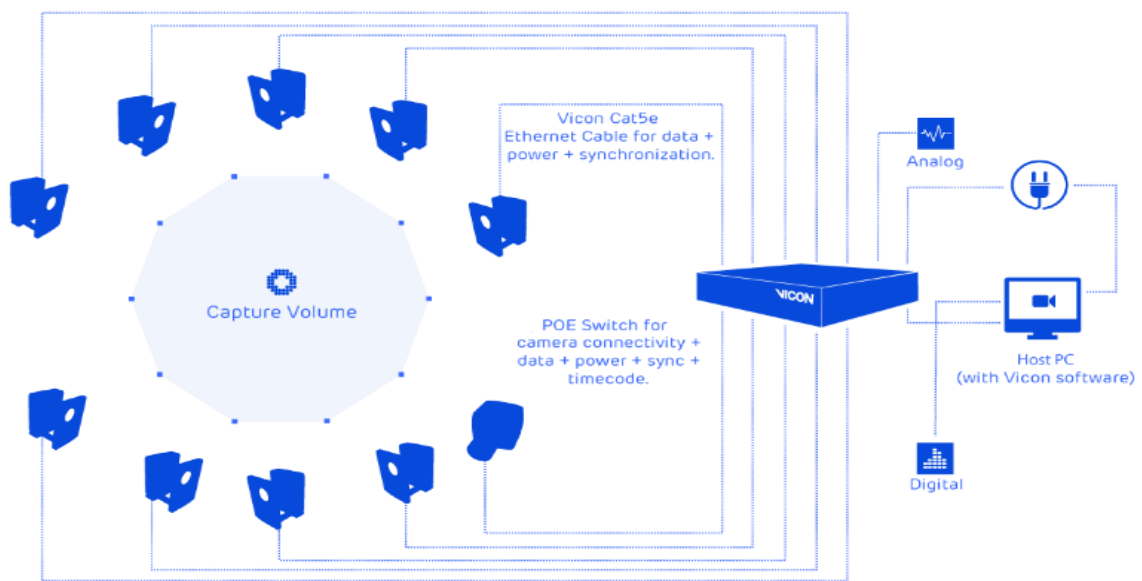


Figure 1. Example of a capture volume being formed by a surrounding Vicon camera and data processing system [5] (Pictures from Vicon.com).

Marker based optical systems are considered the gold standard of motion capture and are frequently used as a 'true value' for motions when other systems are being calibrated or checked for accuracy [6] [7]. This is due to the stability of this system combine with the speed and precision of light-based measurements, which often has the accuracy of a few millimeter or less. However, this fine resolution and the resulting freedom of motion a participant may have is dependent on the number, quality, and dispersion of emitters and receivers about the capture volume [8] [1]. This fact highlights

a major downside to these systems: cost. Most receivers for these systems are specialized, high-resolution video cameras, which cost from \$600 to \$6,000 each [4]. While two cameras are the minimum needed for a system to function, eight is recommended for standard walking observations to guarantee a high level of accuracy [8], and almost every system has more than the minimum to reduce the chance of losing sight of markers partway through a test. It is common for these systems to cost hundreds of thousands of dollars [1].

These systems are also computationally costly. Not only does the data from multiple cameras need to be converted into coordinates, but then combine into agreeing values. After the coordinates are reliably calculated, the joint angle data must be derived through forward kinematics. However, if marker dropout occurs, which is common, inverse kinematics is typically used to fit the remaining markers with simulated markers, orientated at various angles. Finding the angles that yield the best fit can take significant time and/or processing power, which will drive up the computational and energy requirements of these systems.

Marker based systems can be subdivided into two groups: active and passive. Passive markers are usually small and highly reflective in the frequency of light being emitted. They are attached to a participant with tape or adhesive. These markers bounce light from emitters to receivers [2]. Since all passive markers behave similarly, they can be confused for one another, which is called marker swapping [1]. This problem can be minimized by placing markers in specific patterns and relations to one another [9]. Further software methods can eliminate this problem completely.



Figure 2. Comparison between passive (left, Wikipedia.org) and active (right, Berkeley.edu) marker suits.

Active markers are placed on the participant similarly to the passive markers, but instead of reflecting emitted light, they are the emitters. The benefit to active markers is the light travels half the distance [1], which can save either power, while increasing range or accuracy. In addition, each marker can pulse a unique on/off pattern and/or emit a unique photon frequency to avoid marker swapping. The drawback is active markers usually add wires to the participant, which can affect a participant's motion freedom [2].



Figure 3. Kinect's 3D imaging abilities using specialized light patterns (Pictures from yting.com).

Optical systems that do not use markers tend not to be very accurate nor reliable compared to their counterparts. They are usually marketed as novelties rather than scientific instruments, like the Xbox Kinect. The working principle behind this technology is a system emits (usually non-visible) light, which interacts with and reflects off the environment. When the light is reflected into the receiver, its intensity decreases proportional to the distance it traveled. Since there are no markers, the system must send the light in very specific patterns, forming a type of grid over the observation area. This grid is viewed by the receiver, which then see what parts of the environment are closer or farther away from the intensity levels of the grid portions [10]. There is no distinction from the environment and the participant, nor is there distinction between multiple participants. Participant loss and system confusion are common problems. Shape and gesture recognition software are used to aid in tracking, but if there is one emitter/receiver pair, then tracking multiple targets moving in front of one another is not possible, due to the casting of shadows and participant combination. Additional emitter/ receiver pairs at

varying orientations may help, but as is the case of the Kinect, the additional systems may project the same pattern as the first and cause confusion at the receivers of which grid data is which [11]. Confusion can also arise from materials that reflect or absorb the light more than the average rate of the rest of the environment, making certain areas seem closer or farther away than they really are. However, researchers have found uses for this technology for scientific purposes, as well as refining its ability to track [12]. The benefits of this type of system is feedback is real-time; systems are easy to setup, operate, and maintain; and financial and computational costs are very low [1], especially compared to the other optical systems.

2) *Inertial Systems*: Inertial systems are comprised of a series of inertial sensors, arranged specifically on a participant's body and relative to each other. Accelerometers monitor acceleration to deduce velocity and position of the objects they are attached to. Gyroscopes measure the changes in rotation of the objects they are attached to [13]. Commonly, a set of three orthogonal accelerometers are combine with three orthogonal gyroscopes to measure the six degrees of freedom of a rigid body can travel in [14]. Some applications need a global positioning system to give a participant's location in an environment. Using only gyroscopes and accelerometers, deriving a relative position of a participant from a specific reference point would be complicated and flawed, so it is also common to have a magnetic positioning system that measures Earth's magnetic field in three dimensions (often referred to as a digital compass). This combination of sensors is referred to as an inertial measurement unit (IMU) [15]. IMUs normally take the form of three-dimensional circuitry that needs protection from impacts and other external forces and materials. They are often shielded with very hard, rigid cases. These cases are attached

to a participant, similarly to the active markers in optical systems. Unlike the markers, IMUs and their cases have substantial inertia, making it very difficult to attach to a participant rigidly. Sensor vibration and shifting is a common issue with these systems.



Figure 4. Example of a seventeen-sensor inertial motion capture system (left), standard IMU (top right), and waterproof, metal IMU (bottom right) (Pictures from YostLabs.com).

Most full body IMU systems are comprised of sixteen to seventeen sensors. This offers between ninety-six and one hundred and two degrees of freedom being monitored. Many of these are redundant but help the system double check its measurements. There is an issue with having that many sensors: they tend to intrude on the participant's ability to move freely. Research concerned with lowering the required number of IMUs per system has been done in the past. These sparse systems have an error of ten to twenty degrees, after signal processing [16]. Additionally, every inertial system suffers from compounding drift [13], which makes their data collection a rough estimate that can only be relied upon for several seconds [17]. Improved filtering and data processing techniques have been

developed, but most general fixes only reduce the drift effectively in the first six to fifteen seconds [6] [18]. Specific fixes are only applicable for certain regions of the body, where movement, sensor type, signal shape and amplitude, and duration of the test need to be known while developing said solution [18] [7] [6]. The reason long-term filtering is so difficult is the drift is only estimated to be linear and that estimate becomes invalid around the one hundred second mark [18].

Kalman and extended Kalman filters have been used to extend the usefulness of IMU systems. Typically, magnetic north and the direction vector of gravity are referenced continuously to help reset the measurements and discard drift. These filters can yield stable RMS errors of 1.3° to 4.1° for the roll, pitch and yaw for individual IMU units [19] and 6.26° , 5.47° , 7.06° , and 12.24° for hip flexion, abduction, rotation, and knee flexion during walking-speed gait analysis, respectively [20].

A benefit of IMU technology is it has no need for a capture volume and can be used in real-world environments [16]. It is also cheaper than the optical systems by about a factor of ten. Xsens has systems for \$12,000 and the cheapest go for around \$2,500 to \$3,500.

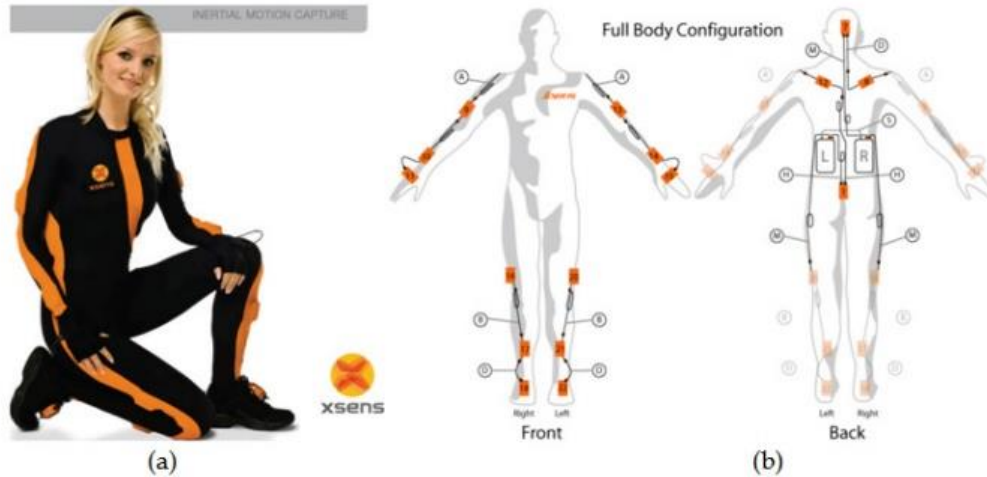


Figure 5. Xsens 22 sensor suit (left) and system layout (right) (Pictures from Xsens.com).

3) *Magnetic Systems:* Magnetic systems are arranged in very similar ways as inertial, with the added requirement of needing a reference, magnetic field transmitter. Three magnetic field generators of known magnitude comprise the individual motion sensors, which are placed at key locations around the body [1]. These body sensors then interact with a static, three-dimensional field that acts as a capture volume, which is a significantly smaller space than typical optical capture volumes [13]. The static field fluctuations are observed and translated to positional changes via a data processing system [21]. This method can produce very good accuracy at a considerably lower cost than optical systems. However, these systems still cost tens of thousands of dollars and are very sensitive to wiring, electrical devices, and conductive metal objects. The noise pollution can be so great that most standard rooms are not usable for these systems due to either the wiring in the walls or the rebar in the concrete structure of the building [1] [21]. This system is so sensitive, the wiring use by the system needs to be given extra shielding to avoid interference, which results in a very restrictive, heavy system for the participant to wear [21].

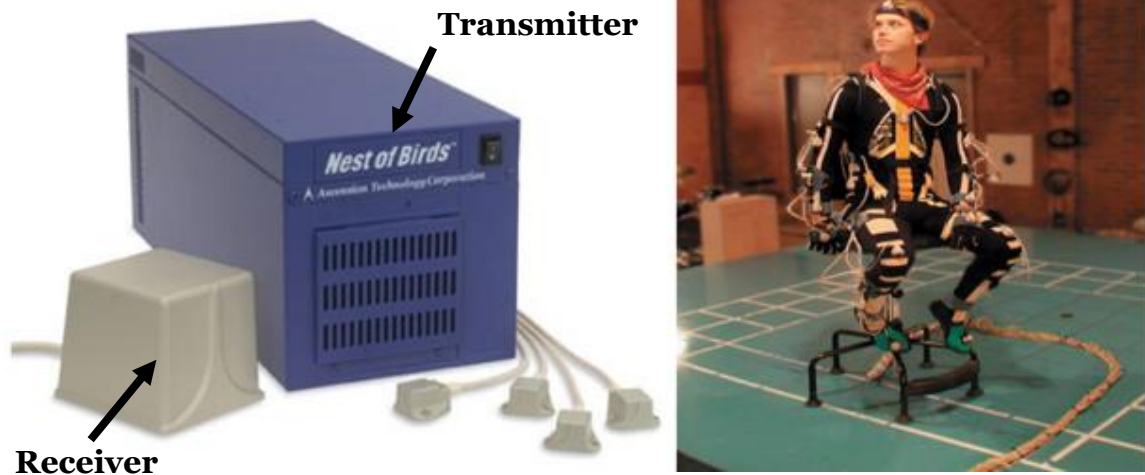


Figure 6. An example of a magnetic motion capture system (from source [13]).

4) *Acoustic Systems*: Acoustic systems operated off similar principles as marker-less optical systems and sonar. These systems let out a special frequency of soundwaves that interact with a capture volume. When there is a participant in the capture volume, the soundwaves interact with the participant, and the receivers analyze the changes in the waves, exactly like the marker-less optical systems. However, these systems are susceptible to echoes and outside noises, which cause major sample pollution [1].

5) *Mechanical Systems*: Mechanical systems were the first type of motion capture and are considered the most intuitive to use, maintain, and collect data from [1]. These systems, often referred to as exoskeletons [13], are very accurate do to their physical interactions with the participant's motion [22]. An issue that they create is that they are very large, heavy attachments that very much restrict movement freedom and change the resulting motion of the participant due to the system's added inertia. Additionally, the system must be fitted and adjusted to every new participant that wears it to ensure proper measurements [1]. While these systems are very accurate and need little to no signal calibration or processing once operational [22], this method is underdeveloped because the physical restrictions on participant's motion make them less attractive than most of the

other systems [1]. Mechanical systems do not use a capture volume or a line of sight, so they have more mobility, in a general sense, than optical systems [22] [13].



Figure 7. The Gypsy 6 mechanical motion capture suit. The Gypsy 7 has a resolution of 0.125 degrees [22] (Pictures from Pinterest.co.uk).

B. Analysis & Problem Identification

Optical, magnetic, and acoustic systems are all able to produce very accurate and reliable data while operating in an optimal environment. However, the ideal environment for magnetic and acoustic systems are not common setting and almost have to be specifically built or shielded to accommodate their needs. Optical systems are more straight forward to accommodate. Marker based systems need environments specifically designed, too, but controlling lighting and placing cameras rigidly requires less room modifications and knowledge than soundproofing or magnetic shielding. Additionally, marker-based systems have fine accuracy and precision when operated correctly, making them a reliable and stable option. Magnetic and acoustic do not cost as much as the optical systems but are susceptible to noise pollutions that are too common to make their tradeoffs pay out.

Traditional Mechanical and inertial sensing systems are unique in that they do not need to customize their operating environment to function. In addition, most if not all the measuring equipment is worn by the participant being monitored. This allows for more

mobility for these two systems. Mechanical systems need very little calibration, are very stable systems, and can produce high level of accuracy when reading a participant's motions. However, the mechanical systems are also rigid, metal exoskeletons tend to limit a participant's range of motion and are of significant mass, which shifts the observed dynamics away from a natural motion. Inertial sensors are light and small, so they can avoid this issue. They are problematic to attach to a participant, though. Due to the IMU's sensitive electrical boards, they need shielding that is rigid and physically large compared to the sensor and the area being monitored. This can allow vibrations or small motions relative to the participant that will pollute measurements if the IMU's are not fully secured. If the sensors are fully secured, they can become a hindrance to the participant's motion or comfort, so much care must be put into the proper attachment methods of this system to properly balance measurement quality and participant's needs. This issue of balance has led to attempts to reduce the number of needed sensors, which can better preserve participant freedom of motion but does drastically increase error percentages. In addition to attachment concerns, inertial systems are susceptible to drift which compounds over time. This drift can cause upwards of ten degrees of error for certain sensor locations, even on the highest quality systems. The drift can be so bad that it is no longer practical for many systems to record measurements longer than one hundred seconds. This requires operators to have a much more complete knowledge of their system and understand to limitations of the filtering systems being used and potentially how to modify them.

If motion accuracy is all that is being observed with few reservations about cost, marker-based systems are the finest systems available. However, if a study cannot be done inside of a laboratory or would benefit from a more practical setting, optical systems

quickly become unfeasible choices. For practical environments, mechanical systems have the greatest accuracy, stability of measurement, and ease of use. Inertial systems pervert the motion and movement freedom much less than mechanical systems do but are more susceptible to noise and calibration drift which can make them difficult to operate and reduces the usefulness of their data. Both mechanical and inertial systems can be seriously affected by participant impacts. As of this point in time, practical and portable motion capture has a limited range of options that come with many tradeoffs in either motion freedom, accuracy and stability, or working limitations such as participants can't take impacts or operators need full knowledge of the capture system. A more robust and practical system is needed to make motion capture more flexible, useful, and dependable in real world environments, as well as in everyday situations.

C. Solution Proposal

A robust, portable, and practical motion capture system is needed to make real world environments and situations more accessible to measure and study. Laboratory environments have a method that is considered the pinnacle of the technology: marker-based optical systems. However, labs are not practically able to accommodate many situations, including most athletic training, and are inconvenient to test large quantities of participants in. Inertial systems are the most portable and developed options currently available, but the systems have attachment issues, have potential for large drift error, are not fail safe, and have the tendency to encumber their participants. While these systems function, they are not in sync with their participants' motions and/or environments.

For a motion capture system to successfully capture practical motions and real-world situations, it is important to define exactly what "real world situations" and "practical

motions” mean. In this study, “participants” will refer to humans being monitored, “motions” and “movements” will refer to the natural ways the human body moves, and “motion/movement freedom” will refer to the range of motion a human body can achieve under no constraints. “Nonrestrictive clothing” can be defined as clothing that is no more restrictive of motion than clothing worn regularly in the situation being examined, which may cause this definition to change on a test-by-test or application-by-application basis. For example, a test involving a participant being observed while shopping wouldn’t need a system as nonrestrictive as one being used to monitor a participant participating in a yoga exercise. If performance is affected, it is important to specify the nature of the restriction. A “real world situation” will be any action that the participant might do as a part of their daily life or exercise regimen. This may include running and jogging (exercises easily measured in a laboratory environment), various sporting activities, interacting with other participants or non-participants, traversing unprepared terrain, etc. This category should be considered general enough so that it can be more easily defined by what is not being considered “a part of daily life.” For example, if a system is vulnerable to water, then swimming may not be possible to monitor but may be excluded from being a part of daily life if the participant does not regularly swim.

As stated, IMUs have difficulties observing a participant’s motions. They are very difficult to fully constrain to the participant’s motion, are attached by lashings and straps that can restrict participant motions and are encased by relatively large, rigid boxes, which not only contribute to polluting vibrations but can be physically in the way. An alternative system should be one that is composed of sensors that are more compatible with the human body. This would require the individual sensors to have very low mass and inertia, small

(preferably no) rigid areas, attachments that can affectively isolate the sensors from any motions outside of the participant's, while not encumbering the participant by lay close to the body or staying out of the participant's way.

An alternative system would also need to be portable. This would require general stability and low weight addition to the participant. Additionally, power consumption rates would need to be low enough to operate on portable batteries, and generate data would need to be transmitted, processed, and displayed in real-time. Ideally, a useful system would have to be durable enough to survive rough environments repeatedly and be made simply enough to be operated, maintained, and repaired with relative ease.

To address these requirements for a plausible alternative system, a series of one dimensional, electroactive polymer strain sensors will be attached to a pair of compression pants in a reticulated manor. A prototype will be designed around biomechanical considerations of the skeletal and muscular systems of the human body, their relative motion to the overlaying region of skin, and empirical data collected through trial and error (more information is presented on this design in MECHANICAL SYSTEM DESIGN D. Physical Design). The success of this system to meet the specified requirements, and to what degree, is the subject of the following sections.

CHAPTER II

MECHANICAL SYSTEM DESIGN

A. Design Concept

The design concept of the reticulated motion capture (ReCap) system being developed is based around a one dimensional, deformation-monitoring sensor. The word “reticulated” is defined in Webster’s New World College Dictionary as being “characterized by or having the form of a grid or network.” This system is reticulated, which is further explained in CALIBRATION METHOD 4) Signal Crosstalk. The type of sensor being used is an electroactive polymer (EAP) strain sensor, due to the similar physical characteristics it shares with skin. (ReCap system will also be referred to as “this system” or “the system”). The type of EAP is a dielectric elastomer (DE), and the sensors will be referred to as both interchangeably. This system is being designed in a way so that each applied EAP sensor can strongly monitor one specific degree of freedom of the human body. This system will attempt to monitor all types of motion of the human body in three-dimensions by monitoring flexion/extension, adduction/abduction, as well as internal/external rotation.



Figure 8. An example of a dielectric, electroactive polymer strain sensor, one-dimensional. (Pictures from Parker Hannifin at Parker.com).

B. Existing Eap Technologies

Electroactive polymer (EAP) is a relatively new material. There is currently a lot of development and research revolving around this technology and the concept of a strain-based motion monitoring system. This is neither a new nor unique effort and has been attempted many times by various, independent groups. Many share similar qualities, including arbitrary sensor arrangement, integration into clothing, and flexion sensing capabilities. Flexion sensing seems to be so intuitive that handing any layperson an EAP strain sensor would probably result in that individual stretching it across their elbow or knee. Every system that has claimed to sense motion has near identical flexion sensor arrangements. Some appear to have more isolated sensor positioning systems [23], others seem to focus on planar motion, and others still seem to form nonsensical arrangements that would greatly reduce reading quality but appear very reminiscent of the inertial sensor setup.



Figure 9. An example of a research, EAP, motion tracking suit (right, image from source [24]). Bend system (left, image from source [23]) claims to monitor knee flexion and glute “involvement,” which may mean sensing topical distortion caused by flexing gluts. The wearable soft sensing suit is a two-dimensional monitor, which still has linear calibration issues, possibly due to the participants’ inability to restrict themselves to pure planar motion.

Based on available resources and public information, there is no EAP-based motion capture system, commercial or otherwise, that has the capacity to sense anatomical rotation in a meaningful way. The only system that has been found to have any capacities to detect rotation was designed with a large variety of sensor arrangements to test what setup would function best. There were two basic type of arrangements: one set vertical and one set following muscle geometry. The logic behind following muscles is unknown, but one end of their anchors is attached near the spine, and the other on the leg, sometimes snaking around the leg. In all cases, the results were not calibrated to any motion or rotation values but were used to find the magnitude of response [25].

While the magnitude of response is important, there are many additional factors to find a feasible arrangement for sensor input than the size of the response to motion, which is further explained in CALIBRATION METHOD 2) Rotation Sensor Geometry. This

study was presented in April of 2017, which indicates that most knowledge of rotation sensing of human joints via strain sensors is very much at an early stage. Rotation is a fundamental motion, which dramatically affects the overall kinematics of a participant and the dynamics of skin-attached objects, such as sensors. This is a critical blind spot in form monitoring, which also prevents the proper calibration of many other sensors. The proper calibration of flexion, abduction, and rotation sensors requires each to be calibrated with the other degrees of freedom they are kinematically linked to. The error of these systems otherwise is almost certainly significant, a claim that is supported by research that claims to have (at worst) 15° of error [24]. A limited explanation of these effects on skin-applied sensors can be found in CALIBRATION METHOD 4) Signal Crosstalk.

C. Work Thus Far

Two previous projects were performed with the goals of crafting and/or improving an EAP-based motion capture system. The first of these projects set out to determine if the sensors could be arranged on the human body in a way that would robustly capture the flexion and rotation information of a participant, due to their pertinence to anterior cruciate ligament (ACL) health. To clarify, this ligament is an integral part of the structural mechanism that contains the knee while allowing it to move, along with the posterior cruciate ligament, lateral collateral ligament, and medial collateral ligament (PCL, LCL, and MCL, respectively). The ACL is very sensitive to the orientation of one's legs during mid to high magnitude impacts or sustained forces, commonly caused by running, jumping, cutting/juking (rapid directional changes, usually from one high speed to another), and power lifting. Because the knee only has one major degree of freedom, the orientation of one's leg relative to the Sagittal plane is determined by the rotation from the hip joint and

the magnitude of the force transmitted through the ACL can be inversely altered by the magnitude of flexion from the knee joint. When the hip expresses internal rotation, an alignment occurs in the directions of the net force of the body or leg and the direction of the ligament, subjecting the ACL to transmit a higher proportion of the net stress than it was designed to handle. This is an issue, particularly in women athletes, that can be held directly responsible for a large percentage of ACL injuries [26].

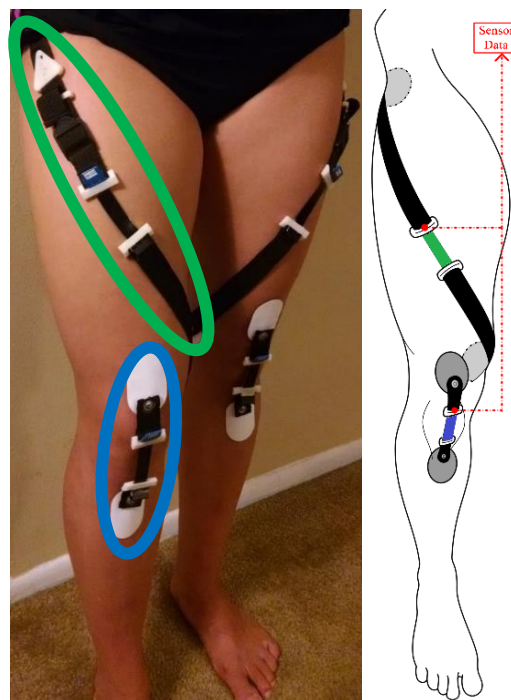


Figure 10. The resulting locations of the leg's flexion (blue) and rotation (green) sensors.

Sensor anchor areas were chosen on the femur at proximal (near joint) locations with the intent of measuring the rotational input of the hip joint on the femur and the flexion of the Tibia about the femur via the knee joint. Testing was performed with several participants; however, the application was directly to the skin and used tape to secure the sensors to their locations. This was not only difficult and unreliable, but it also used system specific information to apply which made application impossible for the entire project's

team, save for the system's designer. Additionally, application was relatively final and did not allow for sensor tension adjustment. As a result of this setup, much data was lost due to poor signal response and slack sensors. The results of this project showed that valid flexion and rotation positions were found, and the system as a whole would benefit from being incorporated into clothing [27]. This project led to two important definitions, described in detail in CALIBRATION METHOD 1) Flexion Sensor Geometry and 2) Rotation Sensor Geometry.

These definitions are important and imply several important details. First, a flexion sensor is a multiple-bodied measurement tool. This means the two anchors of the sensor are on two separate rigid bodies. In this application, the anchors benefit from being as rigid to the bones they are anchored above as possible. Unfortunately, relative motions of these anchors to said bones would cause signal pollution. Due to the amount of muscular tissue between the skin and bone typically found in these regions, this pollution is likely to be consistently present and sporadic in magnitude. A rotation sensor, in direct contrast, must be a single body measurement tool. This is due to rotation being measured indirectly through observing the geometric-based changes in the sensor arrangement. The arrangement travels from a proximal (near the joint originating the motion) location of the long bone and is anchored distally (the further down the bone, axially, the larger the response. The sensor may also cross the long bone to anchor on the lateral side to amplify the response, depending on the underlying anatomy). The sensor measures rotational displacement as the only non-observed, varying component in a right triangle, whose hypotenuse length change is measured by the sensor and is proportional to the rotational motion. The two anchoring positions must be placed along the same bone so that one side

of the triangle is a constant, otherwise additional sensors will be needed to calculate the motion, adding unnecessary errors.

The sensor anchor not proximally placed is like the flexion anchors in that any relative motion to the long bone is a form of pollution. However, the same DOES NOT APPLY to the proximal anchor. If the proximal anchor were rigid to the bone it is observing, this arrangement would not deform or change in length. Due to the proximal locations' proximity to a rotationally isolated rigid body (the other side of the joint) and the skin and muscular tissue continuums, which bridge these two bodies, the rotation is dampened if not eliminated in this area of skin. The proximal anchor instead needs to be as rigid to the static side of the motion joint as possible. The Radial and Ulna pair are unique because they can be considered one axial rigid body, like the femur or humerus. However, their rotation about themselves causes a length change the rotation sensor arrangement can detect with fully rigid anchors, so long each bone has only one anchor.

The mechanical design of the first project involved adhering the anchors directly to the skin and was too complex to be used without a knowledge of anatomical kinematics and a bunch of tape. Even at its most effective, the system was restrictive, unreliable, and awkward. To address these shortcomings, it was decided the system could not be applied to a participant's skin directly. This eliminated the need for human skill to place the sensors for every new participant and avoids the problem of finding an adhesive that is strong enough to solidly attach the sensors to skin, nontoxic and hypoallergenic enough to be used on humans, and easy to remove safely after testing. This led to a motion capture suit. Clothing is generally approachable to all potential audience (claim based on anecdotal evidence) and offers robust anchoring potential, especially near seams. Clothing is

commonly mass-produced and tailored to individuals, making it a cheap and customizable solution.

The second project set out to design a more stable system that is easier to use and apply. This includes being reusable, secure and stable, adjustable in sensor tension, and should not encumber the wearer more than their typical attire. It also set out to design and define effective calibration protocols for the sensors being tested. The redesign began with the idea that clothing would be the best way to achieve all the goals in a practical way. The greatest benefit of incorporating the system into clothing is that it takes a potentially complicated and foreign system and constrains it to an interface most people are very familiar with pants (and eventually shirt). Also, the system is permanently set up on the same place of the human body trial after trial, while being readily removable and chemically inactive.

Compression clothing stays the most static relative to the body parts they cover. This is notable because compression clothing has been specifically made for athletic application, so it may offer minimal interference with motion while providing a comfortable, full body compressive force. The compression is particularly valuable to topical attachments, for it makes the fabric of the clothing move similarly to the skin. The stretch of this elastic fabric can also work as a counter to the tensile force of the deformed sensors by either preventing motion or creating a system of a predictable, linear deformations that can be included into the calibration.



Figure 11. The resulting system of flexion (blue) and rotation (green) sensors integrated into compression pants.

Static and dynamic tests were performed to gather a set of diverse data. Static tests that moved individual joints throughout a range of positions were used to isolate the sensor response for each joint, while dynamic tests were used to measure the long-term stability of the system and the accuracy of a general calibration. The results were acceptable for the knee flexion monitor, with 6.50° error over the dynamic test with simple linear calibration [28]. The rotational sensor was not as straightforward, having a significant difference from the data collected from the optical motion capture. More advanced calibration was needed. A major increase in accuracy came when flexion data was referenced in the calibration of the rotation sensor's signal. While the results were not perfect, the similarities between the optical and strain sensor data were notable (Figure 12). The remaining issue noted was the calibration's inability to be generally applied to datasets the calibration equation was not calibrated on. This meant the array/equation system developed can work but only if a case specific filter is made, which is not very useful. However, the logic behind crosstalk

calibration equation also predicts what may be causing these residual errors left in the rotation data of the calibrated set; the rotation being tracked is from the hip, which is a three degree of freedom joint. When only one of the degrees of freedom is monitored (the rotation), the other two degrees are left as potential, unaccounted pollutants to the rotation and, probably, knee flexion data- the knee data was also recalibrated with rotation data input and improved as well; this process is further explained in CALIBRATION METHOD 1) Work Thus Far.

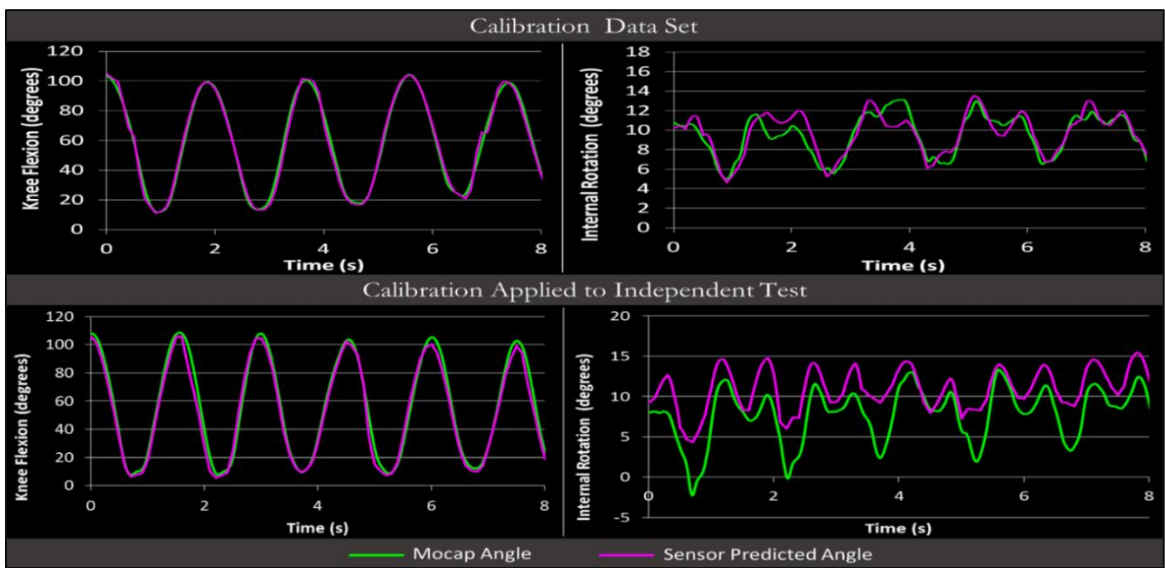


Figure 12. A comparison of a calibration equation’s effects on the calibration data (top) and a dataset from a different test of the same participant (bottom) (graphs and calibration created by Katherine Florek; permission in APPENDIX H).

D. Physical Design

The physical system being designed is set to work around sensors that detect changes in the distance between anchor locations. In this case, the system is designed around one-dimensional, EAP strain sensors. The EAP sensors have several characteristics ideal for use with the human body: they are elastic, non-rigid, low mass, and low power consuming devices. They are high voltage, which makes them dangerous for internal usage; however, the combination of low power/high voltage means the current passing

through each sensor is very small, which is ideal for any electronic in contact with skin and sweat in non-controlled environments. This high voltage makes possible shocks from a damaged circuit more noticeable and less dangerous due to the fact voltage, unlike current, is not lethal. Internally, higher voltages activate muscles. Because of the high water and electrolyte content inside the human body, electrical discharge can be conducted readily to a large volume, making a discharge of any magnitude unpredictable and dangerous. Any malfunctioned discharge these sensors could create would most likely not reach any muscle tissue or internal organ during external usage. This quality is very important and should be present in any electrical device that is in contact with the human body.

1) *Anchors*: This type of anchor design is only relevant for systems that are using clothing not specifically designed to incorporate a strain sensor array and would not be applicable for the design of system specific garments. So long as the deformations are linear and regular, they are easy to calibrate around. The concern is if there are stress concentrations, this may damage or shift the clothing to the participant or attached anchor relative to the clothing in a way that does not repeat. To reduce this happening's potential, an effort was made to create a uniform stress over the largest possible area with the materials at hand.

Nylon was used as the anchoring material. The prevalence of nylon in this design is partly due to its low cost, availability, low rigidity in directions normal to the sensing direction, and ease to work with. For the anchors, the main design concern was avoiding strain concentrations on the clothing they attach to. Since most clothing is made of soft material, any concentration of stress at an anchoring point could cause a substantial or irregular deformation at the site of connection. This deformation could affect how the

system translates force to the sensor, lower the system's useful life, and diminish the deformation absorbed by the sensor. To reduce the possibility of stress concentration, an anchor geometry was design using the Solidworks FEA package.

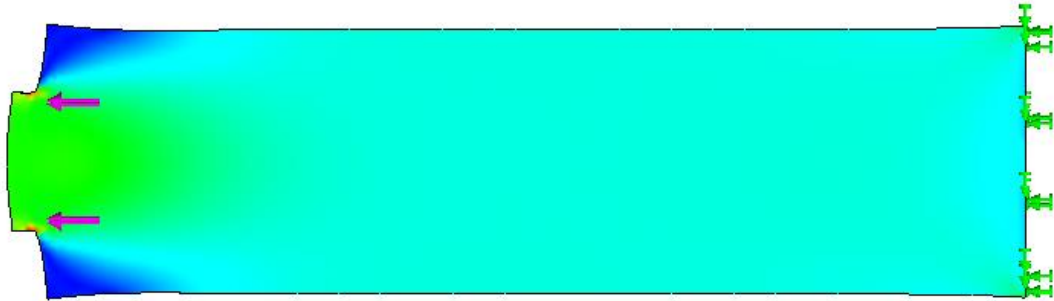


Figure 13. An infinitely long strap modelled and analyzed in Solidworks, based on the dimensions of the anchor material (1.5" standard nylon strapping). "Infinitely long" in this context means the stress/strain flow becomes perfectly distributed before the geometry ends.

First, an infinitely long geometry was made matching the strap material dimension. What made it long was that it was made to a length that the stress had an opportunity to evenly distribute across the cross section partway down the strap's length.

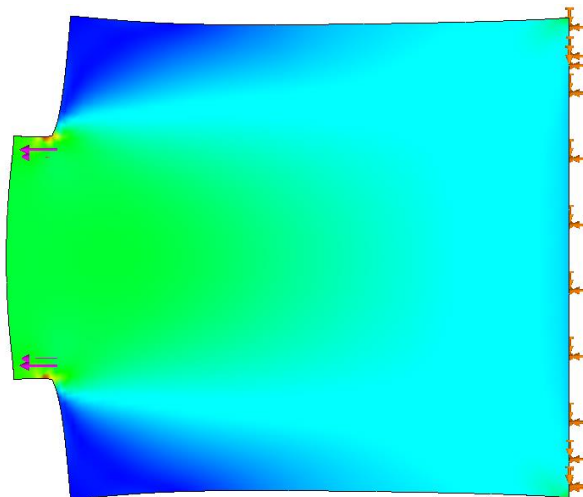


Figure 14. A shortened, yet still infinitely long, strap. Because the perfect distribution of strain just develops at the end of this length, any longer straps will have excess material that does not provide any benefits.

From there, the length was trimmed to be just barely infinitely long. This is considered the blank geometry, since it had no alteration, except for length, from the standard nylon strap. The smaller region where the force is applied is made to represent the connection to the smaller strap that directly holds the sensor.

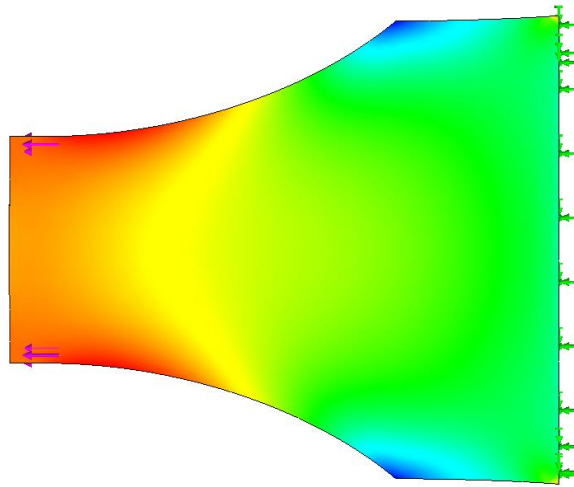


Figure 15. A blank strap with unnecessary material removed.

Cuts were made as an attempt to eliminate unnecessary material. These cuts further affected the stress distribution of the anchor.

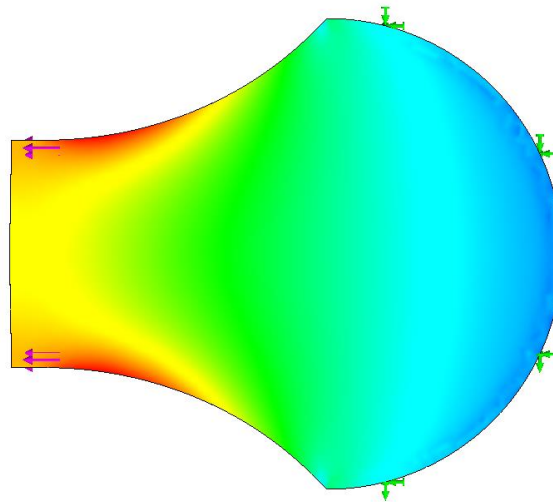


Figure 16. An increase of the attachment perimeter.

To reduce the stress levels at the attachment point as much as possible, the perimeter was increased by creating a circular arc instead of a straight line. The strap was designed to be slightly less than a half circle at the attachment because the stress distribution becomes messy with support perpendicular to the applied force direction.

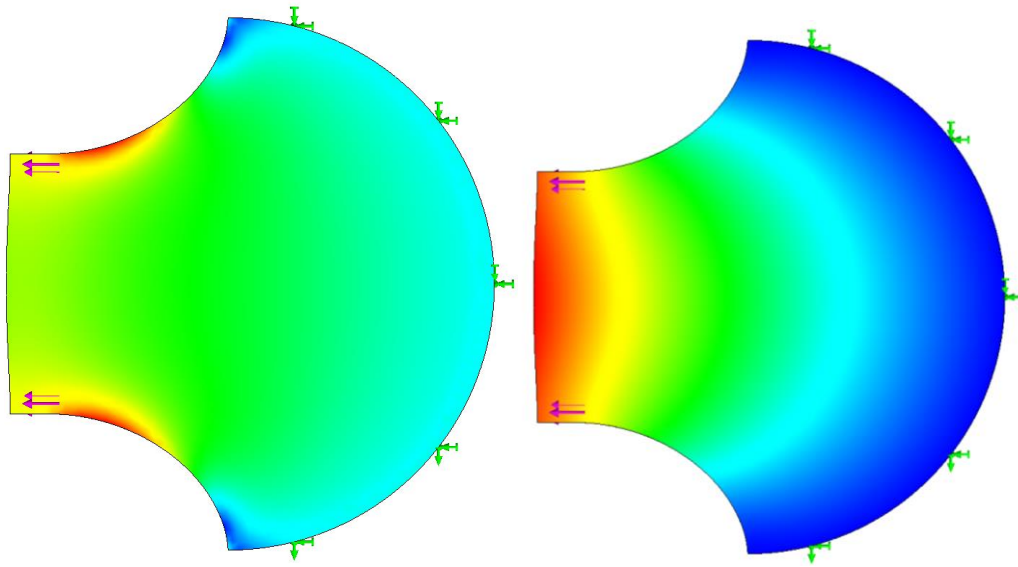


Figure 17. An almost uniform stress (left) and strain (right) distribution of the final anchor geometry.

Geometric relationships were altered and amended through trial and error until the stress distribution formed a smooth color gradient. Because the color gradients assign different values to each color every test, the last geometry was not considered ideal until it was confirmed the attachment area's stress levels were lower than the blank geometries. Since this final iteration had a larger perimeter, the stresses had to be lower, which the FEA results did verify. This approach to anchor geometry is important for any system which must attach the sensors to clothing or skin, causing the force to be absorbed in a very local area. For the purposes of the current system being designed, this geometry will be used as the anchor geometry. These anchoring concerns can be bypassed entirely when a system

uses specifically designed clothing that uses the entire garment to support and secure the sensors, minimizing local deformations.

2) *Straps*: The current sensors being used came in two standard sizes, which were found to be too small for monitoring most positions by themselves. The sensors needed to be extended with relatively rigid straps. The Young's Modulus of Elasticity of nylon is between 2-4_{GPa} ($2-4 \times 10^9$ _{Pa}) [29] compared to the EAP's stiffness of .18_{MPa} (180×10^3 _{Pa}). The strap material is 11,000 to 22,000 times stiffer than the sensors. While this number is most likely for a solid piece of nylon plastic as opposed to a woven strap, this is not much of a concern for several reasons. The strap should deform in a similar way every loading cycle, which can be compensated for and calibrated out; the deformations of the strap due to its geometry will be minimal as a consequence of the low forces involved (the maximum being between 7-10_N, resulting in about 0.04_{mm} deformation over 0.5_m of strapping); and the nylon strap chosen is not only thousands of times stiffer than the sensors but also has a larger cross sectional area.

a) *Clothing*: The ideal properties for clothing used for this system would be they produce little to no relative motion compared to the participant's body, they are flexible and elastic enough to not limit the motions of the participant, and they do not produce excess motion or deformation in the anchoring areas. Relative motion caused by the clothing- either through fabric shifts or material deformation- will affect the sensors' measurements. If this effect is constant and predictable, it can simply be calibrated out and will not affect the accuracy of the readings. However, there is no guarantee these motions will be repeatable. To reduce the possibility of pollution and error from the clothing, clothing motion and deformation will be reduced as much as possible. Compression

clothing become the most obvious choice of garment for low relative motion between the body and clothing that maintains a full range of motion because of their association with athletic activity. The main drawback of using compression clothing is the materials used to make them is high elasticity and easily deformed. While this property allows for the clothing to be tight and fit the form of the wearer with a small amount of tension, limiting the relative motion but not restricting the movement of the participant, it also causes the fabric to deform and shift under small loads, like the tension in a strain sensor. Ideal compression clothing would have more structural material around the areas the anchors attach. The concept of having structural support around joints, while allowing for a full range of motion, fits closely into the principals behind kinesiology tape.

b) *Kinesiology Tape*: Kinesiology tape (taping) is heavily associated with physical therapy and athletic training. Studies suggest taping may have positive effects on the treatment of sprains and other swelling-based injuries for the first 24 hours after occurrence. However, the long-term benefits of taping as a treatment for injuries and as an injury prevention device is still being determined and may not exist [30]. Many athletes, patients, physical therapists, etc., have confidence in taping and believe the compression it adds to their muscles and joints helps stabilize the areas. Many people who suffer an injury are gun-shy about re-injury for months or even years afterwards, which can negatively impact the recovery process from the patient's unwillingness to physically push their body. The fact taping can reduce these doubts could lead to quicker recoveries by restoring the patient's willingness to push their bodies during critical recovery periods. This support is so strongly felt that athletes of all skill levels use tape in practices and in competitions. A notable example of this can be seen in the 2012 and 2016 Summer Olympic Games.

Borrowing the structural components of taping to anchor sensors to a participant could offer a way to create a safe and repeatable way to stick to skin, while taking a familiar form that is trusted to preserve physical performance. To make this method reusable, as well as easier to apply, compression clothing designed to emulate taping's compression will serve as a permanent anchoring system for this project.

E. Present Development

The physical systems used in the second project was made well enough so that no notable aging or wear. The performance was not an issue, beyond the number of motions being monitoring. Rather than start from scratch, these systems were modified from just monitoring hip rotation and knee flexion so they could also monitor hip flexion and abduction (Figure 18). The hip abduction sensor was straight forward to place, as there is only one direction where the largest magnitude of abduction-based motion can be viewed (meaning the other side of the limb in the abduction/adduction plan is the perineum, which would be shared by the other leg, causing the sensor responses to be linked to one another; and would be problematic to anchor to solidly, particularly for male participants). This region on the pants has many structural features, like seams and rigid fabric.

The flexion sensor was more ambiguous due to the distal anchor needing to be located near the ill-defined border of the gluteus curvature and the upper thigh. This is needed to maximize the potential of the anchor moving with the thigh, while minimizing the pollution potential of flexion muscle bellies, as well at the effects of femoral displacement due to hip rotation (this displacement increases distally from the hip joint). Placing a sensor across the belly of the Gluteus Maximus is not ideal because it is the largest muscle in the body and can produce substantial displacements when it flexes. This

is helpful because it is specific to certain motions (which can be calibrated around) and means the flexing of the muscle will primarily happen when it is stretched thin (reducing the muscle's ability to cause displacements of the overlaying skin). Even if this orientation becomes an issue, it is the best choice for the hip flexion sensor. Unlike the abduction sensor, both sides of the limb are available for anchoring in the flexion/extension plane. However, using the ventral surface to anchor a strain-based sensor to measure the flexion-dominated motions of the thigh in that plane means that the sensor needs to be under pretension in a standing position to make measurements. The amount of pretension during the standing position will dictate the resolution of the sensor to the motions and the limits of flexion that can be monitored before the sensor goes slack. This was attempted and created a system that was difficult to work with and added too many limitations to the participant's motions to be practical. The arrangement on the Gluteus Maximus adds no such limitations.

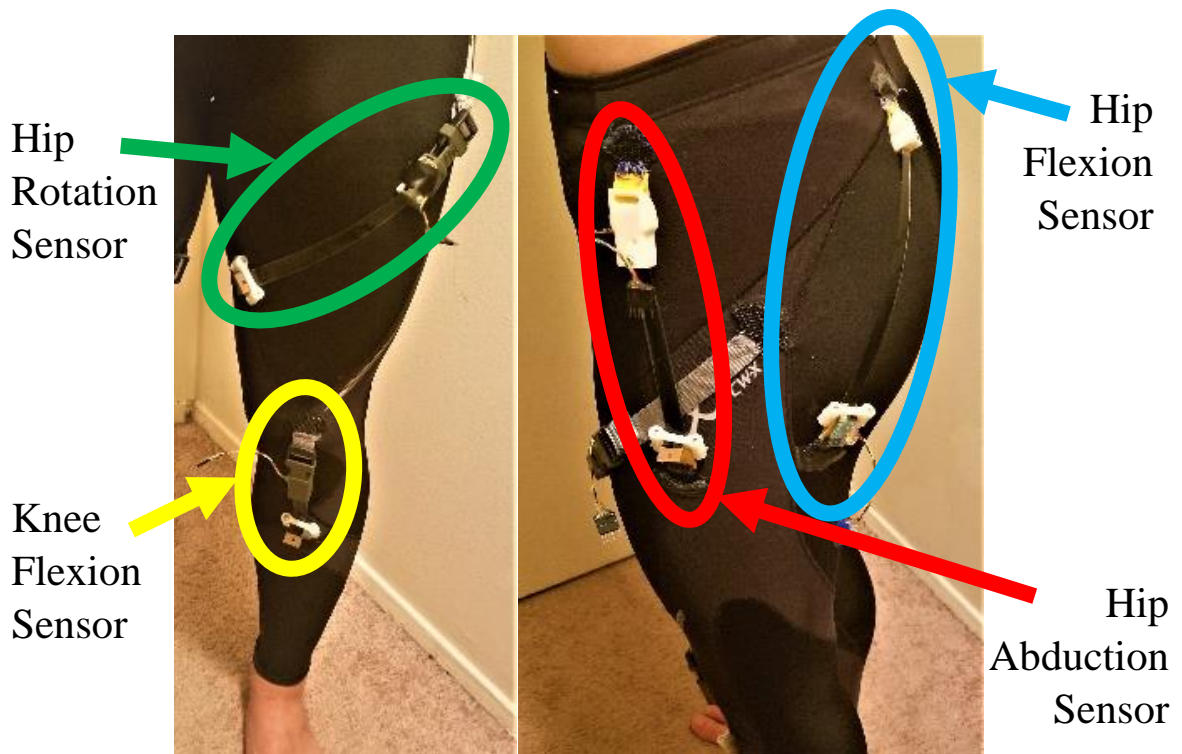


Figure 18. The current system being used (modified from the systems from the previous project). The hip rotation and knee flexion sensors are unchanged (left), while the hip abduction and hip flexion sensors were added.

There are three of these systems, as there were in the second project. They are distinguished by their sizes: small, medium, and large. These three will be used to gauge what effect, if any, height has on the calibration and performance of this method of motion capture. This version of the system will be referred to as the prototype. The cost to build each prototype was less than two hundred dollars, mostly due to the cost of the pants.

F. Future Work

The future development of the system as a mechanical object will be focused on two main issues: making the system mass-producible in a consumer-friendly form and expanding to the entire body.

1) *Mass-Produced Work*: Making anything mass-producible and consumer-friendly can be a daunting task and balancing the two has no universal definition nor criteria

of success. Making a product mass-producible is straight forward, with mostly practical and economic considerations- “is it possible,” and “is it worth it?” Calling something a consumer-friendly product, however, is not as clear cut. Something could be consumer-friendly if it only takes a week to adapt to, like with a new cellphone or computer. However, a pair of tweezers can be marked unfriendly for taking more than ten minutes to acclimate to. The main factors in deciding what is worth the time to learn how to use are the devices perceived complexities and familiarity, perceived services or return value, and perceived entertainment value. An important fact to note is the perception of the consumer can be totally different than the perception of the marketer, whose perception can be totally different from the producers, all of which may differ from the reality of the product or service being offered. Because of the subjective nature of perception, gauging value can be difficult and never guaranteed to be correct. Rather than hope value will be perceived high, efforts will be focused on making the system familiar and easy to use and maintain. It should be noted that potential consumer input is a vital tool for this process, but it is a tangential point to an already loosely connected topic to the purpose of this thesis. Market validation and customer interviews are vital steps that should be explored, and so will be done elsewhere.

As was previously stated, clothing is a universal interface, known to most of the modern world. Efforts will be made to make any additions either not change the wearer’s interactions with the cloths or to make any additions equally as intuitive and familiar.

To make sensors easy to apply and remove from the system, without endangering the health or comfort of the participant, the sensors should be attached with small zippers (clasp locker mechanisms), clothing hooks, Velcro[®] (hook and loop fasteners), or similar

fasteners that maintain rigidity in the observed motion's direction, while being soft in the perpendicular direction to the plan of the skin. This method should add a minimal amount of relative motion, which may be present in Velcro[®], while remaining of-negligible-mass, reusable, and simple.

Wiring to each sensor to a communal power and Wi-Fi transmitter is a more practical solution than equipping each one with independent units. The wiring used for this system needs to share similar mechanical properties as the clothing it is integrated into. Fortunately, wires can be made very thin and flexible (i.e. conductive thread). Care would have to be taken to design the wires with enough slack and excess length to absorb the expansion of the clothing, and at the same time remain out of the way when the clothing is relaxed. If conductive thread is used, there exist a plethora of methods and documentation on choosing and designing the appropriate stitch to allow ample stretching of non-elastic thread. The wires and their connections will also need to be well insulated as to not shock the wearer when in the conductive presence of water or sweat.

Sensor size and shape may influence data collection, the sensor lifespan, the range of observable motions, and the amount of force the sensors exert when deformed. The size and shape of joint specific sensors should be determined to optimize performance and lifespan. Alternatively, a general shape could be found that isn't necessarily ideal for each joint but is more effective than the off-the-shelf shape, while remaining more interchangeable than joint specific sensors.

2) *Expansion Work*: The goal of this research is to produce a system that can monitor thirty-three degrees of freedom in the human body. This excludes the digital (phalangeal; relating to the fingers and toes) degrees and those in the neck. The digital

degrees add up to eighty (four for each digit), which is difficult to monitor in a reasonable amount of space without custom-length sensors. This is a side note, however; the main reason for their exclusion is to focus this research towards degrees of freedom that are prime originators and transmitters of biomechanical forces. The neck is excluded due mostly to the fact that it is not common practice for motion capture, at least in the lab associated with this research, to monitor these motions. Future development may include these degrees.

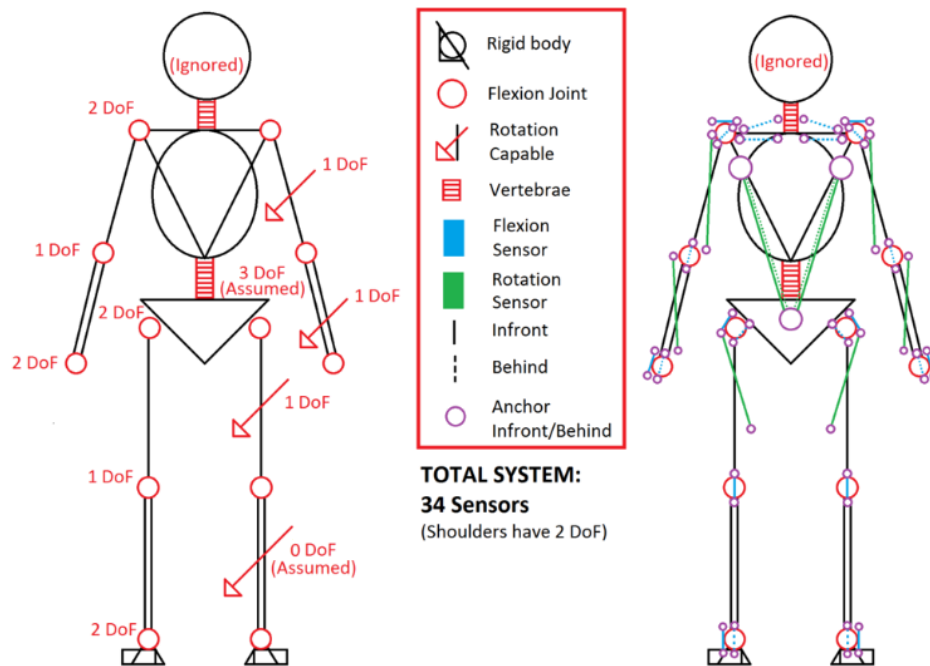


Figure 19. The relevant DoF of the body (left) and possible sensor locations (right). In this diagram, ‘flexion’ refers to the flexion sensor arrangement, which can be used for both flexion and abduction motions. Note to scapula/clavicle complex of the shoulder is assumed to have only two degrees of freedom. This assumption is used to describe the resulting motions possible of the glenohumeral cup and does not look to describe the orientation of the scapula. This assumption may need to be changes, especially if muscle forces need to be solved for.

a) *Everywhere Excluding the Back:* Expansion to the rest of the body will start with the ankle. The ankle has two degrees of freedom that will be monitored with the similar techniques used on the knee and hip. The only unique aspect of this area should be

that the axes of the resulting motions are not perpendicular to each other. This means the ankle produces three-dimensional motions with two degrees of freedom. This should not cause additional challenges, but it may. Since the digital motions are being excluded, this addition will complete the leg motion monitor array.

Expansion to the arm from the leg is expected to be very straight forward due to the anatomical and physiological similarities between the two limbs. The main difference, so far as this system will be concerned, is that the Radial is not assumed rigid to the Ulna, unlike the Fibula to the Tibia. These two bones have significant rotation that needs to be measured. The wrist is very similar to the ankle, except the wrist's degrees of freedom are perpendicular to each other, which should make the measurement straight forward.

Expansion to the shoulder joint itself will be measured similarly to the hip and should pose no major, unique issues. However, the shoulder joint (glenohumeral) is directly connected to another set of joints which create a complex with at least four degrees of freedom. One of these degrees is linked to the shoulder's abduction and becomes active at about the 90° mark, leading to the assumption that it can be grouped together with that motion. Another degree of freedom is responsible for the shrugging motion (scapular elevation). This motion can be monitored by placing a shared anchoring point near the cervicothoracic junction and continuing to the acromion palpation region.

The final motion that is planned to be monitored is protraction and retraction. The essence and importance of this motion is most notably captured in the cinematic masterpiece *Tommy Boy*, during the "Fat Man in a Little Coat" scene [31]. In the scene, the late Chris Farley (the titular Tommy) destroys the notably ill-fitting sport coat of David Spade (Richard) with a bombastic display of shoulder protraction. This motion can be

monitored on ventral or dorsal sides of the body; however, the ventral side is notably less muscular, particularly just below the clavicles. This may prove advantageous compared to the dorsal side in terms of crosstalk complexity. Additionally, the upper sternum would make a good anchoring region, possibly with little contamination between right and left limb motions- a feature probably not present on the back. To make a practical example, examine how clothing hangs on the body. It seems shirts with higher neckline cuts lay on the sternoclavicular joints with little motion, regardless of arm position. This consistency is a good quality for an anchor location. Contrast that with the same location on the back. Aside from loose clothing, a shirt would spend a low percentage of time in physical contact with the skin above the upper spine. Additionally, a high number of flexing muscle and the large motions of the scapulae would most probably cause many additional sources of pollution that the ventral side would not have. The sensor arrangement would likely continue to the acromion palpation region.

At least one degree of freedom exists in the scapula. This is a rotation motion and would be difficult to measure directly with strain sensors unless it were linked to another motion, as with the other rotation motion and arm abduction. Further analysis is needed to determine if additional monitors are needed to adequately describe the motion of the arm (this answer will most likely depend upon the application).

b) *The Back*: The most unique expansion area will be the back. The spine will be assumed to function as one single, large-displacement joint as opposed to an array of interconnected, smaller joints. This assumption comes from the low accuracy potential of monitoring individual vertebra's motion via skin applied sensors. Due to the large volume, variety, and complexity of the musculature of the back, directly measuring the

motion of individual vertebrae, accurately, can only be done by anchoring into individual bones. Because of this restriction, motion capture tends to treat the spine as a single, three-dimensional joint, with the upper torso sitting on it as a rigid object. Resulting kinematics of the spine can be back calculated, to some extent, with physical modeling and inverse kinematics. Since the present goal is to create a viable system of motion capture, and not alter an entire field, this assumption will be enthusiastically embraced.

Since the back is assumed to have 3 degrees of freedom, it can be fully measured with only three sensors. Depending on the chosen arrangement, this would lead to system asymmetric, leaving one side with a sensor the other does not have. More importantly, the three degrees of freedom can combine themselves in complex ways. While three sensors are theoretically able to fully describe three degrees of freedom, additional sensor may be more practical and accurate when dealing with complex motion over a large distance across the body. Redundant sensors can be used to not only ensure symmetry but may also be beneficial when attempting to uniquely describe every combination of motions the back can produce.

Before proving each motion can be described uniquely, the sensor array must be described. The arrangement shown in (Figure 20) displays four sensors arranged in two V patterns; one is on the ventral side of the body, which has its bottom anchor attached around the mons pubis, and the other on the dorsal side of the body, attached in the sacral region. The sensors are then extended to the axillary region. These anchoring regions are chosen because they are at the extreme ends of the spine, while occupying areas with minimal underlying musculature.

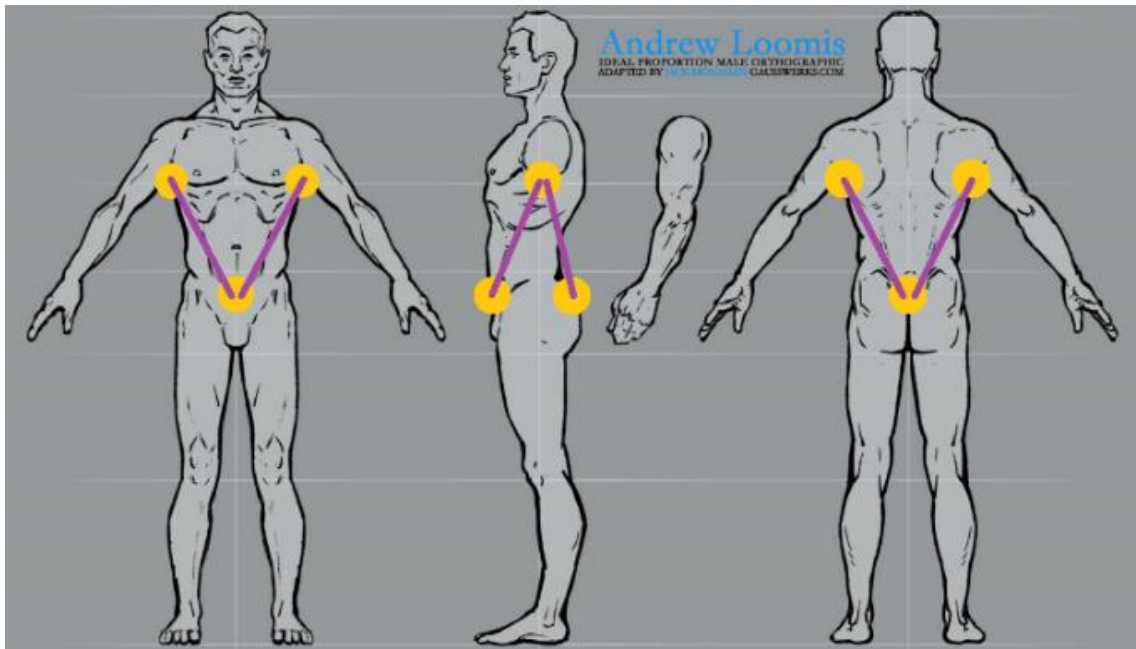


Figure 20. The anatomical orientation of an array of strain sensors used to measure the degrees of freedom of the back (image edited from cec-animation.com).

The lower anchoring locations allows the sensors to observe the entire scope of the lower spine's motion by anchoring on the structure of the hip. The axillary regions do not totally encompass the upper spine's motions, since the ribcage does allow for significant axial rotation (referring to the net spinal column direction as the axial direction). The axillary region is close to the top of the ribcage and is in a location with little musculature, meaning the majority of the motion is taking place below this region and any missed motions may likely be extrapolated from the measured trends, with little pollution potential.

A way to avoid this missed motion issue would be to rotate the array 90° on the body so the lower anchors are located on or near the superior iliac crests of the hip and extend to the upper sternum and between the scapulae. The sternum is not technically rigid, being comprised of three bones and sharing a joint with each long rib, it must translate through the total motion of the spine and may arguably be the indicator of the direction of

the upper thorax. The back-anchoring position would be problematic, for the scapulae and musculature of the back cause great displacement in this area, as mentioned in reference to shoulder protraction.

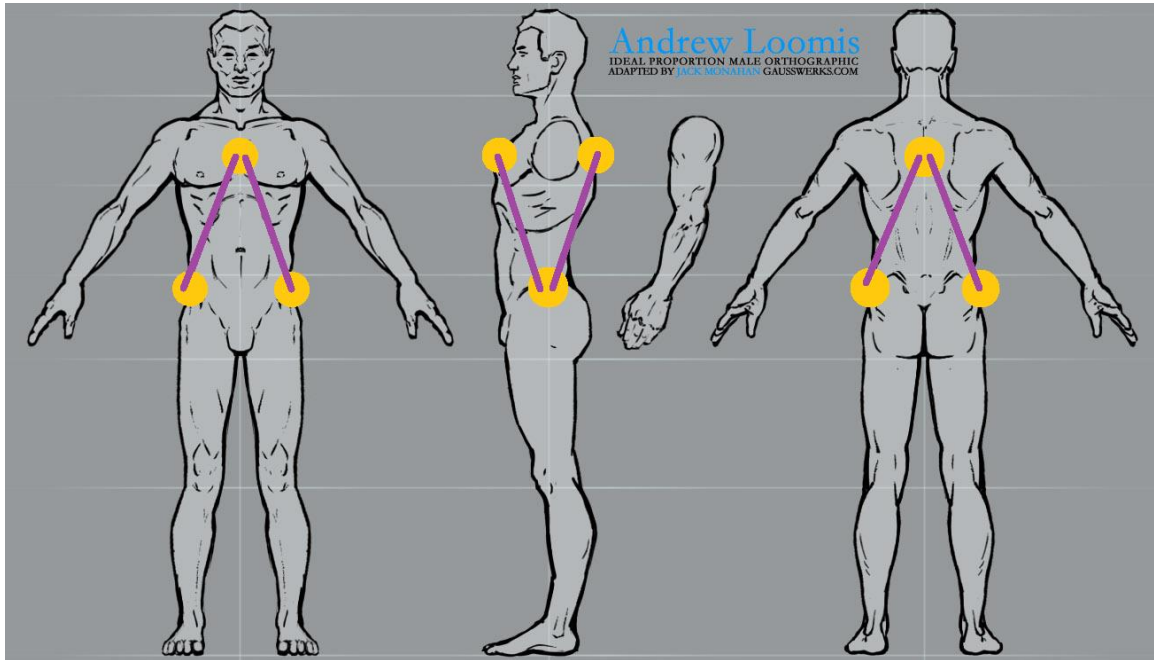


Figure 21. An alternative orientation of an array of strain sensors used to measure the degrees of freedom of the back (image edited from cec-animation.com).

The sternal anchoring location may not be stable connection for persons with large pectoral muscles or females, due to the way the participant's clothing may lay across their chest. Regardless, the arrangement depicted in (Figure 21) is not ideal because it requires sensors to span across the ventral side of the thorax. This may be problematic because this region is very dynamic and heavily involved in most physical activity. Running straps across this area leads to tangling and snagging risks that do not exist (or exist to a much lower extent) in the prior arrangement.

The concept of having sensors in the way during motion is troubling and leads to the ideas that 1) having a redundant sensor may not be an ideal arrangement, and 2) having

three to four sensors traveling diagonally across the thorax may not be practical (note, these issues have not yet been verified to exist and may not). There is an arrangement that can bypass these concerns, minimizing the potential obstruction of a wearer, as depicted in (Figure 22). Three sensors can be placed so that they run exclusively inferiorly and superiorly, with no medial/lateral slants (the anatomical equivalent of vertical). Two of these sensors would run from the superior iliac crests to the axillary regions described prior. The third sensor would begin at the sacrum and continue up the spine, anchoring anywhere from between the scapulae to the cervicothoracic junction. While this superior anchor may not be totally stable, it will mostly move in directions perpendicular to the directions of concern and at a magnitude that would most likely be negligible to acceptable compared to the overall length of the sensor array. If any tradeoffs exist between these arrangements, it will most likely be between wearer restrictions and pollution levels.

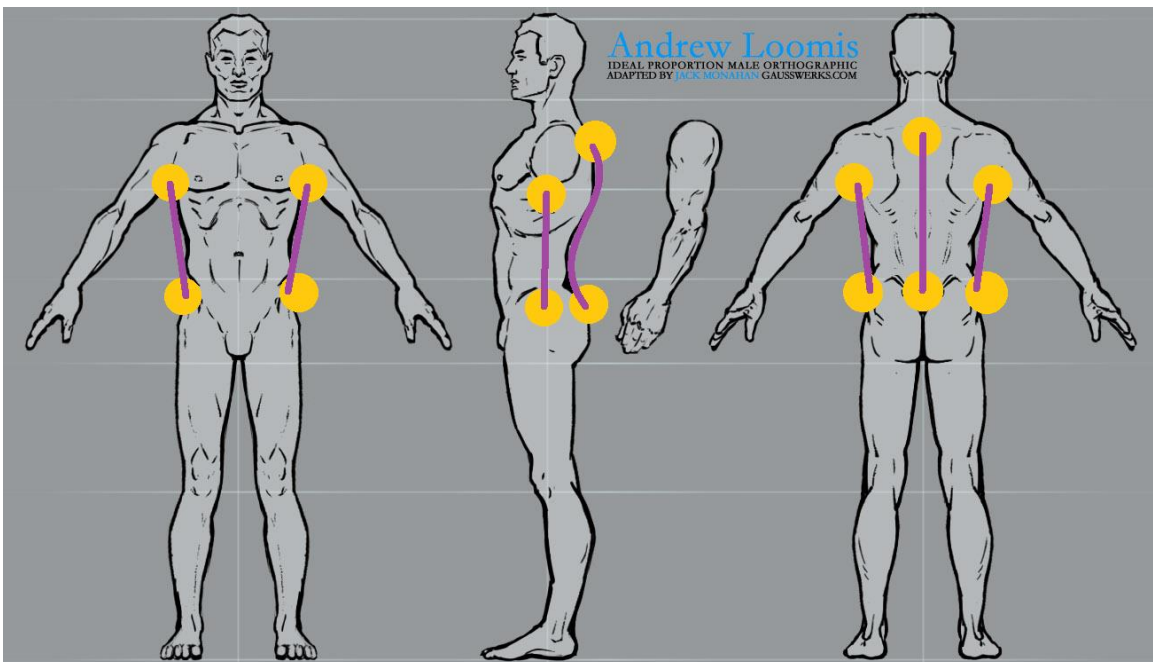


Figure 22. A three-sensor array of strain sensors used to measure the degrees of freedom of the back (image edited from cec-animation.com).

The mechanical arrangement has been sufficiently detailed, but there is no guarantee the data these arrangements record will be able to differentiate between the combination of a forward bend and a twist or a sideways bend and a twist. Until it is shown otherwise, this system has the potential to show the same combination of sensor readings for more than one position. The following charts showcase the possible motion combinations the sensor groups could experience via areas depicting either positive or negative sensor deformation.

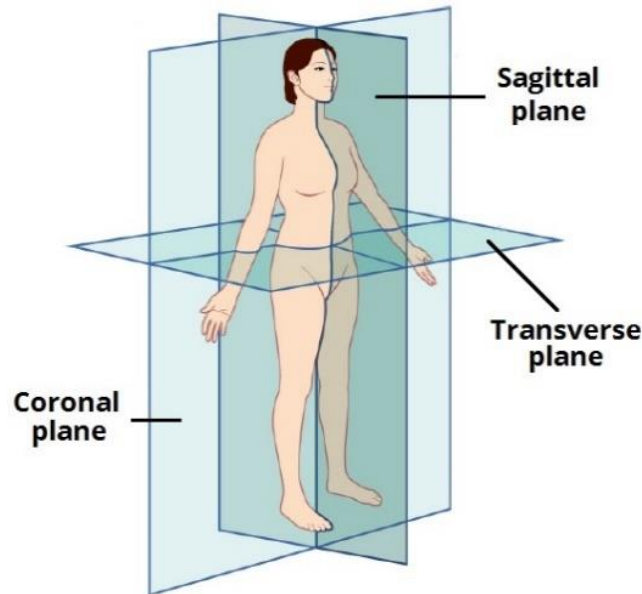


Figure 23. An image defining the anatomical planes (image from TeachMeAnatomy.info).

For reference, the Sagittal, Coronal, and Transverse planes will be used as references. A transverse slice of the torso will be taken. This slice could be anywhere between the anchor positions and the following analysis should hold true for any spot on the spine. Note, the sectors are divided into four to check the first two arrangements.

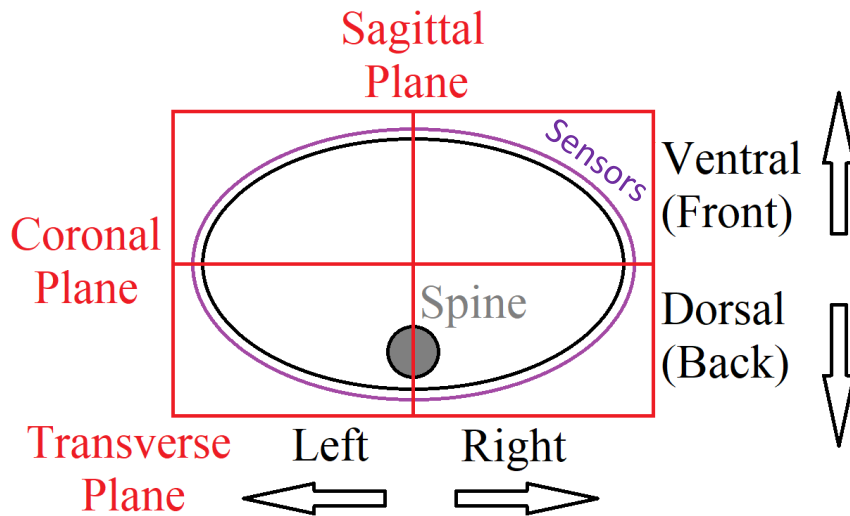


Figure 24. Transverse section of the torso. The spine (grey) is for directional reference.

The most basic motions being monitored are forward/backward bends, leftward/rightward bends, and clockwise/counterclockwise rotations.

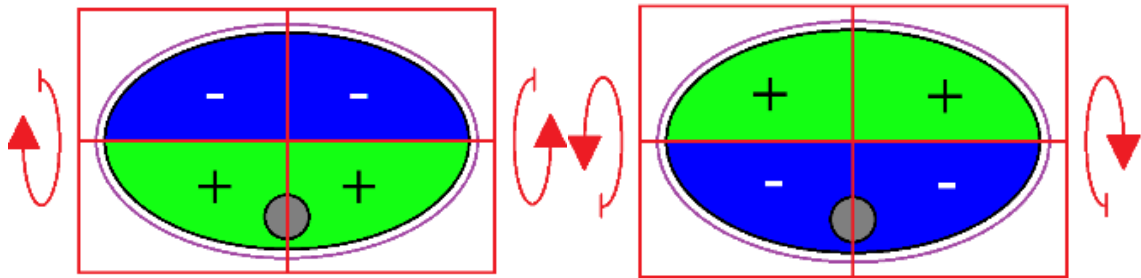


Figure 25. Sensor deformation corresponding to a forward (left) and backward (right) bend (green describes a strain sensor length increase; blue, decrease).

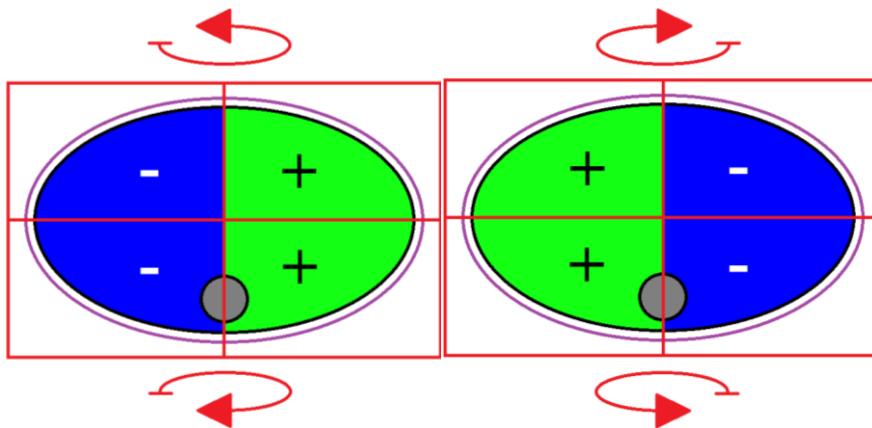


Figure 26. Sensor deformation corresponding to a leftward (left) and rightward (right) bend (green describes a strain sensor length increase; blue, decrease).

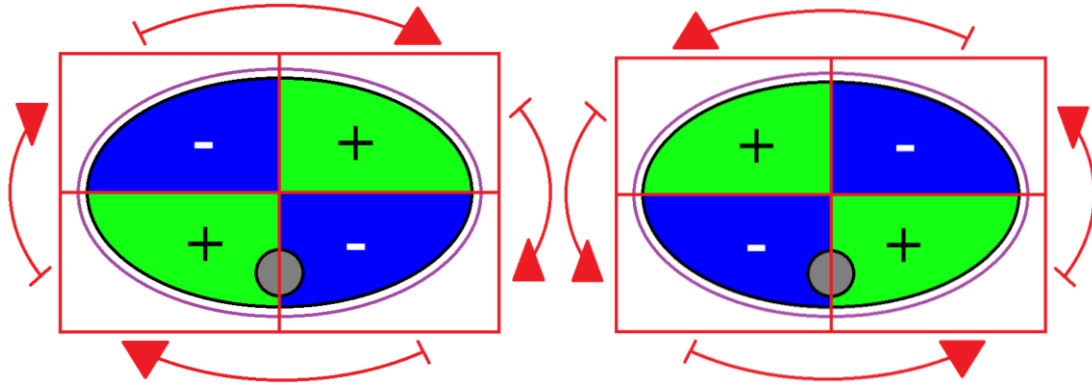


Figure 27. Sensor deformation corresponding to a clockwise (left) and counterclockwise (right) rotation (green describes a strain sensor length increase; blue, decrease).

Each motion, separately, makes a clearly unique combination of sensor strain patterns. Since the changes all have a unique combination of relationships around zero, it is impossible for this array to confuse one motion for another. However, the spine is in no way restricted to planar motions, and all the combinations of these motions must be checked as well.

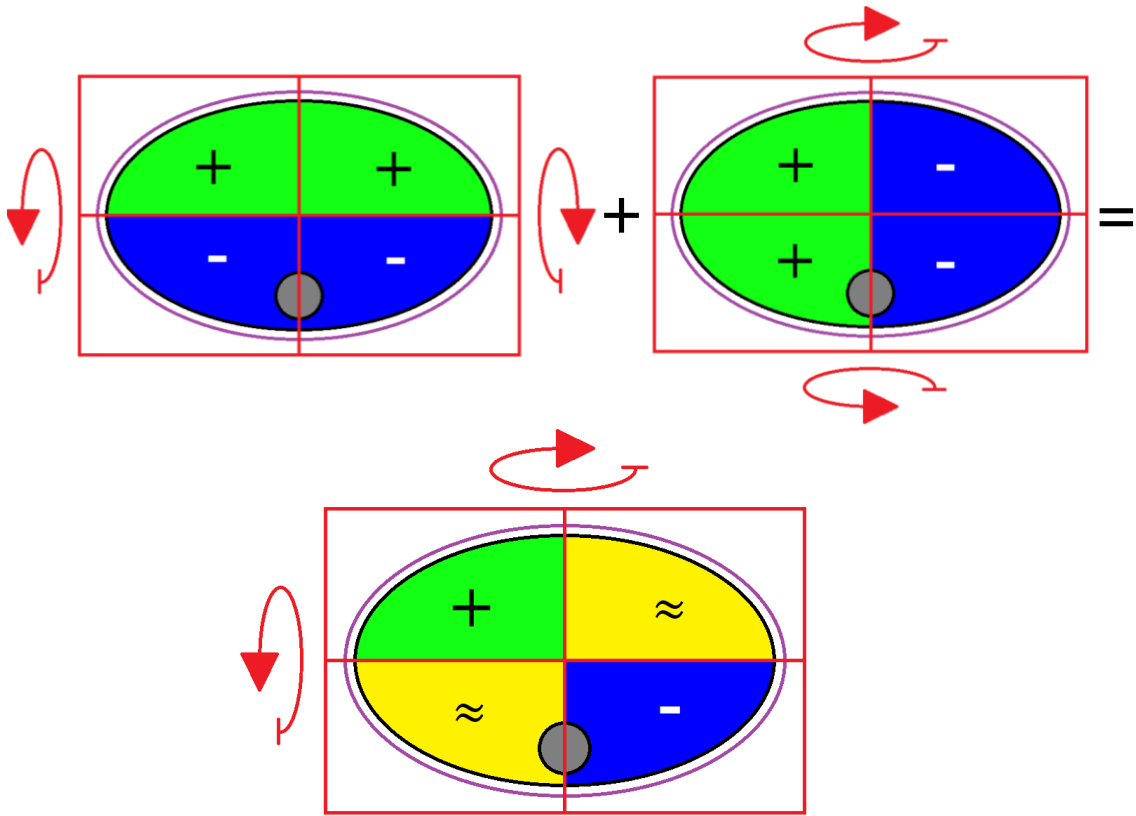


Figure 28. Resulting sensor deformation corresponding to a combine backward and rightward bend (green describes a strain sensor length increase; blue, decrease; yellow, combination of increase and decrease).

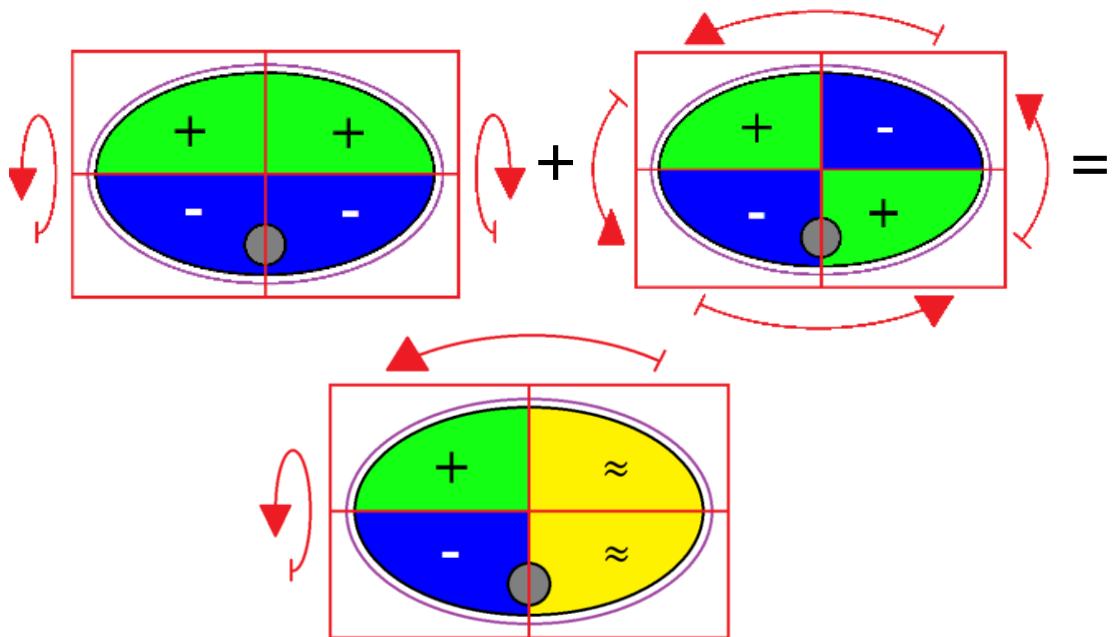


Figure 29. The resulting sensor deformation corresponding to a combine backward bend and counterclockwise rotation (green describes a strain increase; blue, decrease; yellow, combination of increase and decrease).

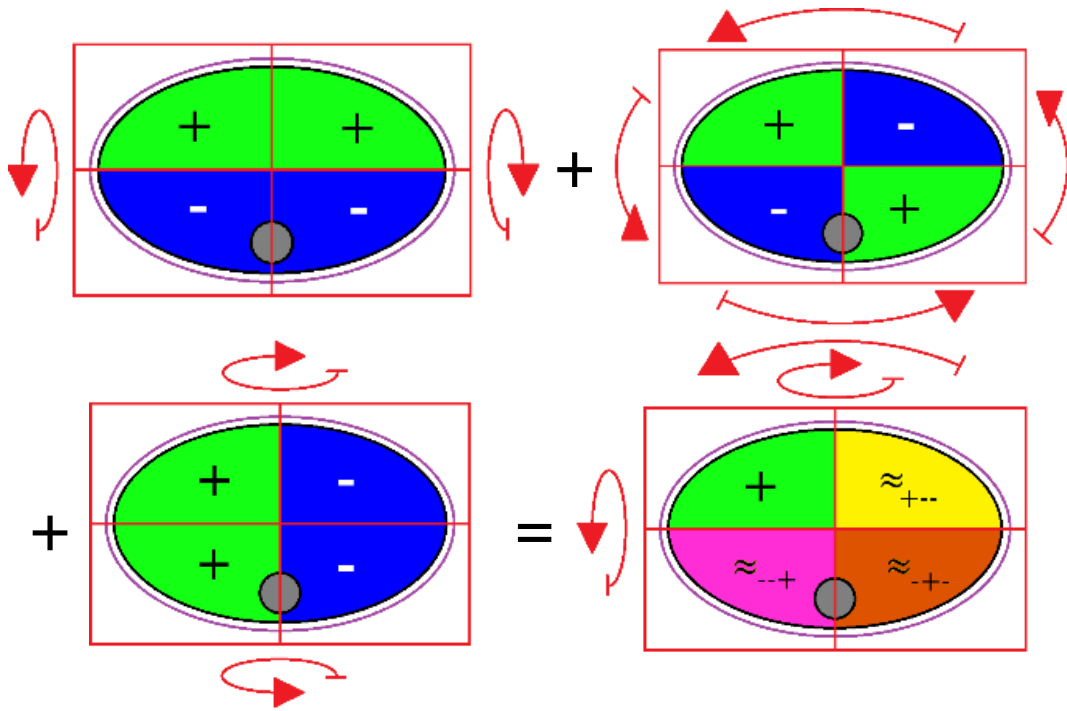


Figure 30. Resulting sensor deformation corresponding to a combine backward bend, counterclockwise rotation, and right bend (green describes a strain increase; blue, decrease; yellow, combination of increase and decrease; pink and orange are not equal in magnitude, but are related by their component motions).

These general variants of sensor response combinations are not similar and can uniquely define each set of movements, making this a valid tool to measure said motions with no reason to believe position confusion or swapping will occur. Inferring from the combination depicted in (Figure 30), it does not appear possible for three sensors to distinguish the difference between every position.

CHAPTER III

CALIBRATION METHOD

A. Introduction

As stated in MECHANICAL SYSTEM DESIGN C. Work Thus Far, the second project relating to this technology had a major impact on the understanding of the calibration needed to formulate a stable output of angular data. The fundamental flaw of this project's calibration was assuming the equations would be adequately described with either a linear or polynomial relationship of just one sensor's data. By making a generic equation without properly analyzing the physical arrangement of the sensors in relation to the desired measurement, the calibration method may not work well with the indirect measurements, like anatomical rotation. Additionally, because the skin is both a continuum and must move with the underlying structures, its net motion can be complex and influenced by multiple degrees of freedom from several joints. Not accounting for these factors was an oversight that was somewhat the product of the knee sensor being straight forward to work with. The knee's calibration equation was correctly formed into a linear relation to the sensor information. Because of the knee's large magnitude motions, the relatively small magnitude of the unfiltered crosstalk present in the output was assumed to

be random error. This calibration resulted in the belief that the hip rotation calibration equation should take a similar, linear or higher order polynomial form. This is believed to be the wrong approach. The geometry involved in the rotation sensor arrangement relates the sensor response to the limb motion via the Pythagorean Theorem, which a polynomial cannot replicate. It seems likely that the calibration equation will need to reflect this relation, too, to serve as a stable, general solution.

1) *Work Thus Far*: The initial set of calibration equations took the form of a first order, linear equality to check the validity of the simplest calibration option:

$$\theta_{Knee} = a_1 + b_1 x_{Knee} \quad (1)$$

$$\theta_{HipRotation} = a_2 + b_2 x_{HipRotation} \quad (2)$$

These equations were derived by Katherine Florek [28] (a_1 , a_2 , b_1 , & b_2 are arbitrary constants and x is the corresponding sensor data).

The results of a calibration system that only included data from the primary sensor monitoring the joint resulted in an RMS error, compared to a MoTek visual motion capture system, for knee flexion/extension of 6.50° in a range of about 90° and an RMS error for hip internal/external rotation of 4.05° in a range of about 8° . The first order knee calibration yielded a very representative picture of the visual systems data, while the corresponding hip rotation calibration produces a poor representation of the visual systems data [28].

An isolated, single input calibration was quickly understood to be insufficient for hip rotation. The hypothesis is the sensors measure skin motion, not skeletal, making their measurements susceptible to any motions that move the area of skin they anchor to. This

would imply the knee's flexing and extending is leaving a mark on the data collected from the rotation sensor, probably coming from the anchoring position nearest the knee joint. To counter this, an additional set of terms was added to the calibration filter to eliminate this crosstalk. This filtering of crosstalk was also done to the knee, too, to determine if similar crosstalk was present. Additionally, the order of the calibration equations was increased to include a factor with both sensors' inputs. The resulting equation took the form of a two-variable, quadratic formula:

$$\theta_{Knee} = a_1 + b_1x_{Knee} + c_1x_{HipRotation} + d_1x_{Knee}^2 + e_1x_2^2 + f_1x_{Knee}x_{HipRotation} \quad (3)$$

$$\theta_{HipRotation} = a_2 + b_2x_{knee} + c_2x_{HipRotation} + d_2x_{knee}^2 + e_2x_2^2 + f_2x_{knee}x_{HipRotation} \quad (4)$$

These equations were derived by Katherine Florek [28] ($a_1, a_2, b_1, b_2, c_1, c_2, e_1, e_2, f_1, \& f_2$ are arbitrary constants and x is the corresponding sensor data).

The results of this calibration were an RMS error for knee flexion/extension of 2.67° in a range of about 90° and an RMS error for hip internal/external rotation of 1.01° in a range of about 8° [28]. It should be noted the data being shown from both calibrations was done with the same set of data. The resulting improvement from the rotation sensor was robust, indicating the improvement was due to the crosstalk. However robust the improvements, an error of 1.01° in a range of 8° is a significant percent. While it is clear this method improved the system's accuracy, further improvement was desired. What was unexpected was the near 2.5 factor improvement to the knee, indicating that the rotational motion of the hip plays a role in the topical motions of the knee. This information implies that accurate monitoring of the knee requires monitoring hip rotation as well, and vice versa, and therefore monitoring one motion in isolation is most likely a flawed approach.

The conclusion of this work was each sensors' data played a vital role in improving the other's accuracy and precision. The resulting knee monitor has an RMS error just below 3%, but the rotation sensor still had 12.5% error. This may be due to residual motion pollution. If the logic of this crosstalk is correct, it is important to note the hip is not a one degree of freedom joint. The rotation sensor's moderate accuracy improvement may be because there are two degrees of freedom being ignored from the hip that are causing the resulting errors. Additionally, if this crosstalk is responsible for error in rotation monitoring, it may also be negatively impacting the knee monitor, too.

2) *Analyzing the Mechanical System*: The fundamental issue in the previous project related to this system was not forming the calibration equations after gaining a physical understanding of the sensor arrangement relative to the monitored motions. In fact, the value of this project is that it highlights the impact the physical arrangement of the sensors can have on the calibration models and the need for sensor correlation with information from all kinematically relevant degrees of freedom to the measurements of that sensor. These issues led to the desire for two completely opposite calibration concepts: a calibration that requires a total, physical analysis of the sensor arrangements, and a calibration that replaces the need for human understanding with computer driven pattern recognition and output correlation.

B. Method Concepts

As stated prior, the calibration of this sensor array can be approached with two main approaches: it can be based on the geometric relationships the sensor's deformations share with the relevant body motions, or it can be based on training a program to relate a combination of inputs to desired outputs via machine learning techniques. The former

results in specific equations that can use physical measurements and motion sets to calibrate but requires a highly accurate mathematical model of the system, while the latter creates a specific relation between the range of inputs and outputs used in the training using no model and does not allow for much flexibility for untrained variables. The two methods are philosophical opposites, both offering specific strengths and weaknesses. This duality offers the opportunity to test the geometric model's validity. Assuming both methods have been constructed properly, any consistent differences between the two values would describe failures in one of the method's implementation. If pollution, crosstalk, etc., exists in a way that is not accounted for in the model, then the trained calibration should consistently be the more accurate of the two methods. If the opposite is true, then the trained calibration would most likely be either overfit or underfit. If the both methods are implemented successfully, the difference between the two methods' results should be random and small.

1) *Geometric Calibration*: A geometric calibration requires knowledge of the arrangement and, if derived correctly, would produce a theoretically correct model of the sensors' relationship to the monitored motions. The benefits of this type of modelling are the equations' abilities to describe the entire range of motions involved, without requiring extensive reference data; and the equations can be calibrated by taking physical measurements from the system and participant once applied. Since the equations are continuous, no interpolation is needed, making the resolution limit of this calibration directly proportional to the resolution of the sensors. Some coefficients in this type of equation have physical meaning that can be measured and input. This allows for full or partial calibration, without having to rely on objective function minimization calculations.

Conversely, a system can be calibrated to its user and the coefficients can reveal important information about the participant, such as height or limb length.

However, these equations are susceptible to influences not accounted for in their geometric models (recurring or otherwise), like flexing of muscles under the sensor's pathway or external impact to the sensor, which would result in errors. This method is also problematic because of its need for consistent setup; if the sensors are not placed in the same place consistently or if their placement shifts during use, the calibration will suffer greatly. To counteract these potential inconsistencies as much as possible, the sensors would need to be located over stable areas on the body, the sensors would need to be placed in areas which have little motion relative to the skin that are easy to identify, and/or the calibration coefficients would need to be modified to the point where they may lose their physical significance- potentially reducing insight into the participant's physical properties.

2) *Gaussian Process Regression*: The gaussian process regression (GPR) is a machine learning technique which requires no initial information of the phenomenon being modeled [32]. This is a very similar quality to neural networks. The main, functional difference in these two methods is the neural network develops a linear equation that is very quick at processing large quantities of data quickly, while the GPR uses linear algebra, which is limited in computational speed relative to the size of the data matrix it needs transform (larger matrix sizes lead to longer computational times) [32]. As a result of the neural networks simplicity, the construction of the neural network is much more important and requires knowledge of the phenomenon being monitored and how that related to the math involved [33], whereas the GPR has a more robust

construction, which needs little to no modification. The GPR is a more robust, reliable solution and is practical when the size of the data being analyzed is small enough to be time effective.

This method is very effective when the fit is appropriate. However, GPR models are susceptible to poor fits. A poor fit is the description of a GPR model which does not reflect the general trend of the data being trained on. There are two types of this poor fitting: underfit and overfit. Underfitting is the method's tendency to not reflect the trends of the training data enough, leading to a loss of insight into the relationship at work. Overfitting is the method's tendency to not only adhere to the trends of the training data but also the random errors. This issue obscures the trend of the training data and can create a false relationship. The quality of fit dictates the usefulness of the GPR model and needs to be checked against the training data to verify the representative nature of the model. The fit can be modified by altering the length and vertical parameters [32].

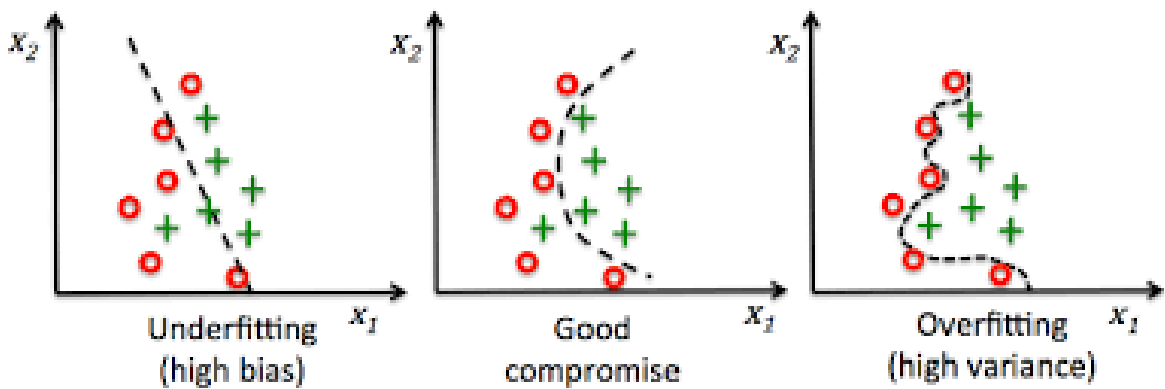


Figure 31. An example of correct (middle) and incorrect (outer left and right) fit possibilities of machine learning-based trendlines. (Pictures from BogoToBogo.com).

Another issue with this method is it offers no insight into the phenomenon it models. While this is often considered a strength, it is also an obstacle because it requires the model to be recalibrated from scratch for each new situation. This makes the GPR model better for statically setup applications and worse for setups which have inherent variation.

3) *Method Comparison*: An ideal system can be perfectly described with geometric equations, but real systems may be difficult or impossible to calibrate this way and would be better served by non-model-based methods. Both methods will be used to create a generalized calibration for each type of sensor, then the resulting calibrations will be compared to a) the corresponding motion data from a passive, visual motion capture system, which will be considered the correct data (this method is the current industry gold standard) and b) each other. The difference between the geometric equation and the neural network will signify either motion contributors are missing from the geometric models or the GPR is improperly fit to the calibration set. The difference between the better of the two methods and the visual system's data will signify the prototype's inability to properly measure the motions being monitored due to the physical system's construction.

C. Method Theory

The construction of the calibration involves putting the principles behind the desired concept and implementing in a practical way to make a filter. Because the signal being analyzed is digital, the output is also digital, and digital filters require less resources to build than hardware filters, the prototype filter will be digital. The benefits of a digital filter are their simplicity to adjust, their ability to be repurposed at no material or machining costs and usually with a much smaller lead time. An issue with digital filters is they take time to process data, causing a lag between an event and its corresponding data output. This leads to data that is not truly live but is approximated as such if the lag time is less than the sampling time. Digital filters can also experience glitches and consume a notable amount of power. The instability and power draw tend to go up with the complexity of the filter. A physical filter is opposite in these regards. They are stable, passive to low energy

draw, and can offer a live feed. They cannot be adjusted substantially, if at all, however. In short, digital filters are great for development and prototyping, but a hardware filter is far more practical mass-produced solution.

1) *Flexion Sensor Geometry*: The geometric equation for the flexion sensor is a straightforward relation, based on equating the deformation of the sensor to the change in arclength around the joint center. The sensor should directly measure this entire change, so the calibration equation needs to convert the sensor output from percent elongation to arclength change to change in flexion angle.

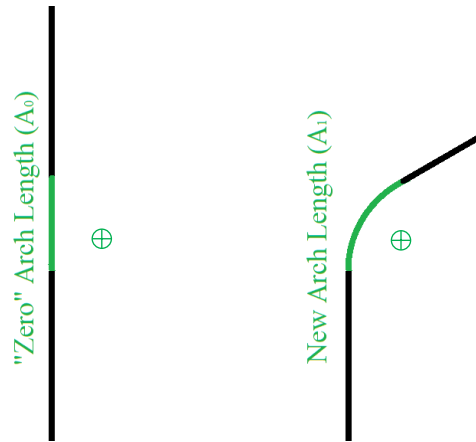


Figure 32. The geometric model of the flexion sensor arrangement. The green area represents the area of skin around the joint that displays significant motion relative to the long bones that make up the joint, while the black areas are comparatively static. Note this makes anatomical flexion/extension a direct measurement.

$$A_1 - A_2 = \Delta A = C_1 \Delta S \quad (5)$$

where:

ΔS = Change in Sensor Signal

ΔA = Change in Arclength of the Joint

C_1 = Constant Converting Percent Strain to Arclength (Scaling Factor)

and:

$$\Delta\theta = \frac{\Delta A}{R} = C_2 C_1 \Delta S \quad (6)$$

where:

$\Delta\theta$ = Change in Joint Angle

R = Radius

C_2 = Constant Converting Arclength to Angle (Inverse Radius)

Both transformations are performed by multiplying the sensor data by constants. Since the change in arclength of a joint is not necessary information and no significant insight is gained by knowing the associated constants, these two transformations and their constants can be combined into one step.

$$\Delta\theta = C_3 \Delta S \quad (7)$$

where:

C_3 = Constant

or:

$$\theta_a = C_3 S_i + C_3 S_0 = C_3 S_i + \theta_0 \quad (8)$$

where:

θ_a = Measured Angle Relative to Anatomical Resting Position

θ_0 = Initial Angle Relative to Anatomical Resting Position

S_i = Measured Angle Sensor Response to Anatomical Resting Position

S_0 = Initial Sensor Response Relative to Anatomical Resting Position

so:

$$\theta_a = C_3 S_i + C_4 \quad (9)$$

where:

C_4 = Constant Signifying the Zeroing Term

While this may vary with application, the value of θ_0 will most likely correspond to setting the zero at resting or anatomical position of the joint. This resulting equation is equivalent to equation 1. Now that the working principle of the flexion sensor has been highlighted, it is both appropriate and necessary to define what a flexion sensor is:

***Flexion sensor:** a non-rigid, strain- or deformation-based sensor that is attached to opposite rigid bodies surrounding a joint, which originates the flexion/extension motion.*

This definition is useful because it establishes a guideline for the development of the calibration. The physical constraints are important- so much so that anything not following those outlined cannot be functionally considered a flexion sensor due to the loss of sensor response and added pollution. The sensor response is important to capture fully because this type of motion is typically large compared to its pollutants, making their effect less influential on the resulting measurement. When less of the motion is captured, pollutant contributions become proportionally more significant, making the sensor arrangement less effective.

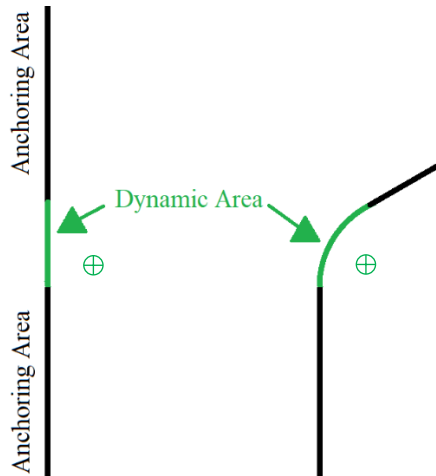


Figure 33. The dynamic area is not the only source of pollution, but it must be encompassed by the anchors to fully capture the magnitude of the joint motion. While it is not shown in this nor the previous figure, other dynamic areas will exist around the joint due to muscles flexing/relaxing and excess skin motions cause by nearby joint motions.

2) *Rotation Sensor Geometry:* The geometric equation for the rotation sensor is less direct than the flexion sensor but is still based on relating the physical deformation of the sensor to the arclength change caused by the motion it monitors. In modeling of the thigh's shape, a common assumption is it can be simplified to a cylinder [34]- partly to help make the model easier, partly to act as a mean value of the shape an active thigh takes.

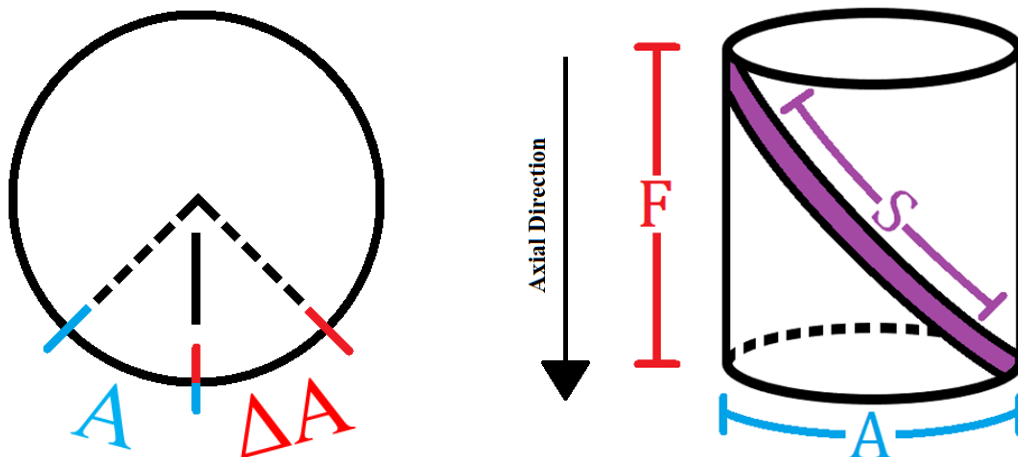


Figure 34. The geometric model of a rotation sensor arrangement on the thigh, relating arclength changes due to internal/external rotation (left) in the cross section to the sensor arrangement on the surface of the thigh. Note that this arrangement makes anatomical rotation an indirect measurement.

However, a three-dimensional shape is more complex to work with than a two-dimensional model. Since the only part of the cylinder that is of concern is the surface, using the assumption the sensor will not be lifted away from or buried into the surface of the thigh, the cylinder can be “unrolled” into a two-dimensional plane. This assumption becomes more reflective of reality by using totally non-rigid sensors, by reducing the mass of the sensor arrangement as much as possible, and by securing the sensor to the surface of the solid body with a sheath or belt loops that follow its path. These additions aid the assumption by reducing the likelihood of the sensor oscillating independent of the solid body by either making it less susceptible to high impulses or by securing it to the body.

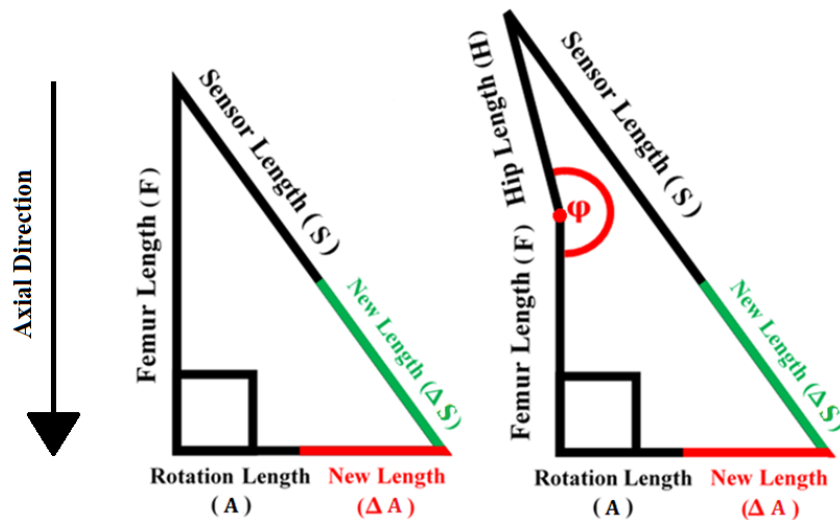


Figure 35. A planar model of a correct, single rigid body, rotation sensor arrangement (left) with one known (green) and one unknown (red), compared to the multiple unknowns that develop from multiple rigid bodies (right) (The hip is used as an example).

The most vital principle of the rotation sensor to understand is the sensor is measuring the change in a hypotenuse of a right triangle that is partly composed of the arclength that needs to be monitored. When one side of this triangle staying constant, the other’s length change can be measured because it is the only unknown side of the triangle. This relation allows for a very basic trigonometric relation between the sensor

data and this arclength change. Because of this relationship, the accuracy of this sensor arrangement is more sensitive to anchoring locations than the flexion sensor since it is vital the sensor be anchored only to the rigid body it is measuring.

This restriction should appear counter-intuitive; measuring the rotation of a rigid body with no external reference shouldn't be possible. This is where the topical nature of this sensor arrangement needs to be understood to create a successful system of strain sensor-based motion capture. Because the attachments are connecting to the skin and not the bone, the sensor is monitoring the motion of the skin. The skin, if healthy, is a continuum that bridges joints throughout their entire range of motion. When skin on a rotating body needs to maintain its connection with non-rotating skin, the topical motion will form a gradient close to the joint, approaching no rotation at the joint location. This phenomenon creates specific areas of skin that can be a rotational reference point that is always a fixed axial distance from the distal attachment. While this point is very mechanical, it is an essential concept for developing both an arrangement and a calibration for this type of sensor. With that highlighted, it is now appropriate to define what a rotation sensor is:

Rotation sensor: *a non-rigid, strain- or deformation-based sensor that is attached in two locations on the axially rigid body originating the rotation. It must be attached close to the proximal location (the origin of the motion) and at a distal location on the same axially rigid body, that balances maximizing the magnitude of sensor response to the motion and minimizing the magnitude of sensor response to pollutants.*

While crossing the rigid body is not necessary, it may offer a magnifying effect to the motion being observed. If this is neglected, the signal change could be too small to robustly define anatomical rotation, but the calibration principles and trigonometric relationships will be the same, regardless. The geometric relation will follow the Pythagorean Theorem:

$$(C \times S + H)^2 = A^2 + F^2 \quad (10)$$

where:

S = Percent Sensor Length including strain

C = Constant transforming Percent Strain to a Length, Also Sensor's Original Length

H = Hypotenuse Length, Minus Sensor Length, which is Constant

F = Axial (Femur) Offset Length = Constant

A = Arclength = L×θ

L = Arc Radius

θ = Internal/External Rotation Angle

Now the relation must be rearranged to solve for the arclength, which corresponds to the displacement caused by anatomical rotation.

$$A^2 = C_c(S + \varepsilon)^2 - F^2 \quad (11)$$

where:

$C_c = C^2$

$\varepsilon = H/C$

or

$$A = L \times \theta = \sqrt{C_c(S + \varepsilon)^2 - F^2} \quad (12)$$

Since the desired output is rotation, both sides need to be divided by constant L.

$$\theta = \frac{\sqrt{C_c(S + \varepsilon)^2 - F^2}}{L} \quad (13)$$

The change in angle from a reference position is much more valuable, so the equation must be amended to conform.

$$\Delta\theta = \frac{\sqrt{C_c(S_i + \varepsilon)^2 - F^2}}{L} - \frac{\sqrt{H^2 - F^2}}{L} = \frac{\sqrt{C_c(S_i + \varepsilon)^2 - C_1}}{C_2} - \frac{\sqrt{C_c(S_0 + \varepsilon)^2 - C_1}}{C_2} \quad (14)$$

where:

$$C_2 = L$$

$$C_1 = F^2$$

S_i = Measured Angle Sensor Response to Anatomical Resting Position

S_0 = Initial Sensor Response Relative to Anatomical Resting Position

or:

$$\Delta\theta = \frac{C_c(\sqrt{(S_i + C_a)^2 - C_b} - \sqrt{(S_0 + C_a)^2 - C_b})}{C_2} = C_{c2}(\sqrt{(S_i + C_a)^2 - C_b} - C_0) \quad (15)$$

where:

$$C_a = \varepsilon$$

$$C_b = \frac{C_1}{C_c}$$

$$C_{c2} = \frac{C_c}{C_2}$$

$$C_0 = \sqrt{(S_0 + C_a)^2 - C_b}$$

and:

$$\Delta\theta = C_{c2}(\sqrt{(S_i + C_a)^2 - C_b}) - C_{c1} \quad (16)$$

where:

$$C_{c1} = C_{c2}C_0$$

or:

$$\theta_a = C_{c2}(\sqrt{(S_i + C_a)^2 - C_b}) - C_{c1} - \theta_0 = C_{c2}(\sqrt{(S_i + C_a)^2 - C_b}) - C_{c3} \quad (17)$$

where:

θ_a = Measured Angle Relative to Anatomical Resting Position

θ_0 = Initial Angle Relative to Anatomical Resting Position

$$C_{c3} = C_{c1} - \theta_0$$

leaving:

$$\theta_a = C_{c2}\sqrt{(S_i + C_a)^2 - C_b} - C_{c3} \quad (18)$$

where:

$$C_a = \varepsilon = \frac{H}{C}$$

$$C_b = \frac{F^2}{C^2}$$

$$C_{c2} = \frac{C^2}{L}$$

$$C_{c3} = \frac{\sqrt{(C \times S_0 + H)^2 - F^2}}{L} - \theta_0$$

These relations are important because H, F, L, and C are physical measurements, H is the distance between the proximal and distal sensor attachments, F is the axial displacement between the proximal and distal sensor attachments minus the sensor length, L is the average radial offset between the distal attachment and the axis of rotation, and C is the unstrained length of the sensor. S_0 is the reading of the sensor at the anatomical resting position, which can be obtained and used to calculate the length of the sensor, C, or the sensor can be manually measured at this position. This highlights the advantage of the geometric mode; all of the constants in the calibration equation can be measured/set, without the assistance of computational power.

3) *Gaussian Process Regression*: The theory behind the gaussian process regression will not be implemented in this work, directly, because the MatLab GPR toolbox will be used. However, the theory will be presented so as to not treat this function as a black box. A gaussian process regression is a tool that can take any finite vector of inputs and outputs, which are related through some function, with a gaussian distribution and generates a regression model by referencing a test data set. The GPR is constructed with kernels known as covariance matrices [32]. There are two types of this used, the first being the covariance of training input verses training inputs.

$$K(X_i, X_j) = p_1 e^{-\frac{(x_i - x_j)^T (x_i - x_j)}{2p_2^2}} \quad (19)$$

where:

$K()$ = Covariance Matrix

X = Training Input Matrix

p_1 = Vertical Scale Constant

p_2 = Length Scale Constant

Each point of the training input is compared to the rest, establishing the relationship of each point to the resulting model. The same is then done for similar reasons to the testing or query points, which is called the covariance of testing inputs verses training inputs.

$$K(Y_i, X_j) = p_1 e^{-\frac{(Y_i - X_j)^T (Y_i - X_j)}{2p_2^2}} \quad (20)$$

where:

Y = Testing Input Matrix (Query Points)

The length and vertical scaling constants dictate the fit of the GPR model. If the model is overfit, p_2 is too small and needs to be increased. The same logic applies to underfitting, where p_2 is too large and needs to be decreased. If the model is poorly scaled, p_1 must be changed in a similar manor [32]. The construction of the GPR model involves both of these covariance matrices and the training data output. The GPR model combines these kernels with the testing outputs to generate the likely query points' outputs.

$$f(Y, X) = \frac{K(Y_i, X_j)}{(K(X_i, X_j) + \sigma^2 I)} \tau \quad (21)$$

where:

$f()$ = GPR Model

σ = Standard Deviation of the Data's Distribution

τ = Testing Output Matrix

I = Identity Matrix

The advantage of this method is most of the work is done through linear algebra. There are two free choices, which have distinct and robust effects on the model. MatLab automates the choosing of these factors, but they can be input manually. The disadvantage is when the testing or training matrices are large, the calculation of the model's outputs slows down. All equations in this section are from this source [32].

4) *Signal Crosstalk*: The concept of reticulated motion capture is to use the sensors information as a network, or a reticulation, rather than isolated measurements. This idea comes from the fact that most joint do not move purely in one direction and the ones that do are in close enough proximity to another joint where the skin overlaying it is affected by the activity from both. Because the sensors used in this motion capture system are essentially measuring the change in distance between two point of skin on the body, the compound skin motion from multiple joints or multiple joint directions is what is measured. To combat this crosstalk and isolate each joint contribution, the GPR model will be given multiple sensor data streams as inputs and factors to the geometric model will be added that also incorporate additional sensors into the calibration equations. However, details into these measures will not be given to protect the relations from emulation. Unlike other proprietary information in this report, this crosstalk elimination would not be sufficiently protected by a patent or copyright, and its specifics will be kept secret.

D. Programing

The sensors being used currently interface with a visual programming language known as LabVIEW. This program currently operates four sensors and outputs a text file, a 5-by-n matrix of time and four percent strain readings. To convert this data into the desired angular measurements, the text file will be read into MatLab and passed the data

through one of the calibration methods. This program will read the visual motion capture data, calibrate the range of motion portion of the strain sensor data to the visual data, filter the remaining strain sensor data through the calibrated equations, and plot both sets.

1) *Geometric Equation Code*: The main functionality of the geometric code will be to calibrate and compare the geometric- and crosstalk-based equations to the visual motion capture angular data. The visual motion capture system is considered the gold standard of accuracy in motion capture and will be considered correct, unless there are specific reasons not to trust this data (i.e. high amounts of noise, dramatic angle changes, impossible joint motions). The visual system's data is sampled at 100hz and is initially a series of x, y, and z coordinates that represent the positions of each marker observed, as well as containing time and force-plate data. These positions must be converted to angles to be useful for this application, so the data was processed before being imported into the calibration codes. This processing is highlighted in TESTING & DATA PROCESSING 1) Processing Visual Motion Capture Data. Before importing any data, the relevant files must be manually searched to identify any initial readings that are unstable or full of placeholders. Placeholders often exist in the strain sensor datasets, in the form of zeros. To eliminate these false readings, a set-specific amount of the beginning of the strain sensor data is excluded. The processed angular data is imported into the program. The force-plate data is also imported to determine the time of impact of the foot during walking gait. The trusted portion of the strain sensor data is loaded into the program as well, which was sampled at 10hz. Because these sets of data were collected via two separate systems, these datasets must be aligned in time. To do so, first, their initial time readings are set to zero and increase from that reference. Next, the calibration portion of the visual data and strain data

are plotted on the same graph versus time (the visual data was plotted in black and the strain data was plotted in red). These datasets will not be aligned, but by observing the similar features in each line, their RMS error (error being defined as the difference between the points of the two lines), and the time offset between them, alignment can be achieved within a few iterations.

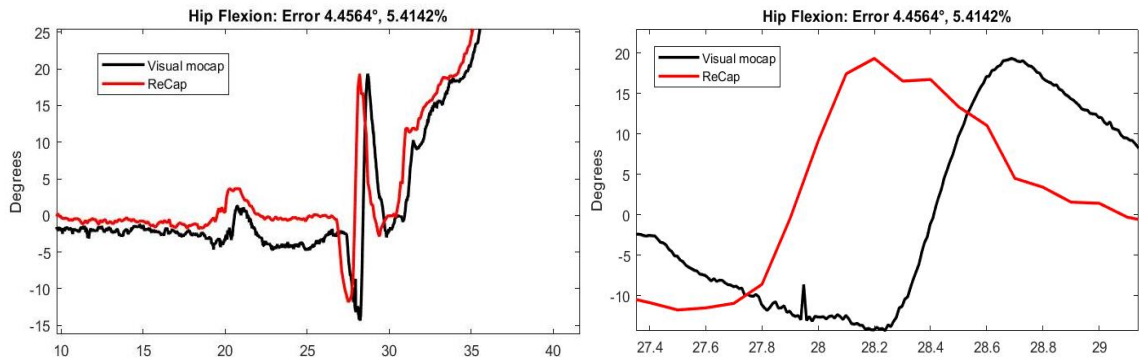


Figure 36. An example of unaligned visual (black) and strain (red) datasets. The offset can be estimated to be about 0.6 seconds. Because the visual data’s sampling rate is 0.01 seconds, the maximum resolution that makes sense is half that value, or 0.005 seconds. This limiting factor is important so that alignment is taken far enough, but not too far. For example, the offset was estimated to by 0.6 seconds. To make this value a final solution, it would need to be 0.600 seconds, meaning 0.595 and 0.605 seconds were shown to not lower the RMS error.

For the RMS error to be calculated, a point of data must exist at the same timestamp in each dataset. This cannot be counted upon to occur, so the optical motion capture data will be down sampled and interpolated to guarantee the alignment and minimize the loss of accuracy. Note, this must happen after alignment, yet alignment must be performed to interpolate correctly. What results is a few iterations of improperly aligned data being interpolated, compared, and plotted. This yields errors and plots that are not perfect accurate accounts of the datasets and their differences, but it is effective enough to highlight the general offset, which can be addressed with several iteration, rather than one. Once aligned and resampled, the data is ready to be calibrated.

A function, *Calibrator*(), was written to calibrate the sensor data from each of the four sensors to align with each of the four motions being monitored (hip flexion, hip abduction, hip rotation, and knee flexion). This function uses the equations 6 & **Error! Reference source not found.**, outlined in 1) Flexion Sensor Geometry and 2) Rotation Sensor Geometry. In addition, crosstalk factors are added to the ends of these equations to help eliminate contributions from other motions. Details about this crosstalk elimination will not be given to protect this method from discovery and exploitation by other interested groups, for the inevitable goal of this project is to aid in the creation of a marketable product. The nature of this crosstalk elimination may not be patentable, and if it is, similar but unprotected equations could be constructed as a work around. Because of this, the *Calibrator*() function used will be treated as a semi-black box and will not be included in this report, but it will be partially described. The equations are created using unknowns that act as placeholders for the calibration constants. This unsolved equation is then entered into an objective function that computes the total, absolute difference between the visual data and the equation-altered strain data. This objective function is then fed through MatLab's *fmincon*() function. The outputs of *Calibrator*() are the calibration constants, the strain angle data, and the RMS error between the visual and strain angles. Once the strain angles are calculated for the calibration portion of the data, they are plotted against the corresponding optical motion capture data.

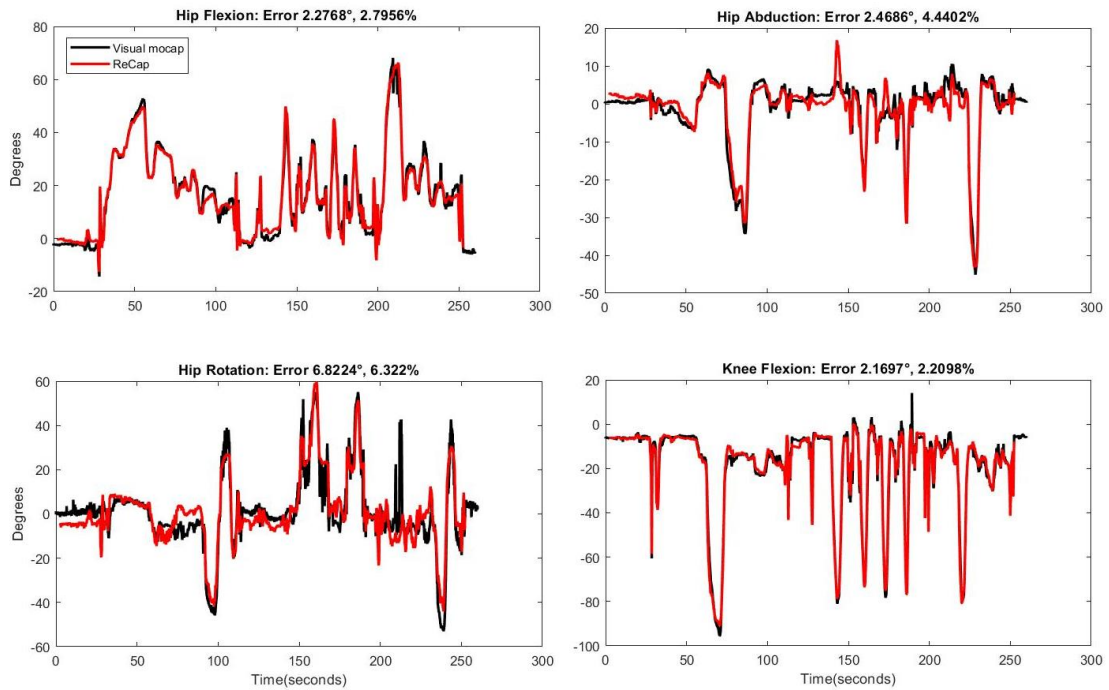


Figure 37. An example of a calibration data set plot.

The calibration constants and the remaining strain sensor data are then used as inputs to *Calibrator()*, and *Calibrator()* is set to be used as a calibrated filter, rather than a literal calibrator. The outputs are the filtered, strain angles. These angles are plotted against their visual counterparts in a series of way to analyze specific function of the calibration. First, the whole data set is plotted for each degree of freedom being monitored.

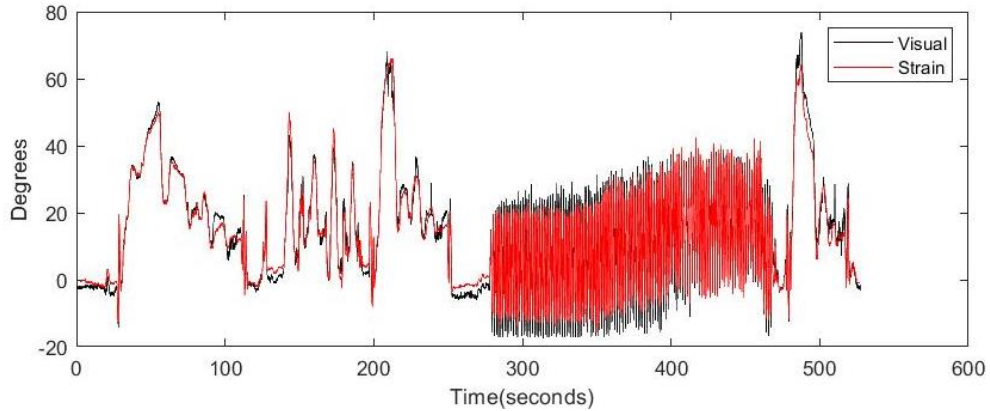


Figure 38. An example of a total hip flexion data set plot. In this data set, the time frame from 0 seconds to about 275 seconds corresponds to the section of data generated by the passive range of motion (ROM) and squat sets, which was used to calibrate the sensor models. From about 275 seconds to about 475 seconds corresponds to the data generated during the gait cycle test. After about 475 seconds, the data resembles the beginning section of the data because this corresponds to the second set of ROM and squat tests, which is used to check the calibration’s stability.

Then, the three walking trials are divided into separate gait plots with all the monitored degrees of freedom presented.

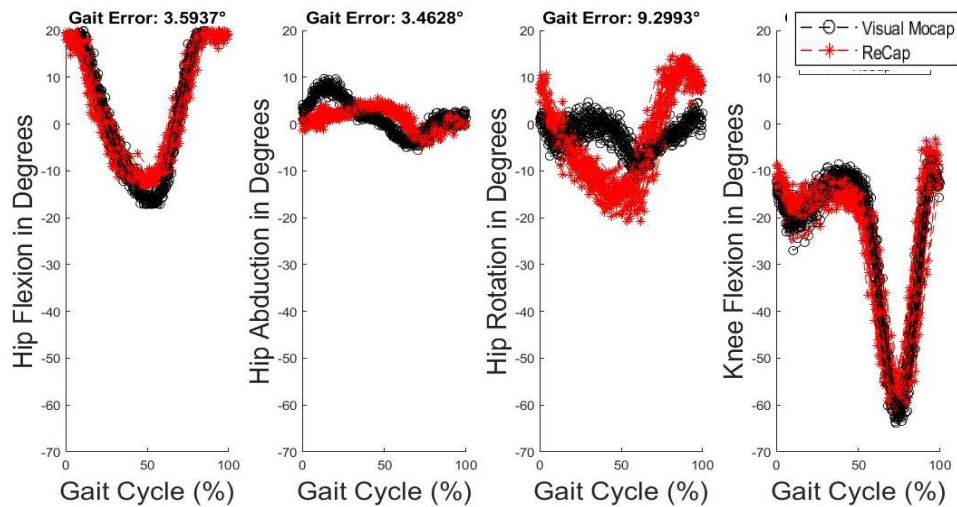


Figure 39. An example of the gait graphs. This example displays normal or toes-forward gait.

Finally, the last ROM test is plotted, along with that section’s error. This is done to check the stability of the calibration.

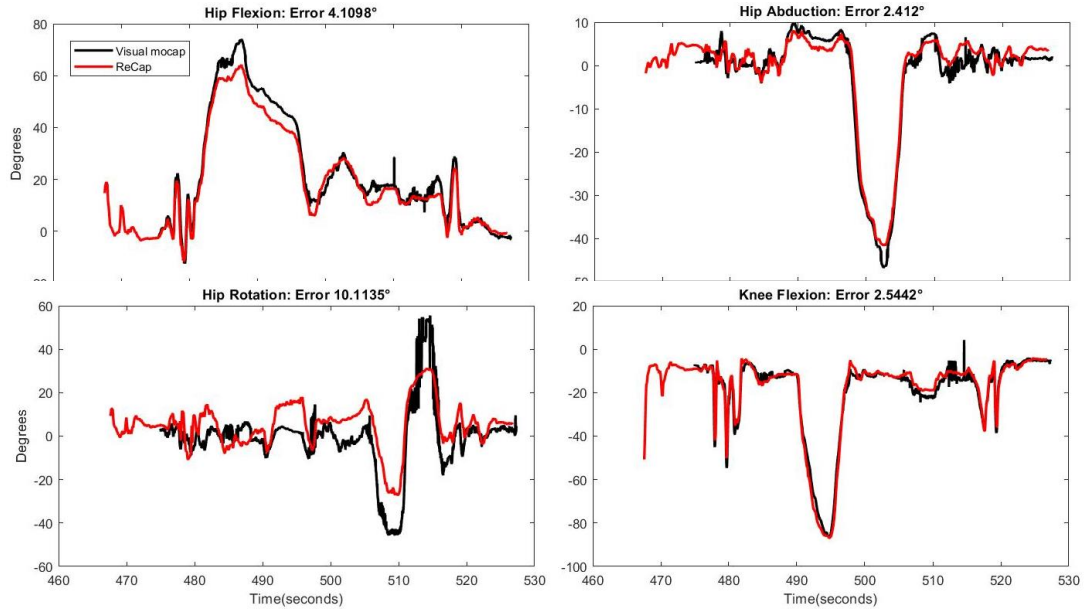


Figure 40. An example of a stability check plot.

2) *Gaussian Process Regression Code*: The gaussian process regression code's main functionality must be near identical to the geometric equation code to yield a meaningful comparison. The only major difference is instead of using *Calibrator*(), MatLab's built-in gaussian process regression functions, *fitrgp*() and *predict*(), are used in its place.

E. Future Work

The current work in creating and calibrating sensor arrangements is being performed on developing the arrangements that need the fewest sensors to operate. As a general rule, simpler is better. This is because each sensor adds error, uncertainty, and complexity to the arrangement. However, there may be circumstances where the simplest arrangements are impractical or incompatible with situations that need motion capture. To increase the flexibility of this system, multiple arrangements need to be available to measure the same motions. The most restricted motion so far is rotation, so the focus will

be to define two additional rotation sensor arrangements that will require more than one strain sensor. The first of these is similar to the rotation sensor being tested with the current prototype, except that it spans two solid bodies.

Combine Data Rotation sensor- a rotation sensor that has its proximal anchor located on a rigid body that is isolated from the rotational motion and uses corresponding joint sensor data to isolate the rotational motion.

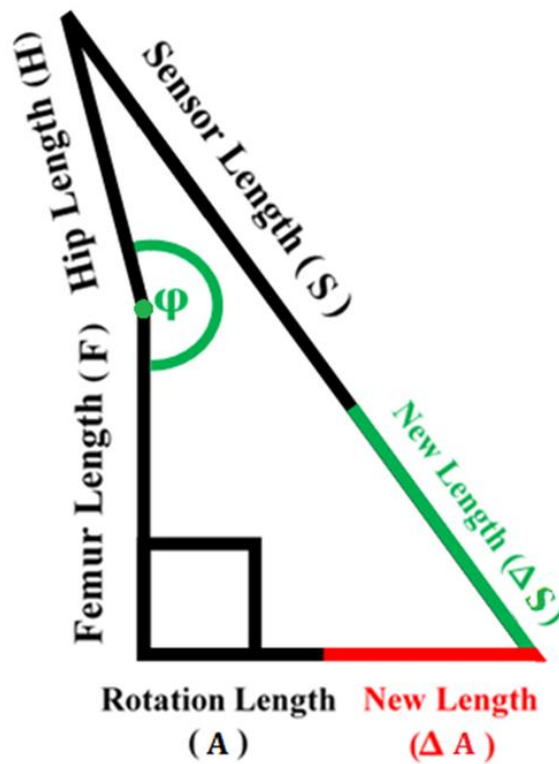


Figure 41. A planar model of a correct, multi-bodied rotation sensor setup with one unknown (red), which uses corresponding sensor data to determine variable angle ϕ (The hip is used as an example, meaning angle ϕ is a multi-dimensional vector).

The second arrangement does not touch the solid body producing the motion at all. This arrangement would only be useful at measuring rotation if there is only one body rotating axially between the two anchors.

Double Combine Data Rotation sensor- a combine rotation sensor that has its non-proximal anchor on a separate rigid body that is not isolated from the rotational motion being observed but from all others and then uses corresponding joint sensor data to isolate the rotation data.

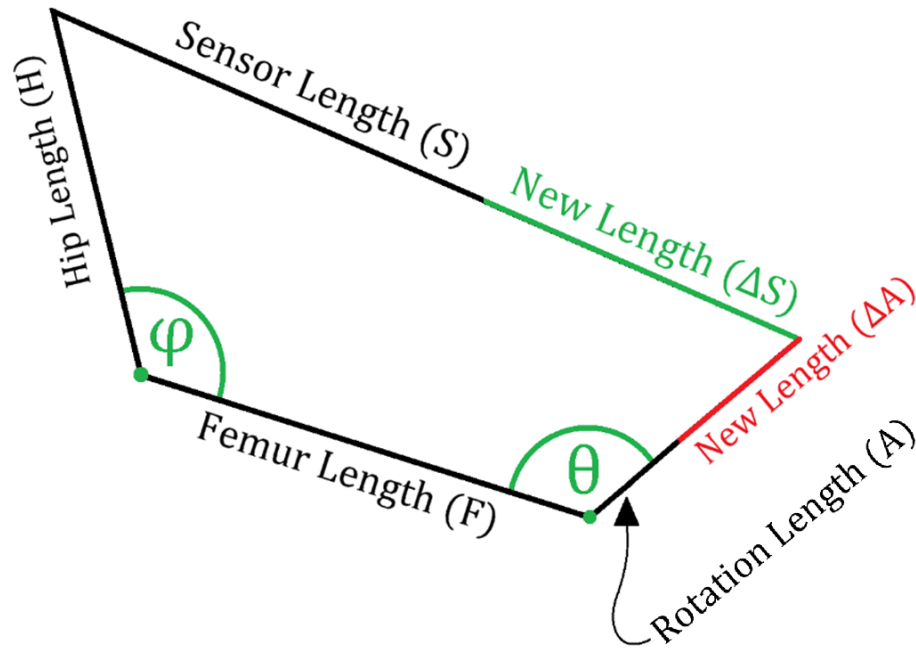


Figure 42. A planar model of a correct, multi-bodied rotation sensor setup with one unknown (red), which uses corresponding sensor data to determine variable angles φ and θ (The hip is used as an example, meaning angle φ is a multi-dimensional vector). Angle θ can have more than one degree of freedom, so long as none produce axial rotation.

The Combine Data Rotation (CDR) and Double Combine Data Rotation (2CDR) sensors' proximal anchors can be attached to more rigid areas that are isolated from the rotation, which do not necessarily need to be in a proximal location (the naming will stay the same to highlight that these anchors are attached to a reference that exhibits little to no motion, much like the flexion and rotation sensors' proximal anchors). The 2CDR has the benefit of magnifying the rotational data by anchoring further away from the origin, while also not contacting nor restricting the rigid body being observed. A benefit of these arrangements is the increased choices in anchoring positions, many of which are far from

the origin of the joint motion, which may reduce pollution or crosstalk. The drawback to both is they rely more heavily on other sensors' data, adding to their uncertainty, increasing their potential error, and making their calibration more complex. These sensor variants offer several choices to measure the same value, offering system flexibility and customization for specific applications and constraints. The accuracy differences between the rotation, CDR, and 2CDR sensors will be determined in future works.

CHAPTER IV

TESTING & DATA PROCESSING

A. Protocol Planning

The initial testing concept will be based around standard range of motion (RoM) test exercises. These exercises are being chosen to test knee flexion & extension, hip internal & external rotation, hip flexion & extension, and hip adduction & abduction because these are the corresponding bodily motions being monitored by this version of the reticulated prototype. Ankles are not currently being monitored because they are far from other joints and the skin overlaying them is assumed to be isolated from motions developed by the knees and hip. If residual error persists, the ankle will be monitored first to test if this assumption is incorrect.

The RoM tests are standard tools used in the physical therapy and health science fields. In the world of engineering, RoM can usually be summed up by the minimal amount of motion needed to interact with a computer station or work bench, so to accurately describe and test these ranges, a member of the physical therapy field was asked to assist in the selection, modification, and implementation of these tests. Michael Hanson is a doctoral student in Cleveland State University's Physical Therapy Department, who has

helped formulate similar test protocols in previous projects on this topic. His familiarity with these tests and this project makes him an obvious first choice to assist.

In addition to testing RoM, a more dynamic, mixed response, real-world situation will be analyzed to gauge this prototype's ability to measure human motions. A regiment of walking will be performed after the RoM tests, then it will be followed by the same RoM tests to determine not only the system's ability to perform accurately but also to the system's stability. If the RoM tests before and after yield similar results under the same calibration, the system is stable, and if the same calibration can read the motions of the walking session accurately, the system and its calibration are suited for dynamic, practical motions as well. If this is not the case, or if there is significant error associated with certain portions of this protocol, then the system and its calibration will have significant and unaddressed pollutants present that will need to be identified and dealt with to create a more useful system.

B. Range of Motion Tests

The range of motion exercises used for this testing are the hip flexion with knee straight test, hip flexion with knee flexed test, internal and external hip rotation test, hip abduction and adduction test, and the double leg squat test. These various tests are used to both isolate individual motions and combine several motions at once, which makes an ideal combination of motions to train and test a calibration.

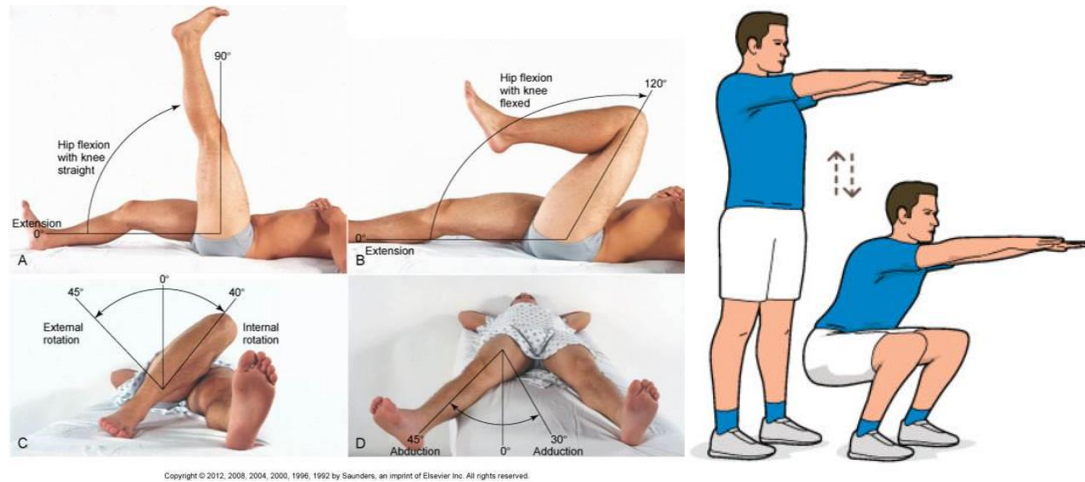


Figure 43. An examples of active versions of hip flexion with knee straight test (upper left), hip flexion with knee flexed test (upper right), internal and external hip rotation test (lower left), and hip abduction and adduction test (lower right) (left-most picture, from Joint Range of Motion and Muscle Length Testing: Third Edition), and the double leg squat test (right-most picture, from FourFourTwo.com).

To maintain repeatability of the RoM tests, the participants will perform these actions passively, meaning the limb of the participant will be moved by either Michael Hanson or another tester who is competently able to guild the participant.

1) *Test Modification:* As previously stated, these RoM tests are standard tools used to measure a joints mobility. However, these tests will not only be limited by a joint’s performance but also the prototype monitoring the joint. While a system could be constructed in a way where the joints is the limiting factor, the current prototype is not at that level of performance due to limited resources and time. As a result, the actual range of motion tested will be abridged as deemed appropriate by Michael Hanson under the constraints dictated by the prototype- mostly to keep the strain sensors taught but not over 120% strain.

Specifically, the constraint in this testing regiment exists as a limited range in knee flexion. The knee is typically not allowed to bend past 90°. While this constraint exists,

the RoM tests encompasses normal walking motions, meaning this prototype can be calibrated and tested to see if the model can correctly monitor walking motions.

C. Finalized Protocol

The finalized protocol will function as a skeleton that will help structure the testing sessions to maintain consistency of actions between participants and to ensure all major tests are completed. The practicality of this protocol will not be known fully until it is implemented during testing, which means it may not have the ideal layout or succession of events. If this is the case, amendments will be made and noted. Amendments will mostly serve to restructure the protocol to avoid redundancy or participant discomfort, or to reduce the amount of time needed to preform said tests. Notes will be taken of any changes made so any inconsistencies or any changes that would inappropriately affect the testing results can be identified either immediately or in the future. This is being done partly to preserve as much transparency as possible so these tests can be reproduced with equivalent results. This is also being done to avoid any bias of the tester (consciously or otherwise) to make changes that may result in more favorable results. The finalized protocol can be referenced in APPENDIX G.

D. Testing

Testing is being performed in the Parker-Hannifin Laboratory for Human Motion and Control at Cleveland State University. Each test participant will be asked to perform a series of motions and walking forms on a treadmill, outfitted in both the prototype and the visual motion capture markers. Parameters were taken from the xSens system to serve as a reference. Because there are three sets of pants and two biological genders, six test

participants make sense to test, while giving a margin of error. In the case one of the data sets is of poor-quality data, there will still be data for that size.

1) *Processing Visual Motion Capture Data*: The data produced by the visual motion capture system is initially not in a useful form for this research. The system outputs the X, Y, and Z coordinates of each marker relative to a set reference point. The data needs to be transformed into joint angles. This is a very computationally costly transformation with a relatively simple concept. The process entails grouping markers into solid bodies that represent body parts, including the pelvis, thigh, shank, and foot, then making a local coordinate system for each solid body and calculating the angular offsets between these coordinate systems.

First, the code imports the raw visual system data and divides it into the corresponding twelve markers (LASIS, RASIS, LPSIS, RPSIS, LGTRO, FLTHI, LLEK, LATI, LLM, LHEE, LTOE, AND LMT5). The code also needs LMM and LMEK to approximate the joint centers of the ankle and knee, respectively. To simulate these markers, physical measurements are taken from the participant, and the assumptions that the joint center is halfway in between the medial and lateral markers and that the joint's X axis will always be in the direction of the global X axis are used. The hip's joint center is approximated using a common proportionality assumption.

Using the joint centers as origins, local coordinate systems are made for each solid body. The pelvis' is assumed to be in line with the global, the thigh's Y axis is in line with the shaft of the femoral bone, the shank's Y axis is in line with the shaft of the tibia, and the foot's Y axis is defined as the global Y. The X axes are all in line with the global X axis, and the Z is the cross product of the X and Y axes.

A forward kinematics model was created around these solid bodies. The pelvis (with 6 DOF) is connected to the thigh (3 DOF of rotation), then the shank (3 DOF of rotation), and finally like the foot (3 DOF of rotation). The joint rotations were defined under the ISB standard [35]. The generalized coordinates were solved using inverse kinematic analysis [36]. This analysis uses an initial guess for the joint angles and compares the resulting coordinates to the actual marker coordinates. An optimizing algorithm repeats this guessing until it produces angles that yield the smallest error between these two sets of coordinates. This process is used on each frame of the dataset. The first frames initial guess is a set of angles equaling zero because each test begins with the participant standing in a neutral pose, where the joints are near their zero angle positions/orientations. The remaining frames use the prior's optimized angles as an initial guess. This is done to save time because the body can only move so quickly in between frames and the participant is not necessarily in a neutral pose. This means the all-zeros initial guess would likely take more computation time to optimize than the prior pose, which must be similar to the current due to time constraints.

The codes used to process this data in three-dimensional space is heavily based on a two-dimensional code written by Dr. Antonie J. van den Bogert and was modified under his guidance. These codes can be referenced in APPENDIX A through APPENDIX C.

2) *Initial Test*: The initial test was performed as a rehearsal to the statistical testing so a protocol could be created, tested, and amended without having to file and refile permissions with the Institutional Review Board. A condition to this testing is that the data from the initial testing cannot be used in the study, so as to prevent gaming of the system. The data collected will be processed to develop, refine, and troubleshoot the calibrations

and codes to be used in the statistical tests, but this data will not be disclosed otherwise. During the preparation for the initial test, an observation was made that led to an anecdotal conclusion. The details and discussion of this test are described in 1) Observations of the Initial Test.

Early attempts to run the initial statistical test ran into difficulties. One major difficulty was the delicate nature of the wiring that ran to the sensors. Wires tended to break from the circuit board that powered the sensors due to the wires running from the side of the boards bearing the weight of the cables that powered and monitored the sensors. This asymmetric mounting causes excessive strain on these wires. To combat this, the wires were soldered back into place when needed and reinforced with silicon via a hot gun. Additional tension relief was added by taping the wires to the sensor clamp casings.

a) *Protocol Amendments*: There are no protocol amendments to report, meaning that the previously defined protocol was followed completely and with no additional procedures.

b) *Initial Conclusion*: The initial testing of the prototype showed this suit tends to shift for the first several minutes it's worn, which notably affects the calibration quality. This is the result of the pants used to make the prototype not having an ideal fit to the participant. This is a limitation that is a consequence of only having available three sizes of pants that are specifically made to fit on parts of the body. As a result, the tension in the clothing seems to fight the tension from the sensors in various areas until the internal forces balance out over the range of motions the participant is performing. To combat this,

if possible, participants will be asked to spend five or ten minutes before their test in the garment and walk around or do some light stretching.

The initial accuracy of the calibration was calculated against the accuracy of a ten camera, passive marker, optical motion capture system (Motion Analysis Corp., Santa Rosa, CA). This accuracy was initial going to be considered absolute, but due to the angle toggling in some degrees of freedom, questions started to arise about the visual system's ability to monitor larger angle changes, as this particular system was designed to monitor the range of motions associated with walking gait. It should be noted this accuracy is actually the difference between the two systems. All things considered, the accuracy will be split up into sections: total (all of the test data after the calibration), normal gait, toes in gait, and toes out gait.

The initial data was collected to test the protocol before the submission of approval to Cleveland State University's IRB. This was done to ensure the protocol was effective, efficient, and yielded data which was sufficiently useful. While this is an acceptable and encouraged practice, it is only allowed as a check and the results are not allowed to be kept or used in the associated research. To comply with this standard, the results of the initial test will not be presented. However, while looking at the errors produced through the initial data processing, a fundamental question popped up: is this error in an acceptable range or not? To determine a quantifiable standard to this potentially subjective question, a reference was needed from the commercial world. The logic behind this decision is that if there is a customer segment willing to consistently pay for a product, its error tendencies must be worth the cost, making it an acceptably accurate system. In this case, the relevant commercial space must include a motion capture system that is portable- portable meaning

the system can operate outside of a prepared area. IMU systems are the most mobile motion capture known to this research, with xSens as a leader in accuracy by word of mouth reviews. A study was completed in September of 2018, which was posted on the xSens website as documentation of their technology’s effectiveness [37]. It is assumed this data is the most recent and accepted accuracy analysis of the xSens systems because it is so recent and condoned by the company. The accuracy of the relative joint angles will serve as a reference for the errors of the ReCap system, and are as follows:

Table 1: xSens Walking Gait Data [37]				
Property	Hip Flexion	Hip Abduction	Hip Rotation	Knee Flexion
RMSe±(σ)	5.7±2.1°	4.1±2.0°	6.5±2.8°	4.4±2.0°
ρ	0.99	0.91	0.68	0.99

Note this is walking gait data, which corresponds to only a portion of the testing performed in this research.

3) *Statistical Testing*: The Institutional Review Board of Cleveland State University approved of IRB-FY2019-73 Validation Study of Reticulated Motion Capture on March 3rd, 2019. There are three sizes of pants and two participants are tested in each size, so each size can be calibrated with a male and female.

Table 2: Relevant Participant Information							
Number	Gender	Age	Height (m)	Weight (kg)	Pant Size	Ankle Malleolus (m)	Knee Epicondyle (m)
1	F	29	1.78	68	L	0.064	0.100
2	M	25	1.83	84	L	0.074	0.100
3	F	22	1.66	68	M	0.067	0.092
4	M	20	1.73	61	M	0.062	0.098
5	F	22	1.55	60	S	0.068	0.105
6	M	25	1.57	59	S	0.063	0.095

The data being collected is processed with the geometric model with crosstalk terms, the geometric model without crosstalk terms, and the GPR model for comparison. The numbers used in the tables are assigned to align the data sets in groups of pant size and is different than the random number chosen by each participant during testing, which was not necessarily between one and six. This change in numbering both attempts to increase the security of participant privacy and organize the data in a logical way. The root-mean-square error (RMSe) is the difference between the down-sampled visual motion capture data and the processed strain sensor data. This value is calculated for each type of gait, the ROM tests and the overall test to function as a metric of accuracy. The average and standard deviation of the RMSe is taken to put the data in a form that is similar to the reference xSens data. The average Pearson correlation coefficient (ρ) was also taken to determine the fit, so this will be emulated as well. Only the normal walking gait data can be compared to with this reference, and ρ will only be found for the total data analyses, for it offers the most insight into the fit. This is not ideal if the errors of the other gait styles are different than the normal walking gait. The other metrics will be compared to one another only. It should be noted the xSens data was taken at several speeds. The speed $0.8^m/s$, which is the speed this projects data was taken at, is the lower end of the range of speeds used in the xSens tests. This may be significant because higher speeds of gait could produce higher errors.

Also note participant three's data ends halfway through the walking trial. All of the normal walking gait and half of the toes-out walking gait is intact, which will be used. The toes-in data was not captured, nor the final stability test. This data is still useful, but

it should be noted the toes-out gait and total error are calculated without the full protocol being performed.

a) *Geometric Results with Crosstalk Compensation*: The results presented in this section were processed with the geometric calibration model with crosstalk compensation, which will be abbreviated as the GC model. All notes and limitations of the data highlighted prior still hold true for these results.

Number	Hip Flexion RMSe	Hip Abduction RMSe	Hip Rotation RMSe	Knee Flexion RMSe
1	3.52°	3.96°	9.68°	4.07°
2	5.11°	4.89°	6.44°	6.89°
3	3.06°	2.37°	4.32°	5.58°
4	5.90°	6.92°	5.95°	5.88°
5	4.45°	4.77°	5.39°	6.81°
6	5.68°	5.04°	8.15°	7.75°
Avg±σ	4.62±1.16°	4.66±1.49°	6.66±1.95°	6.16±1.29°
ρ	0.95	0.82	0.89	0.96

Number	Hip Flexion RMSe	Hip Abduction RMSe	Hip Rotation RMSe	Knee Flexion RMSe
1	3.59°	3.46°	9.30°	4.63°
2	4.12°	1.94°	4.85°	7.11°
3	3.45°	2.91°	4.37°	6.54°
4	2.97°	8.07°	6.84°	4.62°
5	3.20°	3.63°	2.93°	6.26°
6	5.57°	4.27°	7.75°	9.83°
Avg±σ	3.82±0.94°	4.05±2.12°	6.01±2.37°	6.50±1.93°

Table 5: Toes-Out Walking Gait Error of the GC model

Number	Hip Flexion RMSe	Hip Abduction RMSe	Hip Rotation RMSe	Knee Flexion RMSe
1	3.39°	6.56°	6.81°	4.58°
2	5.28°	2.61°	7.89°	5.69°
3	3.15°	2.19°	5.49°	5.87°
4	2.53°	6.68°	6.61°	6.85°
5	2.91°	4.11°	4.01°	7.67°
6	5.78°	5.25°	5.73°	8.19°
Avg±σ	3.84±1.35°	4.57±1.93°	6.09±1.33°	6.48±1.35°

Table 6: Toes-In Walking Gait Error of the GC model

Number	Hip Flexion RMSe	Hip Abduction RMSe	Hip Rotation RMSe	Knee Flexion RMSe
1	3.10°	3.20°	13.22°	4.89°
2	5.65°	7.13°	6.74°	7.04°
3	n/a	n/a	n/a	n/a
4	11.62°	9.86°	6.18°	8.67°
5	5.31°	5.93°	8.53°	7.31°
6	6.45°	4.93°	5.46°	7.27°
Avg±σ	6.43±3.16°	6.21±2.50°	8.03±3.12°	7.04±1.36°

Table 7: ROM Stability Comparison of the GC model

Number	Hip Flexion RMSe	Hip Abduction RMSe	Hip Rotation RMSe	Knee Flexion RMSe
1	2.28°/4.11°	2.47°/2.41°	6.82°/10.11°	2.17°/2.54°
2	3.09°/6.12°	1.75°/5.69°	4.09°/5.80°	2.84°/7.84°
3	n/a	n/a	n/a	n/a
4	2.01°/2.49°	2.08°/2.99°	4.82°/5.21°	2.16°/3.45°
5	3.66°/6.08°	3.36°/5.66°	4.56°/5.26°	2.49°/6.92°
6	4.85°/5.28°	3.99°/4.93°	7.32°/9.08°	3.65°/8.02°
Avg±σ	3.18°/4.82°	2.73°/4.34°	5.52°/7.09°	1.49°/5.75°

b) *Geometric Results with No Crosstalk*: The results presented in this section were processed with the geometric calibration model without crosstalk compensation, which will be abbreviated as the GNC model. All notes and limitations of the data highlighted prior still hold true for these results.

Table 8: Total Error of the GNC model				
Number	Hip Flexion RMSe	Hip Abduction RMSe	Hip Rotation RMSe	Knee Flexion RMSe
1	5.14°	5.50°	11.05°	4.33°
2	7.62°	6.71°	7.75°	7.97°
3	5.43°	4.85°	6.45°	5.03°
4	5.15°	7.83°	8.66°	5.82°
5	5.34°	6.54°	5.90°	7.41°
6	7.55°	6.43°	9.34°	8.50°
Avg±σ	6.04±1.20°	6.31±1.03°	8.19±1.91°	6.51±1.69°
ρ	0.93	0.61	0.86	0.96

Table 9: Normal Walking Gait Error of the GNC model				
Number	Hip Flexion RMSe	Hip Abduction RMSe	Hip Rotation RMSe	Knee Flexion RMSe
1	3.70°	3.46°	4.42°	4.13°
2	3.20°	4.48°	6.35°	7.66°
3	4.87°	4.55°	5.47°	5.76°
4	2.37°	6.16°	8.80°	6.85°
5	4.31°	3.66°	3.97°	8.47°
6	4.10°	4.69°	6.85°	10.52°
Avg±σ	3.76±0.88°	4.50±0.96°	5.98±1.77°	7.23±2.21°

Table 10: Toes-Out Walking Gait Error of the GNC model

Number	Hip Flexion RMSe	Hip Abduction RMSe	Hip Rotation RMSe	Knee Flexion RMSe
1	5.68°	5.41°	7.14°	3.98°
2	4.41°	6.70°	7.01°	5.71°
3	7.71°	6.92°	8.78°	5.41°
4	1.90°	11.28°	6.18°	6.41°
5	3.78°	6.90°	5.30°	7.08°
6	4.96°	6.23°	10.96°	6.40°
Avg±σ	4.74±1.94°	7.24±2.06°	7.56±2.03°	5.83±1.08°

Table 11: Toes-In Walking Gait Error of the GNC model

Number	Hip Flexion RMSe	Hip Abduction RMSe	Hip Rotation RMSe	Knee Flexion RMSe
1	3.51°	4.73°	18.09°	6.05°
2	12.30°	8.50°	9.53°	9.94°
3	n/a	n/a	n/a	n/a
4	9.84°	7.59°	13.50°	7.05°
5	6.08°	7.40°	8.37°	8.49°
6	11.22°	3.34°	6.14°	8.64°
Avg±σ	8.59±3.67°	6.31±2.18°	11.13±4.72°	8.03±1.51°

Table 12: ROM Stability Comparison of the GNC model

Number	Hip Flexion RMSe	Hip Abduction RMSe	Hip Rotation RMSe	Knee Flexion RMSe
1	5.48°/7.48°	5.86°/8.52°	11.21°/11.38°	3.25°/3.52°
2	4.92°/7.91°	4.28°/6.31°	5.21°/7.68°	3.24°/7.78°
3	n/a	n/a	n/a	n/a
4	2.73°/3.31°	5.43°/7.06°	6.13°/6.14°	3.13°/3.55°
5	6.63°/6.82°	6.92°/8.13°	4.97°/5.78°	3.65°/6.26°
6	8.37°/8.99°	10.25°/9.83°	9.99°/12.67°	4.40°/7.95°
Avg	5.63°/6.90°	6.55°/7.97°	7.50°/8.73°	3.53°/5.81°

c) *Gaussian Process Regression Results*: The results presented in this section will be identical to that of the previous sections, save for the fact the data was processed with the GPR toolbox in MatLab, rather than the geometric calibration model. All notes and limitations of the data highlighted prior still hold true for these results. The *fitrgp()* function was run without specifying any parameters or hyperparameters away from their default settings. The automated GPR hyperparameter and model optimization was attempted on one set of data, but no notable change was observed from the optimized and the default calibration, so this result was not recorded, and the default was used instead. These default settings of the hyperparameters for the kernel functions are described on Mathworks' webpage [38] as follows:

“Default initial value of the length scale parameter is the mean of standard deviations of the predictors, and the signal standard deviation is the standard deviation of the responses divided by square root of 2”

Specific optimums were not found for the hyperparameters. This was avoided partly to avoid finding set-specific optimums because this would not emulate a general calibration solution. This was also avoided to maintain a focus on the geometric aspect of the calibration. The optimization of the GPR model may be worthwhile but would involve enough work to merit its own study.

Number	Hip Flexion RMSe	Hip Abduction RMSe	Hip Rotation RMSe	Knee Flexion RMSe
1	8.15°	6.04°	12.60°	6.74°
2	8.47°	4.45°	10.68°	8.77°
3	5.33°	3.51°	6.94°	9.88°
4	4.95°	5.81°	17.62°	7.85°
5	4.25°	4.18°	5.11°	8.34°
6	9.89°	5.73°	6.28°	9.59°
Avg±σ	6.84±2.29°	4.95±1.04°	9.87±4.74°	8.53±1.16°
ρ	0.87	0.74	0.76	0.91

Number	Hip Flexion RMSe	Hip Abduction RMSe	Hip Rotation RMSe	Knee Flexion RMSe
1	4.16°	3.51°	3.74°	5.00°
2	5.62°	1.95°	9.50°	8.23°
3	4.59°	2.78°	4.32°	12.15°
4	3.25°	3.15°	5.49°	5.79°
5	5.05°	3.53°	3.34°	7.58°
6	12.14°	6.90°	2.77°	10.64°
Avg±σ	5.80±3.21 °	3.64±1.70°	4.86±2.46°	8.23±2.76°

Number	Hip Flexion RMSe	Hip Abduction RMSe	Hip Rotation RMSe	Knee Flexion RMSe
1	14.53°	5.20°	6.81°	6.73°
2	12.08°	3.62°	9.39°	9.34°
3	7.63°	4.18°	14.25°	11.67°
4	3.79°	8.56°	18.14°	9.65°
5	2.81°	4.08°	4.37°	11.22°
6	11.53°	6.54°	6.32°	11.51°
Avg±σ	8.73±4.76°	5.36±1.88°	9.88±5.29°	10.02±1.89°

Number	Hip Flexion RMSe	Hip Abduction RMSe	Hip Rotation RMSe	Knee Flexion RMSe
1	4.85°	5.52°	23.54°	9.92°
2	8.83°	5.38°	14.89°	9.52°
3	n/a	n/a	n/a	n/a
4	8.63°	6.41°	31.49°	11.03°
5	5.57°	5.86°	8.37°	8.04°
6	8.99°	5.26°	9.35°	6.46°
Avg±σ	7.37±2.00°	5.69±0.46°	17.53±9.86°	8.99±1.78°

Number	Hip Flexion RMSe	Hip Abduction RMSe	Hip Rotation RMSe	Knee Flexion RMSe
1	0.68°/7.40°	0.26°/9.48°	1.49°/9.34°	0.66°/6.75°
2	1.20°/5.96°	0.83°/5.65°	2.04°/6.37°	0.94°/7.95°
3	n/a	n/a	n/a	n/a
4	0.84°/4.61°	0.69°/5.34°	1.22°/14.16°	0.68°/7.03°
5	1.19°/3.53°	1.25°/3.44°	1.52°/3.63°	1.32°/7.37°
6	1.58°/6.18°	1.03°/4.03°	1.69°/6.13°	1.48°/9.21°
Avg	1.10°/5.54°	0.81°/5.59°	1.59°/7.93°	1.02°/7.66°

d. *Protocol Amendments*: There are no protocol amendments to report, meaning that the previously defined protocol was followed completely and with no additional procedures.

E. *Data Analysis*

The initial and statistical testing yielded important results. An important note for the initial test data is that it cannot be used nor disclosed to comply with IRB standards. The useful information from this test that is to be discussed came in the form of observations of the system performance or general output patterns and not the data the statistical test is gathering.

1) *Observations of the Initial Test:* During initial test preparation, the uncalibrated strain sensor data was observed in a graphical format that showed when an isolated rotation, flexion, or adduction motion was performed, the main sensor reacted to the motion, as well as most, if not all, of the other three sensors- typically to a lesser extent. This demonstrated the presence of the hypothesized motion crosstalk present in deformation-based motion capture techniques. This crosstalk can be so extreme that identifying which data stream corresponds to the sensor responsible for monitoring joint movement becomes difficult.

An impromptu test was performed by abridging the squat tests described in the protocol. With the feet planted at various distances apart, the participant flexed their knees to the extent allowed by the prototype and rose back to a standing position several times. The response from the sensors showed the knee flexion and hip rotation sensor responses changed when performing identical motions with this varied hip adduction.

Referring to the main issue from the previous projects, prior calibration attempts were successful with individual trials. However, when a general calibration was applied, the calibration became useless. It is now clear the unwatched hip flexion and adduction motions polluted the knee flexion and hip rotation readings in a way that could not be accounted for. Further imperial tests done more formally will not only work to confirm this crosstalk but will also determine to what extent is it causing the calibration to perform poorly.

2) *Observations of the Statistical Testing:* The statistical testing showed the prototypes are not easily set up and reset for new participants. The main issue was attaching the sensors to the clamps. This was an issue because the clamps work by tightening and loosening screws. This requires a screwdriver. That is an obvious point but

one that holds more weight when one realizes that the sensor must simultaneously be stretched to an appropriate length to properly attached. This combination proved difficult to pull off when the pants were on a participant. The most effective method was to secure the sensors before the pants were worn and then adjusting the sensors' initial tension as needed after they were put on.

Several of the strain sensors had a habit of being stretched to 120% to 140% strain. This is a concern because they are only rated for 100% strain. Even when the percent strain was not exceeded, several sensors were clamped midway and stretched to high percentages. In addition, if the clamps were tightened too much, they would press holes through the silicon laminate of the sensors. Several sensors were replaced over the course of these tests, most likely as a result of these factors wearing them prematurely.

The hip rotation sensor was initially made with a 100mm sensor and not a 50mm to have a greater resolution to capture the motion with. This thinking was wrong. The 100mm and 50mm sensors are made with the same circuitry, hardware, and software. There only difference is their size. This equates to the larger having a lower resolution because both are designed to stretch to 100.00% with a resolution of 0.01%. When the rotation sensor was stretched, it would rarely reach as high as 30% and would not drop much below 10%. This 20% range offered about 2000 values, which would have been doubled if the smaller sensor was used.

There were several observed instanced when the strain sensors went slack during testing and other instances when the pants shifted from the beginning of the test to the end. Additionally, there are several regions where the visual mocap data quickly shifts, or toggles, between two angular values too quickly to be human motions. This issue may be

the result of the motion capture system used being tailored to observe the smaller movements of walking gait and not the relatively dramatic motions of the double-leg squat or the range of motion tests used in the test protocol.

CHAPTER V

SUMMARY & CONCLUSION

A. System Summary

The prototype used in this project was not ideal. The setup issues highlighted in TESTING & DATA PROCESSING 2) Observations of the Statistical Testing were mostly caused by the clamping mechanisms. The clamps used to hold the strain sensors to the suit are bulky and hard compared. When a female side-release buckle end is added to these clamps, these clamps become about as long as the sensors. This leads to too much of the length of the flexion or rotation sensor being rigid, causing non-continuous sensor contact with the joint and the body. In short, they are ineffective tools that take up too much space and effect the interaction of the sensors with the body. It is possible the data collected could have been made a degree less accurate across the board by these clamps, with the probable exception of the hip flexion sensor. The only benefits they have are they can be 3-D printed, they are conceptually obvious, and they wear very little. These devices are not useable in a prototype that is to be used out of a lab or by an individual not intimately familiar with this prototype. To create an effective motion capture system that can be practically operated and can maintain sensors for a reasonable lifecycle, the sensor attachment method would need to be changed.

In addition to the rigid attachments, the wiring needs to be much more discreet and less free moving to be appropriately suited to operate in sports. This is for several reasons: to not tangling the participant during movements, particularly intense ones; to not cause high stresses at the wire attachments to the sensor; and to present the feeling the participant is wearing standard clothing. The wiring caused many issues and posed much potential for additional issues over the life of this project. For initial validation, these risks were acceptable. For practical uses, this arrangement is totally unusable.

The clothing used in this prototype was bought off the shelf. It was specifically chosen because it is quality made and durable, while emulating the feel of kinesiology tape on the knee. Because of this added pressure and the limited number of sizes the pants are available in, the fit of these pants was not ideal on most participants, and the added support caused the pants to shift notably. Additionally, this clothing did not have support in every area where a sensor was being attached. This is in part due to the focus of the pants to address the knee and nothing else. A custom design of clothing is needed to create a more forgiving fit that does not create excess shifting if the wearer is not the perfect size, which also emulates a series of kinesiology tape patterns to offer support for all the sensor arrangements on the leg.

B. Test Result Summary

The summary of the testing data will look at the averages of each calibration method's performance at each of the trials and groupings presented in TESTING & DATA PROCESSING 3) Statistical Testing.

	Hip Flexion RMSe	Hip Abduction RMSe	Hip Rotation RMSe	Knee Flexion RMSe
xSens	5.7±2.1°	4.1±2.0°	6.5±2.8°	4.4±2.0°
GC	3.8±0.9°	4.1±2.1°	6.0±2.4°	6.5±1.9°
GNC	3.8±0.9°	4.5±1.0°	6.0±1.8°	7.2±2.2°
GPR	5.8±3.2 °	3.6±1.7°	4.9±2.5°	8.2±2.8°

To determine if there is a statistically significant difference between these models and the xSens system, a two-tailed, paired t-test was performed and the p-value was calculated for the difference of the average RMS error between the GC, the GNC, and the GPR models from the xSens system and the mean values of these differences were compared to zero (to test the null hypothesis the methods produce the same magnitude of error). If the p-value is lower than 0.05, the two methods are considered significantly different.

	Hip Flexion P-value	Hip Abduction P-value	Hip Rotation P-value	Knee Flexion P-value
GC vs Xsens	0.021	1	0.71	0.06
GNC vs Xsens	0.021	0.132	0.662	0.028
GPR vs Xsens	0.947	0.597	0.251	0.019

These values show, in normal gait, the GC and GNC models of the prototype are significantly more accurate than the xSens in hip flexion monitoring and the Xsens is significantly more accurate in knee flexion monitoring than all of the models. The other measurements are shown to be similar.

Both geometric calibration equations were able to create comparable accuracies to commercially available motion capture systems for six participants of varying heights. This is surprising and indicates that the range of motions used in typical gait may not require crosstalk compensation. The GC model seems to perform better with the knee measurements, perhaps due to the knee's larger range of motion, but the GNC was close in

all measurements with fewer terms that needed to be calibrated. The GPR model was mostly successful, except with the knee measurements.

	Hip Flexion RMSe	Hip Abduction RMSe	Hip Rotation RMSe	Knee Flexion RMSe
GC	3.8±1.4°	4.6±1.9°	6.1±1.3°	6.5±1.4°
GNC	4.7±1.9°	7.2±2.1°	7.6±2.0°	5.8±1.1°
GPR	8.7±4.8°	5.4±1.9°	9.9±5.3°	10.0±1.9°

The GC model performed similarly with the toes-out gait as with the normal gait.

The GNC and GPR models performed notably worse in this trial than the GC model.

	Hip Flexion RMSe	Hip Abduction RMSe	Hip Rotation RMSe	Knee Flexion RMSe
GC	6.4±3.2°	6.2±2.5°	8.0±3.1°	7.0±1.4°
GNC	8.6±3.7°	6.3±2.2°	11.1±4.7°	8.0±1.5°
GPR	7.4±2.0°	5.7±0.5°	17.5±9.9°	9.0±1.8°

The GC model performed notably worse with the toes-in gait as with the normal gait. The GNC and GPR models performed notably worse in this trial than the GC model.

	Hip Flexion RMSe	Hip Abduction RMSe	Hip Rotation RMSe	Knee Flexion RMSe
GC	4.6±1.2°	4.7±1.5°	6.7±2.0°	6.2±1.3°
GNC	6.0±1.2°	6.3±1.0°	8.2±1.9°	6.5±1.7°
GPR	6.8±2.3°	5.0±1.0°	9.9±4.7°	8.5±1.2°

The GC model performed with similar accuracy over the entire test as with its normal gait. The GNC and GPR models performed notably worse over the entire test than the GC model. To determine if there is a statistical difference between these methods, the p-value was calculated for the difference of the average RMS error between the GC verses

the GNC model and the GC versus the GPR model for each subject and the mean values of these differences were compared to zero. This comparison was done with the total error values.

	Hip Flexion P-value	Hip Abduction P-value	Hip Rotation P-value	Knee Flexion P-value
GC vs GNC	0.035	0.001	0.005	0.21
GC vs GPR	0.066	0.58	0.155	0.002

The p-values show the GC model is significantly more accurate than the GNC model, with the exception of knee flexion monitoring. The GPR is on the verge of being significantly less accurate in hip flexion monitoring than the GC and is less accurate in knee flexion monitoring but is otherwise to be similar. This may be the result of too few tests being performed in conjunction with this model's high standard deviations in the case of hip rotation monitoring.

	Hip Flexion RMSe	Hip Abduction RMSe	Hip Rotation RMSe	Knee Flexion RMSe
GC	3.2°/4.8°	2.7°/4.3°	5.5°/7.1°	1.5°/5.8°
GNC	5.6°/6.9°	6.6°/8.0°	7.5°/8.7°	3.5°/5.8°
GPR	1.1°/5.5°	0.8°/5.6°	1.6°/7.9°	1.0°/7.7°

The stability test checks the calibration's initial fit to its calibration set to the fit of that calibration to the end ROM tests. The initial fit will most likely yield the lowest error in the entire data set, and will probably not be reproducible throughout the test, due to random errors and perturbations. The main purpose of displaying the initial values is to determine if they are too low or too high. The GPR values are very low, which may indicate the trend is fitting to error too. The fit of the final ROM tests is a test to determine if the error grows over time or is comparable to other trials earlier in the test. The GPR final ROM test values are lower than several of its tests, which may indicate that the calibration

does not have a stability problem, but a fitting problem. When looking at the GPR data, the calibrated strain sensor data is tight to the visual data and also follows the discontinuities of the measurements, which are erroneous.

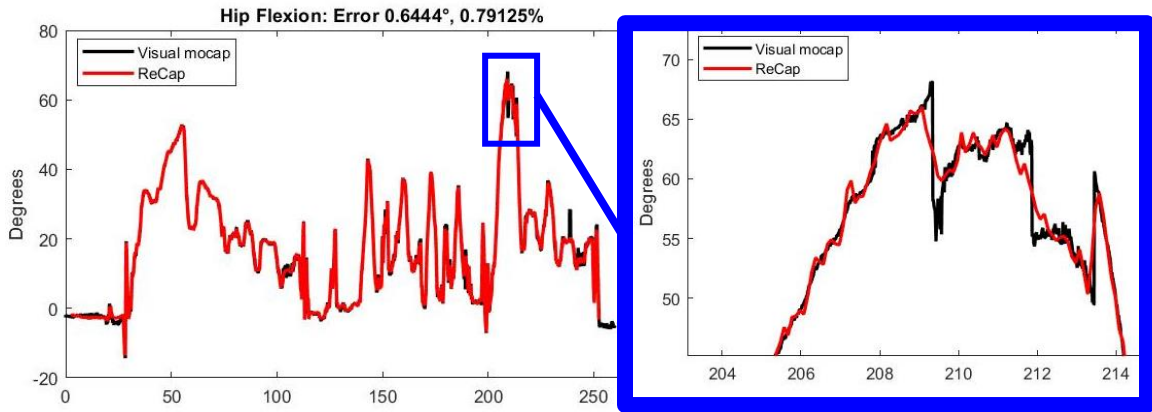


Figure 44. An example of the GPR calibration model overfitting a calibration set and fitting to error.

The stability comparison shows ROM test accuracies similar to the test and trial accuracies of the GC and GNC models. This indicates the calibrations do not drift over time. The initial values also seem reasonable. With the data from the other trials, the GNC's initial values may be said to be too high, resulting in the calibration losing too much of the trend of the calibration data.

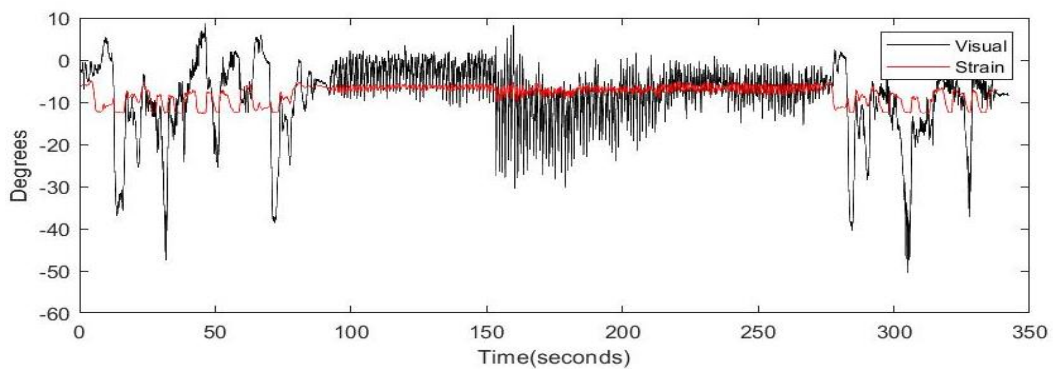


Figure 45. An example of the GNC model failing to emulate the trend of the line. Due to the data's low range, the RMS error was 6.45° .

The Pearson correlation coefficient is used to gauge the correlated output between two functions. In this case, it is gauging the similarities in angles produced by the visual motion capture system and the other system used to make measurements (the xSens and the GC, GNC, and GPR calibrated prototype). For reference as to what these values mean, this source [39] claims the following:

Weak	Moderate	High	Very High
0-0.35	0.35-0.67	0.67-0.9	0.9-1

	Hip Flexion	Hip Abduction	Hip Rotation	Knee Flexion
xSens	0.99	0.91	0.68	0.99
GC	0.95	0.82	0.89	0.96
GNC	0.93	0.61	0.86	0.96
GPR	0.87	0.74	0.76	0.91

These coefficients indicate the GC model is a better fit than the GNC and GPR as well. Compared to the xSens system, the GC is slightly worse with hip and knee flexion and notably worse with hip abduction but is notably better with hip rotation.

These results indicate the geometric model with crosstalk compensation is the most stable and accurate calibration solution for the prototype, however the GPR model has not been shown to be significantly worse in each degree of freedom and more testing would offer clarity to whether or not a substantial difference in model performance exists. The data also indicates this system is as accurate as existing commercial systems, with two exceptions; it is more accurate in hip flexion monitoring, and it is less accurate in knee flexion monitoring.

C. Implications & Conclusion

The implications of the results gathered by this and previous, related projects lead to several conclusions:

- 1) Any sensor array that attempts to measure the motions of a human, or similar, body by measuring the change in distance between two or more points on the overlaying skin, clothing, etc., will need to choose such points in a manner that makes geometric and anatomical sense.
- 2) Any similar sensor array will encounter crosstalk due to its attachment points being a continuum of skin that spans both relatively static and dynamic areas, as well as covering dynamically shaped musculature and will have to compensate for said pollutants in any resulting calibrations.
- 3) Any similar sensor array that attempts to measure simple motions (one dimensional) will need to also monitor all other degrees of freedom the immediate area is capable of to eliminate skin motion-based crosstalk.
- 4) Any similar sensor array that attempts to measure simple motion (one dimensional) without monitoring all other degrees of freedom the immediate area is capable of will probably yield inconsistent measurements.

With the magnitude of error collected being comparable to commercially available systems, it can be said that the fundamental working principles dictating the performance of this system are known and understood well enough to craft a useful human motion monitor. Because of this, immediate development of this system should take the form of expansion into new regions of the body, such as the ankle, arms, wrists, and the back, to apply the existing technology to the entire body so this system can offer an acceptable

resolution of motion capture in these areas. Additional work is needed to determine what factors affect the calibration to the point the system needs to be recalibrated, including if a calibration can handle the wearer removing and putting back on the system in a non-precise manner. Other factors, like a recalibration method dependent on motions and practical measurements is needed to remove dependency from other motion capture technology.

D. Personal Annotations

The findings of this project are significant in part due to the implications it holds relative to both the motion capture and the wearables industries. As it stands, there are few true wearable technologies on the market today. By true wearable technologies, it is meant these are unique innovations or devices that are exclusively more functional and beneficial than a portable devices and function by being strapped or attached to the human body. Take the example of the smartwatch; it is considered a wearable, yet it has identical functionality to a smartphone (a portable device), except in the case heart monitoring hardware was added. Even in the case of a pedometer, most smartphones have this functionality, but most would not qualify a phone as a wearable. True wearable technology is a subset of portable devices and should only be classified as such if it fundamentally needs to be worn to offer its benefits. A wearable could have non-wearable technology included, such as GPS, Wi-Fi reception, communication capacities, but the device itself would only offer a benefit, beyond convenience, if worn. Again, look to the smartwatch as an example; if one took their smartwatch off their arm, the main functions are not interrupted. In stark contrast, a motion monitoring suit or a heart monitor needs to be worn, otherwise it cannot function, making these true wearable technologies. The reason for this

annotation is to highlight several issues the current markets of motion capture and wearables are facing.

Currently, the topically applied rotation sensor and reticulated motion capture system do not exist outside of the previously described projects and these projects have demonstrated the necessity of network-based calibration to create any feasible, deformation monitoring, motion capture system (this does not include marker based visual or IMU-based motion capture because of the care of placing sensors and markers on relatively rigid areas of the body), yet systems currently exist and are for sale, without rotation sensing, which means they cannot have a stable calibration. The reason these should not be considered true wearables is for the fact they fundamentally cannot function properly. The message that can be taken away from this situation is that the market is currently desperate for technology in this area and will attempt to resell existing technologies with an added strap or produce half-finished products that are unvalidated.

Caution and skepticism should be used when dealing with technology that claims to be wearables and functional validation should be presented before it is accepted as such. Fortunately, this issue does not seem to be having a large, present effect. Most people are not running around in tights that almost read their motions and base their exercise and physical health decision on said flawed data. In the case of smart watches, consumers seem to be fully aware of what they are buying and feel this is a worthwhile purchase. Will this always be the case for wearables? Probably not. Many see the wearables industry as the future, or at least the short-term future. It should be expected that within the decade, wearables will become increasingly frequent and publicized, much like the personal computer and smartphone booms before it.

Fortunately, these previous industries have been mostly dominated by quality and competition from the very beginning. Wearables are still new or maybe even on the verge of arriving, and the scope they could cover is massive, especially compared to the initial markets of personal computers (1980s) and smartphones (mid to late 2000s). For example, Apple, Windows, and Linux will always be competing for portions of the personal computer market, just like Apple, Samsung, and Motorola will always compete for phone sales. With wearables, however, a group that develops a motion capture suit will not necessarily compete with other biometric technologies like heart monitors, blood pressure readers, body temperature monitors, pressure-sensitive insoles, etc. This diversity could yield low competition, at least in the initial growth of the market, allowing for low quality products to exist in a profitable form.

Wearables very well could be the future and have the potential to positively change aspects of healthcare, athletics, and beyond. Initially, wearables as a market pose a problem. At any moment, the wrong product could be released at the wrong time and cripple the market's potential. To be fair, a seemingly inevitable development that can carve out its chunk of a multi-billion-dollar, virgin market is exciting and tantalizing. On the consumer side, cinema constantly bombards audiences with fantastical technologies, with the backdrop of scientific experts speculate about what is on the horizon. Like when the iPhone was release, people are naturally infatuated with new technology that seems like the future. Unlike the iPhone, though, wearables pose a threat to health if they don't perform right or as anticipated. If participants trust them with their health, regardless of what the device is made for or claims, and does not meet expectations, people will be hurt. Wearables should be embraced, developed, and praised, but the level of scrutiny each

innovation is subjected to should appropriately rise to match the seriousness of the claims it makes and the impact it could have.

REFERENCES

- [1] P. Nogueira, "Motion Capture Fundamentals," *Faculdade de Engenharia da Universidade do Porto*, 2011.
- [2] R. Roesler, "Optical Motion Capture Guide: A Guide to Optical Motion Capture," Stanford University, 29 March 2011. [Online]. Available: http://physbam.stanford.edu/cs448x/old/Optical_Motion_Capture_Guide.html#head-07a3f975a4b5da3e8f10c61179968f27bf15c63d. [Accessed 10 September 2017].
- [3] A. J. van den Bogert, T. Geijtenbeek, O. Even-Zohar, F. Steenbrink and E. C. Hardin, "A real-time system for biomechanical analysis of human movement and muscle function," *Medical & Biological Engineering & Computing*, vol. 51, no. 10, pp. 1069-1077, 2013.
- [4] OptiTrak, "OptiTrack.com," 2017. [Online]. [Accessed 1 September 2017].
- [5] Vicon, "Vicon.com," 2017. [Online]. [Accessed 1 September 2017].
- [6] S. Ahuja, W. Jirattigalachote and A. Tosborvorn, "Improving Accuracy of Inertial Measurement Units using Support Vector Regression," Stanford University, Stanford, 2011.
- [7] V. Bonnet, S. Ramdani, C. Azevedo-Coste, P. Fraisse, C. Mazzà and A. Cappozzo, "Integration of Human Walking Gyroscopic Data Using Empirical Mode Decomposition," *Sensors*, pp. 370-381, 2013.

- [8] P. Eichelberger, M. Ferraro, U. Minder, T. Denton, A. Blasimann, F. Krause and H. Baur, "Analysis of accuracy in optical motion capture- A protocol for laboratory setup evaluation," *Journal of Biomechanics*, pp. 2085-2088, 2016.
- [9] NaturalPoint Corporation, "Rigid Body Tracking," NaturalPoint Corporation, 18 February 2019. [Online]. Available: https://v21.wiki.optitrack.com/index.php?title=Rigid_Body_Tracking#Unique_Marker_Placements. [Accessed 4 28 2019].
- [10] B. Freedman, A. Shpunt, M. Machline and Y. Arieli, "Depth mapping using projected patterns". United States of America Patent US20100118123A1, 2 April 2007.
- [11] C. Morato, K. N. Kaipa, B. Zhao and S. K. Gupta, "Toward Safe Human Robot Collaboration by Using Multiple Kinects Based Real-Time Human Tracking," *Journal of Computing and Information Science in Engineering*, vol. 14, no. 1, 2013.
- [12] V. Castaneda and N. Navab, *Time-of-Flight and Kinect Imaging*, München: Technische Universität München, 2011.
- [13] A. Gmitterko and T. Lipták, "Motion Capture of Human for Interaction with Service Robot," *American Journal of Mechanical Engineering*, vol. 1, no. 7, pp. 212-216, 2013.
- [14] SparkFun, "Accelerometer, Gyro and IMU Buying Guide," SparkFun, [Online]. Available: www.sparkfun.com. [Accessed 10 September 2017].
- [15] G. Wetzstein, "Inertial Measurement Units I," 19 July 2017. [Online]. Available: <https://stanford.edu/class/ee267/lectures/lecture9.pdf>. [Accessed 10 September 2017].

- [16] T. v. Marcard, B. Rosenhahn, M. Black and G. Pons-Moll, "Sparse Inertial Poser: Automatic 3D Human Pose Estimation from Sparse IMUs," *Eurographics*, p. 349–360, 2017.
- [17] P. Neto, J. N. Pires and A. P. Moreira, "3-D Position Estimation from Inertial Sensing: Minimizing the Error from the Process of Double Integration of Accelerations," in *Industrial Electronics Society, IECON 2013 - 39th Annual Conference of the IEEE*, Vienna, 2013.
- [18] R. Takeda, G. Lisco, T. Fujisawa, L. Gastaldi, H. Tohyama and S. Tadano, "Drift Removal for Improving the Accuracy of Gait Parameters Using Wearable Sensor Systems," *Sensors*, pp. 23230-23247, 2014.
- [19] A. M. Sabatini, "Quaternion-Based Extended Kalman Filter for Determining Orientation by Inertial and Magnetic Sensing," *IEEE TRANSACTIONS ON BIOMEDICAL ENGINEERING*, vol. 53, no. 7, pp. 1346-1356, 2006.
- [20] M. Nitschke, "Sensor-based Movement Analysis Using Optimal Control Simulation of a 3D Biomechanical Model," Friedrich-Alexander-Universität Erlangen-Nürnberg, Lauingen, 2017.
- [21] Meta Motion, "Magnetic Motion Capture," Meta Motion, [Online]. Available: <http://metamotion.com/motion-capture/magnetic-motion-capture-1.htm>. [Accessed 10 September 2017].
- [22] Meta Motion, "Gypsy 7™ Motion Capture System," Meta Motion, [Online]. Available: <http://metamotion.com/gypsy/gypsy-motion-capture-system.htm>. [Accessed 10 September 2017].

- [23] ElectricFoxy, "Bend," ElectricFoxy, 2015. [Online]. Available: <http://www.electricfoxy.com/bend/>. [Accessed 4 October 2017].
- [24] Y. Mengüç, Y.-L. Park, H. Pei, D. Vogt, P. M. Aubin, E. Winchell, L. Fluke, L. Stirling, R. J. Wood and C. J. Walsh, "Wearable Soft Sensing Suit for Human Gait Measurement," *The International Journal of Robotics Research*, vol. 33, no. 14, pp. 1748-1764, 2014.
- [25] R. Pettys-Baker, C. Compton, S. Utset-Ward, M. Tompkins, B. Holschuh and L. E. Dunne, "Design and Development of Valgus-Sensing Leggings," in *Proceedings of the 2017 Design of Medical Devices Conference*, Minneapolis, 2017.
- [26] S. G. McLean, X. Huang and A. J. van den Bogert, "Association between lower extremity posture at contact and peak knee valgus moment during sidestepping: Implications for ACL injury," *Clinical Biomechanics*, vol. 20, no. 8, pp. 863-870, 2005.
- [27] N. Sunpituksaree, C. Schroeck, G. Trovato, B. McKinney and M. Hanson, "Electroactive Polymer Strain Sensor: Application in Knee Flexion & Orientation Monitoring in Athletic & Rehabilitative Settings," Cleveland State University, Cleveland, 2016.
- [28] N. Sunpituksaree, K. Florek and C. Schroeck, "Electroactive Polymer Strain Sensor As a Monitoring Devices in Preventative Sports Medicine," Cleveland, 2017.
- [29] The Engineering Tool Box, "Modulus of Elasticity or Young's Modulus - and Tensile Modulus for common Materials," The Engineering Tool Box, [Online]. Available:

https://www.engineeringtoolbox.com/young-modulus-d_417.html. [Accessed 20 October 2017].

- [30] A. Kalron and S. Bar-Sela, "A Systematic Review of the Effectiveness of Kinesio Taping®- Fact or Fashion?," *European Journal of Physical and Rehabilitation Medicine*, vol. 49, no. 5, pp. 699-709, 2013.
- [31] P. Segal, Director, *Tommy Boy*. [Film]. United States of America: Broadway Pictures; Paramount Pictures, 1995.
- [32] C. Williams and C. Rasmussen, *Gaussian Processes for Machine Learning*, Boston: The MIT Press, 2006.
- [33] R. J. Schalkoff, *Artificial Neural Networks*, New York: McGraw-Hill Companies, Inc, 1997.
- [34] S. B. Heymsfield, A. Martin-Nguyen, T. M. Fong, D. Gallagher and A. Pietrobelli, "Body Circumferences: Clinical Implications Emerging from a New Geometric Model," *Nutrition & Metabolism (London)*, vol. 5, no. 1, 6 October 2008.
- [35] G. Wu, S. Siegler, P. Allard, C. Kirtley, A. Leardini, D. Rosenbaum, M. Whittle, D. D. D'Lima, L. Cristofolini, H. Witte, O. Schmid and I. Stokes, "ISB recommendation on definitions of joint coordinate system of various joints for the reporting of human joint motion—part I: ankle, hip, and spine," *Journal of Biomechanics*, vol. 35, no. 4, pp. 543-548, 2002.
- [36] T.-W. Lu and J. J. O'Connor, "Bone position estimation from skin marker co-ordinates using global optimisation with joint constraints.," *Journal of Biomechanics*, vol. 32, no. 2, pp. 129-134, 1999.

- [37] A. Karatsidis, "Kinetic Gait Analysis Using Inertial Motion Capture: New Tools for Knee Osteoarthritis," University of Twente, 2018.
- [38] The MathWorks, Inc, "fitrgp," The MathWorks, Inc, 2019. [Online]. Available: https://www.mathworks.com/help/stats/fitrgp.html?searchHighlight=fitrgp&s_tid=doc_srchtile#input_argument_namevalue_d119e335756. [Accessed 2 May 2019].
- [39] R. Taylor, "Interpretation of the Correlation Coefficient: a Basic Review," *Journal of Diagnostic Medical Sonography*, vol. 6, no. 1, pp. 35-39, 1990.

APPENDIX A

(MatLab Program leg_main.mat: heavily based off of Dr. Antonie van den Bogert's code by the same name, used to process 12 markers in three-dimensional space)

```
clear all
close all
clc

% main program to run inverse kinematics on data from a file

% specify the data file and frame numbers to process
filename = 'mocap001.txt';

% load the file and extract the marker coordinates we want
% LASIS XYZ in columns 3-5 (1-3)
% RASIS XYZ in columns 6-8 (4-6)
% LPSIS XYZ in columns 9-11 (7-9)
% RPSIS XYZ in columns 12-14 (10-12)
% LGTRO XYZ in columns 18-20 (13-15)
% FLTHI XYZ in columns 21-23 (16-18)
% LLEK XYZ in columns 24-26 (19-21)
% LATI XYZ in columns 27-29 (22-24)
% LLM XYZ in columns 30-32 (25-27)
% LHEE XYZ in columns 33-35 (28-30)
% LTOE XYZ in columns 36-38 (31-33)
% LMT5 XYZ in columns 39-41 (34-36)
data = load(filename);
time = data(:,1)-data(1,1);

columns = [3:14 18:41];
data0 = data(:, columns);
data = data0;

%%%%%%%%%%%% counter LLM & LHEE marker switching
%%%%%%%%%%%%
% load('switcher.mat');
%
% data(switcher, 28:30) = data0(switcher,25:27);
% data(switcher, 25:27) = data0(switcher,28:30);
%
% load('switcher2.mat');
%
% data(switcher, 31:33) = data0(switcher,34:36);
% data(switcher, 34:36) = data0(switcher,31:33);
```

```

%%%%%%%%%%%%%%%%%%%%%%%%%%%%%%%%%%%%%%%%%%%%%%%%%%%%%%%%%%%%%%%%%%%%%%%%
%%%%%%%%%%%%%%%%%%%%%%%%%%%%%%%%%%%%%%%%%%%%%%%%%%%%%%%%%%%%%%%%%%%%%%%%
nframes = size(data,1);
nmarkers = size(data,2)/3;

LASIS = (mean(data(10:150,1:3), 1))';
RASIS = (mean(data(10:150,4:6), 1))';
LPSIS = (mean(data(10:150,7:9), 1))';
RPSIS = (mean(data(10:150,10:12), 1))';
LGTRO = (mean(data(10:150,13:15), 1))';
FLTHI = (mean(data(10:150,16:18), 1))';
LLEK = (mean(data(10:150,19:21), 1))';
LMEK = LLEK + [0.098 ; 0 ; 0];      % we do not have the LMEK marker, so
derive it from RLEK
LATI = (mean(data(10:150,22:24), 1))';
LLM = (mean(data(10:150,25:27), 1))';
LMM = LLM + [0.062 ; 0 ; 0];      % we do not have the LMM marker, so
derive it from RLEK
LHEE = (mean(data(10:150,28:30), 1))';
LTOE = (mean(data(10:150,31:33), 1))';
LMT5 = (mean(data(10:150,34:36), 1))';

% determine the joint centers
DASIS = norm(RASIS-LASIS);      % distance between RASIS and LASIS
% from femur.m, where X was forward and Z to the right:
% Rhip = [RGTRO(1) ; RASIS(2)-0.30*DASIS ; RASIS(3)-0.14*DASIS]; % hip
using Bell et al. 1990
Lhip = [LASIS(1)+0.14*DASIS ; LASIS(2)-0.30*DASIS ; LGTRO(3)];
Lknee = (LLEK + LMEK)/2;      % knee center is assumed at midpoint between
epicondyles
Lankle = (LLM + LMM)/2;      % ankle center is assumed at midpoint between
malleoli

% determine thigh and shank length
Lthigh = norm(Lhip-Lknee);
Lshank = norm(Lknee-Lankle);

% determine the local coordinate systems (O,Ex,Ey,Ez)
% hip
Oh = Lhip;
Exh = (RASIS-LASIS);      % vector pointing from LASIS to RASIS
Exh = Exh/norm(Exh);      % now it is a unit vector

```

```

MSISL = (RPSIS+LPSIS)/2 - (RASIS+LASIS)/2;          % Mid Superior Iliac
Spinal line, points ??????????????poteriorly????????????????????
Eyh = cross(MSISL,Exh);          % local x axis direction
Eyh = Eyh/norm(Eyh);            % now it is a unit vector
Ezh = cross(Exh,Eyh);          % the local z axis
Thip_stand = [ [Exh Eyh Ezh Oh] ; 0 0 0 1];        % position and orientation of hip
frame during standing

% determine local XYZ coordinates of the markers we will use to track the hip
xyzh = [LASIS, RASIS, LPSIS, RPSIS];

xyzh = reshape(xyzh,3,4);          % transform into a 3x4 matrix

locxyzh = Thip_stand \ [xyzh ; ones(1,4)]; % transform marker coordinates to
local xyz coordinates
locxyzh = locxyzh(1:3,:);

% determine the local coordinate systems (O,Ex,Ey,Ez)
% femur
Of = Lhip;
Eyf = (Lhip-Lknee);              % vector pointing from knee center to hip center
Eyf = Eyf/norm(Eyf);            % now it is a unit vector
TEL = LMEK - LLEK;              % trans-epicondylar line, points medially
Ezf = cross(TEL,Eyf);           % local x axis direction
Ezf = Ezf/norm(Ezf);           % now it is a unit vector
Exf = cross(Eyf,Ezf);           % the local z axis
Tfemur_stand = [ [Exf Eyf Ezf Of] ; 0 0 0 1];      % position and orientation of
femur frame during standing

% determine local XYZ coordinates of the markers we will use to track the femur
xyzf = [LGTRO, FLTHI, LLEK];

xyzf = reshape(xyzf,3,3);          % transform into a 3x2 matrix

locxyzf = Tfemur_stand \ [xyzf ; ones(1,3)]; % transform marker coordinates to
local xyz coordinates
locxyzf = locxyzf(1:3,:);

%tibia
Ot = Lknee;
Eyt = (Lknee-Lankle);           % vector pointing from ankle center to knee center
Eyt = Eyt/norm(Eyt);           % now it is a unit vector
TML = LMM - LLM;               % trans-malleoliar line, points medially

```

```

Ezt = cross(TML,Eyt);      % local x axis direction
Ezt = Ezt/norm(Ezt);      % now it is a unit vector
Ext = cross(Eyt,Ezt);     % the local z axis
Ttibia_stand = [ [Ext Eyt Ezt Ot] ; 0 0 0 1];    % position and orientation of tibia
frame during standing

% determine local XYZ coordinates of the markers we will use to track the tibia
xyzt = [LLEK, LATI, LLM];

xyzt = reshape(xyzt,3,3);          % transform into a 3x3 matrix

locxyzt = Ttibia_stand \ [xyzt ; ones(1,3)]; % transform marker coordinates to
local xyz coordinates
locxyzt = locxyzt(1:3,:);

%paw (foot)
Op = Lankle;
Eyp = [0; 1; 0];      % local y axis direction matches global y
Eyp = Eyp/norm(Eyp);  % now it is a unit vector
TML = LMM - LLM;      % trans-malleoliar line, points medially
Ezp = cross(TML,Eyp); %
Ezp = Ezp/norm(Ezp);  % now it is a unit vector
Exp = cross(Eyp,Ezp); % the local z axis
Tpaw_stand = [ [Exp Eyp Ezp Op] ; 0 0 0 1];    % position and orientation of tibia
frame during standing

% determine local XYZ coordinates of the markers we will use to track the foot
xyzp = [LLM, LHEE, LTOE, LMT5];
xyzp = reshape(xyzp,3,4);          % transform into a 3x4
locxyzp = Tpaw_stand \ [xyzp ; ones(1,4)]; % transform marker coordinates to
local xyz coordinates
locxyzp = locxyzp(1:3,:);

% put data and show parameter in a global variable
global leg_solve_glb
leg_solve_glb.Lthigh = Lthigh;
leg_solve_glb.Lshank = Lshank;
leg_solve_glb.locxyzh = [locxyzh, ones(length(locxyzh),1)]; % transform to a
4x4 matrix (as needed by leg_fk)
leg_solve_glb.locxyzf = [locxyzf, ones(size(locxyzf,1),1)]; % transform to a
3x4 matrix (as needed by leg_fk)
leg_solve_glb.locxyzt = [locxyzt, ones(length(locxyzt),1)]; % transform to a
4x4 matrix (as needed by leg_fk)

```

```

leg_solve_glb.locxyzp = [locxyzp, ones(length(locxyzp),1)]; % transform to a
3x4 matrix (as needed by leg_fk)

% process the frames
q = zeros(15,1); % initial guess for frame 1
q(2) = 1;
% data = data(20:120,:);
% nframes = size(data,1);
qresults = zeros(nframes,15);
d = zeros(nframes,12);
rms = zeros (nframes,12);

% figure(1);
figure(1)
tic
for i = 1:nframes
    if toc > 60.0
        tic
        fprintf('Solving frame %d ...\n', i);
    end
    leg_solve_glb.i = i;
    % framedata
    =[LASIS,RASIS,LPSIS,RPSIS,LGTRO,FLTHI,LLEK,LATI,LLM,LHEE,LTOE,
LMT5];
    framedata = data(i,:);
    framedata = reshape(framedata,3,nmarkers)';
    % framedata(3,:) = [0 0 0];
    % framedata(1,:) = [0 0 0];
    [q, dd, rms1] = leg_solve(framedata, q);
    qresults(i,:) = q';
    d(i,:) = dd;
    rms(i,:) = rms1;
    if rem(i,1000) == 0
        subplot(2,1,1)
        plot(1:i,qresults(1:i,:))
        xlabel('Frame Number')
        ylabel('Meters & Radians')
        legend('hip x','hip y','hip z','hip flexion','hip abduction','hip rotation','thigh
flexion','thigh abduction','thigh rotation','knee flexion','knee abduction','knee
rotation','foot plantarflexion','foot abduction','foot rotation')
        title('Processed Data Q')
        subplot(2,1,2)
        plot(1:i,d(1:i,:))

```

```

    title('Distance between Measured & Model Markers')

legend('LASIS','RASIS','LPSIS','RPSIS','LGTRO','FLTHI','LLEK','LATI','LLM','
LHEE','LTOE','LMT5')
    xlabel('Frame Number')
    ylabel('Meters')
    drawnow
end
end
subplot(2,1,1)
plot(1:i,qresults(1:i,:))
xlabel('Frame Number')
ylabel('Meters & Radians')
legend('hip x','hip y','hip z','hip flexion','hip abduction','hip rotation','thigh
flexion','thigh abduction','thigh rotation','knee flexion','knee abduction','knee
rotation','foot plantarflexion','foot abduction','foot rotation')
title('Processed Data Q')
subplot(2,1,2)
plot(1:i,d(1:i,:))
title('Distance between Measured & Model Markers')
legend('LASIS','RASIS','LPSIS','RPSIS','LGTRO','FLTHI','LLEK','LATI','LLM','
LHEE','LTOE','LMT5')
xlabel('Frame Number')
ylabel('Meters')

Sub.q = qresults; Sub.rms = rms; Sub.d = d; Sub.time = time;save Subject006.mat
Sub;

```

APPENDIX B

(MatLab Program leg_solve.mat: heavily based off of Dr. Antonie van den Bogert's code by the same name, used to process 12 markers in three-dimensional space)

```

function [q, d, rms] = leg_solve(data, q0)
% solve the inverse kinematic problem
%
% Input:
% data (Nmarkers x 3)      measured coordinates of markers at hip, knee,
ankle, heel, toe
% q0 (NDOF x 1, optional)  initial guess for the solution
%
% Output:
% q (NDOF x 1)  generalized coordinates: hip x, hip y, hip z,
%              thigh angle, knee angle, ankle angle,
% d (Nmarkers x 1) distances between model markers and measured markers

% default initial guess is close to standing
if (nargin < 2)
    q0 = [0 (Lthigh+Lshank) 0 0 0 0 0 0 0 0 0 0 0];
end

% put data and show parameter in a global variable
global leg_solve_glb
leg_solve_glb.data = data;

% This version uses the fminsearch optimization function
% fmincon is probably faster.
% for an even faster algorithm, use Levenberg-Marquardt (Numerical Recipes,
chapter 15)
A=[];b=[];Aeq=[];beq=[];
lb= -1* [.5 0 1 .30 .75 1 0.30 pi/2 pi/2 pi .0323 -.0077 1 pi/2 pi/2];
ub=  [.1 2 1 .75 .25 1 1.75 pi/2 pi/2 .25 -.0323 .0077 1 pi/2 pi/2];
nonlcon=[];
options = optimoptions(@fmincon,'Display','off');
q = fmincon(@leg_ssquares, q0,A,b,Aeq,beq,lb,ub,nonlcon,options);

[~,d, rms] = leg_ssquares(q);

end
%=====
=====

function [ssq, d, rms] = leg_ssquares(q)
% compute sum of squared residuals for inverse kinematic problem

```

```

%
% Input:
% q (NDOF x 1) generalized coordinates: hip x, hip y, thigh angle, knee
angle, ankle angle
%
% Output:
% ssq (scalar) sum of squared differences between marker data and
forward kinematic model in pose q
% res (Nmarkers x 1) RMS residuals for each marker, i.e. distance (in m)
between measured marker position and
% corresponding model marker when model is in pose q.
%
% Before calling this function, global variable leg_solve_glb must contain:
% data (Nmarkers x 3) measured coordinates of markers at hip, knee, ankle,
heel, toe
global leg_solve_glb

% extract marker data
data = leg_solve_glb.data;

visible = find(data(:,1) ~= 0);
leg_solve_glb.visible = visible;
i = leg_solve_glb.i;

% use forward kinematics function to determine where the model's markers are,
this is fi(q) in the equations presented
fiq = leg_fk(q);
% figure(1)
% hold off
% plot3(data(:,1),data(:,2),data(:,3),'g','LineWidth',4);
% hold on
% plot3(fiq(:,1),fiq(:,2),fiq(:,3),'ro');
% axis equal
% pause(0.01)

% compute sum of squared residuals of all 13x3=39 coordinates
ssq = sum(sum((data(visible,:) - fiq(visible,:)).^2));

rms = zeros(1,12);
rms(visible) = sqrt(sum((((data(visible,:) - fiq(visible,:)).^2)')/(3)));

% compute distance between each measured marker and the corresponding model
marker

```

```
d = zeros(1,12);  
d(visible) = sqrt(sum((data(visible,:)-fiq(visible,:)).^2)); % for each marker,  
distance is computed as sqrt((xmeas-xmodel)^2 + (ymeas-ymodel)^2)  
end
```

APPENDIX C

(MatLab Program leg_fk.mat: heavily based off of Dr. Antonie van den Bogert's code by the same name, used to process 12 markers in three-dimensional space)

```
function [r] = leg_fk(q)
% leg model forward kinematics function
%
% Input:
% q (13 x 1) generalized coordinates: hip x, hip y, hip z, hip
% flexion, hip abduction, hip rotation, thigh flexion, thigh abduction,
% thigh rotation, knee flexion, ankle plantar flexion, ankle Supination,
% ankle rotation (=0)
%
% Output:
% r (14 x 3) global coordinates of the 12 markers

% Call on global variable leg_solve_glb for:
% Lthigh (scalar)
% Lshank (scalar)
% locxyzf (4 x 3) local coordinate system of the femur
% locxyzt (4 x 3) local coordinate system of the tibia
% locxyzp (4 x 3) local coordinate system of the foot (paw)

global leg_solve_glb

% extract marker data and Lthigh
Lthigh = leg_solve_glb.Lthigh;
Lshank = leg_solve_glb.Lshank;
locxyzh = leg_solve_glb.locxyzh;
locxyzf = leg_solve_glb.locxyzf;
locxyzt = leg_solve_glb.locxyzt;
locxyzp = leg_solve_glb.locxyzp;

% generate the segment pose matrices
Tpelvis = hmc3_transrotX([q(1); q(2); q(3)],
q(4))*hmc3_transrotZ(zeros(3,1),...
q(5))*hmc3_transrotY(zeros(3,1), q(6));

Thip = hmc3_transrotX(zeros(3,1), q(7))*hmc3_transrotZ(zeros(3,1),...
q(8))*hmc3_transrotY(zeros(3,1), q(9));

Tthigh = Tpelvis * Thip;
```

```

Tthigh_shank = hmc3_transrotX([0; -1*Lthigh; 0],
q(10))*hmc3_transrotZ(zeros(3,1),...
q(11))*hmc3_transrotY(zeros(3,1), q(12));           % translate along thigh Y,
then rotate by q(10)

Tshank      = Tthigh * Tthigh_shank;

Tshank_foot = hmc3_transrotX([0, -1*Lshank, 0],
q(13))*hmc3_transrotZ(zeros(3,1),...
q(14))*hmc3_transrotY(zeros(3,1), q(15));           % translate along shank Y,
then rotate by q(11), q(12), & q(13)

Tfoot      = Tshank * Tshank_foot;

%%%%%%%%%%%%%%%%%%%%%%%%%%%%%%%%%%%%%%%%%%%%%%%%%%%%%%%%%%%%%%%%%%%%%%%%
% generate the global coordinates of the markers

rLASIS = Tpelvis * locxyzh(1,:);
rRASIS = Tpelvis * locxyzh(2,:);
rLPSIS = Tpelvis * locxyzh(3,:);
rRPSIS = Tpelvis * locxyzh(4,:);

rLGTRO = Tthigh * locxyzf(1,:);
rFLTHI = Tthigh * locxyzf(2,:);

rLLEK = Tshank * locxyzt(1,:);
rLATI = Tshank * locxyzt(2,:);
rLLM = Tshank * locxyzt(3,:);

rLHEE = Tfoot * locxyzp(2,:);
rLTOE = Tfoot * locxyzp(3,:);
rLMT5 = Tfoot * locxyzp(4,:);

% store the XYZ coordinates of the markers in a 12x3 matrix
r = [rLASIS(1:3)'; rRASIS(1:3)'; rLPSIS(1:3)'; rRPSIS(1:3)'; rLGTRO(1:3)';...
rFLTHI(1:3)'; rLLEK(1:3)'; rLATI(1:3)'; rLLM(1:3)'; rLHEE(1:3)';...
rLTOE(1:3)'; rLMT5(1:3)'];
end

```

APPENDIX D

(MatLab Program CalibrationTestCode.mat: redacted of protected calibration information)

```
clear
clc
%%%%%%%%%%%%%%%%%%%%%%%%%%%%%%%%%%%%%%%%%%%%%%%%%%%%%%%%%%%%%%%%%%%%%%%%
%%%%%%%%%%%%%%%%%%%%%%%%%%%%%%%%%%%%%%%%%%%%%%%%%%%%%%%%%%%%%%%%%%%%%%%%
%%%%%%%%%%%%%%%%%%%%%%%%%%%%%%%%%%%%%%%%%%%%%%%%%%%%%%%%%%%%%%%%%%%%%%%% CalibrationTestCode
%%%%%%%%%%%%%%%%%%%%%%%%%%%%%%%%%%%%%%%%%%%%%%%%%%%%%%%%%%%%%%%%%%%%%%%%
%%%%%%%%%%%%%%%%%%%%%%%%%%%%%%%%%%%%%%%%%%%%%%%%%%%%%%%%%%%%%%%%%%%%%%%%
%%%%%%%%%%%%%%%%%%%%%%%%%%%%%%%%%%%%%%%%%%%%%%%%%%%%%%%%%%%%%%%%%%%%%%%%

%%%%%%%%%%%%%%%%%%%%%%%%%%%%%%%%%%%%%%%%%%%%%%%%%%%%%%%%%%%%%%%%%%%%%%%% Loading Force Plate Data
%%%%%%%%%%%%%%%%%%%%%%%%%%%%%%%%%%%%%%%%%%%%%%%%%%%%%%%%%%%%%%%%%%%%%%%%
% Visual Mocap File
filename = 'mocap001.txt';           %Format
>Name.FileType'.
dataVDB = load(filename);

%Defining Y Force
Fy1 = dataVDB(:,52);                %Left Y direction force
plate data.
clear dataVDB                       %Saving space.

%Defining Step Times
difFy = zeros(size(Fy1));           %Initializes delta force
matrix to make it the same size as force matrix.
step = difFy;                       %Records step locations in
matrix.
difFy(2:end) = diff(Fy1);           %Calculates delta force.
ppp = 0;                             %Makes sure step only happens
when the foot left the ground.

for i = 1:length(Fy1)                %Finding time when step
happens based on force & delta force.
    if Fy1(i) > 40.3 && difFy(i) > 33 && ppp == 0
        step(i) = 1;
        ppp = 1;
    elseif Fy1(i) < 40 && difFy(i) < 0 && ppp == 1
        ppp = 0;
    end
end
end
```

```

clear difFy Fy1 %Saving space.
%%
%%%%%%%%%%%%%%%%%%%%%%%%%%%%%%%%%%%%%%%%%%%%%%%%%%%%%%%%%%%%%%%%%%%%%%%% Loading Test Data Files
%%%%%%%%%%%%%%%%%%%%%%%%%%%%%%%%%%%%%%%%%%%%%%%%%%%%%%%%%%%%%%%%%%%%%%%%
% Visual Mocap Data
load('Subject001.mat'); % Visual Mocap
Inverse Kinematics-processed .mat file.
timeVDB = Sub.time; %Format .mat to have 1
structure 'Nic' with 3 variables:
qrs = Sub.q(:,7:10) * 180/pi; % 'time' for time, 'q' for
angles, 'rms' for rms of marker positions.
rmsVDB = Sub.rms(:,7:10); %For reference- non-
essential.
clear Nic

%Strain Sensor ReCap Data
data = load('test001.txt'); %Strain sensor .txt file-
formatted: [time, hip flexion (HF), hip abduction (HA), hip rotation (HR), knee
flexion (KF)].
% time0 = data(1,1); %Finding initial time
stamp value.
data = data(30:end,:); %Finds testing window.

time1 = sum([60 1].*data(:,2:3),2) + 2.125; %Zeroing
ReCap time to match Visual Mocap time for HR & KF.
time2 = sum([60 1].*data(:,2:3),2) + 2.125; %Zeroing
ReCap time to match Visual Mocap time for HF & HA.

SME = data(:,4:7); %Assigning variable for
strain sensor data.
clear data %Saving space.
SME1 = SME(1:2000,:); %Finds calibration
window.

%Interpolating the Higher Sampled Visual Mocap (100hz) to Match Recap (10 hz)
qVDBa = interp1(timeVDB, qrs, time1); %Match Visual
Mocap time for HR & KF.
qVDBb = interp1(timeVDB, qrs, time2); %Match Visual
Mocap time for HF & HA.
qVDB = [qVDBb(:,1:2), qVDBa(:,3:4)]; %Combobulating
data.
qVDB1 = qVDB(1:2000,:); %Finds calibration
window.

```

```

clear qVDBa qVDBb                                %Saving space.

close all                                         %Close figures after reading data
files for quick recalibration point.
%%%%%%%%%%%%%%%%%%%%%%%%%%%%%%%%%%%%%%%%%%%%%%%%%%%%%%%%%%%%%%%%%%%%%%%% Optimization
%%%%%%%%%%%%%%%%%%%%%%%%%%%%%%%%%%%%%%%%%%%%%%%%%%%%%%%%%%%%%%%%%%%%%%%%
%Initial Calibration Factor Guesses
[REDACTED]

%structure = Calibrator(Direction,Function Mode, Strain Sensor Data, Initial
Guess, Visual Mocap Data)
X = Calibrator('HF', 'fit', SME1, [REDACTED], qVDB1);           %X
is a structure with three variables:
cHF = X.c;                                       %c (calibration constant)
calEqHF = X.eq;                                 %eq (equations)
RMSeHF = X.rms;                                 %rms (root mean square
error)

X = Calibrator('HA', 'fit', SME1, [REDACTED], qVDB1);
cHA = X.c;
calEqHA = X.eq;
RMSeHA = X.rms;

X = Calibrator('HR', 'fit', SME1, [REDACTED], qVDB1);
cHR = X.c;
calEqHR = X.eq;
RMSeHR = X.rms;

X = Calibrator('KF', 'fit', SME1, [REDACTED], qVDB1);
cKF = X.c;
calEqKF = X.eq;
RMSeKF = X.rms;

clear SME1                                       %Saving space.
%Calculating ReCap Angles of Calibration Curves
q = [calEqHF(cHF), calEqHA(cHA), calEqHR(cHR), calEqKF(cKF)];

x = range(qVDB1);
rmsME = [RMSeHF,RMSeHA,RMSeHR,RMSeKF];          %rms
of ReCap vs Visual Mocap.
rmsMEp = rmsME./x*100;                          %rms percentage of
max range.

```

```

%%%%%%%%%%%%%%%%%%%%%%%%%%%%%%%%%%%%%%%%%%%%%%%%%%%%%%%%%%%%%%%%%%%%%%%% Calibration Curves
%%%%%%%%%%%%%%%%%%%%%%%%%%%%%%%%%%%%%%%%%%%%%%%%%%%%%%%%%%%%%%%%%%%%%%%%
%Both Angular Data Sets Plotted Together
figure(1)
hold on

subplot(2,2,1);
plot(
timeVDB(1:26000,:),qrs(1:26000,1),'k',time2(1:2000,:),q(:,1),'r','LineWidth',2)
title(['Hip Flexion: Error ',num2str(rmsME(1)),char(176),',
',num2str(rmsMEp(1)),'%'])
ylabel('Degrees')

subplot(2,2,2);
plot(
timeVDB(1:26000,:),qrs(1:26000,2),'k',time2(1:2000,:),q(:,2),'r','LineWidth',2)
title(['Hip Abduction: Error ',num2str(rmsME(2)),char(176),',
',num2str(rmsMEp(2)),'%'])
legend('Visual mocap','ReCap')

subplot(2,2,3);
plot(
timeVDB(1:26000,:),qrs(1:26000,3),'k',time1(1:2000,:),q(:,3),'r','LineWidth',2)
title(['Hip Rotation: Error ',num2str(rmsME(3)),char(176),',
',num2str(rmsMEp(3)),'%'])
xlabel('Time(seconds)')
ylabel('Degrees')

subplot(2,2,4);
plot(
timeVDB(1:26000,:),qrs(1:26000,4),'k',time1(1:2000,:),q(:,4),'r','LineWidth',2)
title(['Knee Flexion: Error ',num2str(rmsME(4)),char(176),',
',num2str(rmsMEp(4)),'%'])
xlabel('Time(seconds)')

%Calibration Curves
figure(2)
hold on

subplot(2,2,1);
CaliCurve('hf',q(:,1),qVDB1(:,1),0,1)
subplot(2,2,2);
CaliCurve('ha',q(:,2),qVDB1(:,2),0,0)

```

```

subplot(2,2,3);
CaliCurve('hr',q(:,3),qVDB1(:,3),1,1)
subplot(2,2,4);
CaliCurve('kf',q(:,4),qVDB1(:,4),1,0)
clear q qVDB1 %Saving space.
%%
%%%%%%%%%%%%%%%%%%%%%%%%%%%%%%%%%%%%%%%%%%%%%%%%%%%%%%%%%%%%%%%%%%%%%%%%%% Calculating ReCap Angles
%%%%%%%%%%%%%%%%%%%%%%%%%%%%%%%%%%%%%%%%%%%%%%%%%%%%%%%%%%%%%%%%%%%%%%%%%%
%Angle Calculation
qHF = Calibrator('HF', 'run', SME, cHF);
qHA = Calibrator('HA', 'run', SME, cHA);
qHR = Calibrator('HR', 'run', SME, cHR);
qKF = Calibrator('KF', 'run', SME, cKF);
clear SME %Saving space.

qME2 = [qHF, qHA, qHR, qKF];

%RMS Error Calculation
rmsHF2 = (mean((qHF(2500:end)-qVDB(2500:end,1)).^2)).^0.5;
rmsHA2 = (mean((qHA(2500:end)-qVDB(2500:end,2)).^2)).^0.5;
rmsHR2 = (mean((qHR(2500:end)-qVDB(2500:end,3)).^2)).^0.5;
rmsKF2 = (mean((qKF(2500:end)-qVDB(2500:end,4)).^2)).^0.5;
clear qHF qHA qHR qKF %Saving space.

%%%%%%%%%%%%%%%%%%%%%%%%%%%%%%%%%%%%%%%%%%%%%%%%%%%%%%%%%%%%%%%%%%%%%%%%%% Method Comparison Curves
%%%%%%%%%%%%%%%%%%%%%%%%%%%%%%%%%%%%%%%%%%%%%%%%%%%%%%%%%%%%%%%%%%%%%%%%%%
%HF
figure(5)
hold on

subplot(2,1,1);
plot(timeVDB,qrs(:,1),'k',time2,qME2(:,1),'r')
legend('Visual','Strain')
xlabel('Time(seconds)')
ylabel('Degrees')

subplot(2,1,2);
CaliCurve('hf',qME2(:,1),qVDB(:,1),1,1)
title(['Hip Flexion: Error',num2str(rmsHF2),char(176),',',num2str(rmsHF2*100/range(qVDB(:,1))),'%'])

%HA
figure(6)

```

```

hold on

subplot(2,1,1);
plot(timeVDB,qrs(:,2),'k',time2,qME2(:,2),'r')
legend('Visual','Strain')
xlabel('Time(seconds)')
ylabel('Degrees')

subplot(2,1,2);
CaliCurve('ha',qME2(:,2),qVDB(:,2),1,1)
title(['Hip Abduction: Error
',num2str(rmsHA2),char(176),',',num2str(rmsHA2*100/range(qVDB(:,2))),'%'])

%HR
figure(7)
hold on

subplot(2,1,1);
plot(timeVDB,qrs(:,3),'k',time1,qME2(:,3),'r')
legend('Visual','Strain')
xlabel('Time(seconds)')
ylabel('Degrees')

subplot(2,1,2);
CaliCurve('hr',qME2(:,3),qVDB(:,3),1,1)
title(['Hip Rotation: Error
',num2str(rmsHR2),char(176),',',num2str(rmsHR2*100/range(qVDB(:,3))),'%'])

%KF
figure(8)
hold on

subplot(2,1,1);
plot(timeVDB,qrs(:,4),'k',time1,qME2(:,4),'r')
legend('Visual','Strain')
xlabel('Time(seconds)')
ylabel('Degrees')

subplot(2,1,2);
CaliCurve('kf',qME2(:,4),qVDB(:,4),1,1)
title(['Knee Flexion: Error
',num2str(rmsKF2),char(176),',',num2str(rmsKF2*100/range(qVDB(:,4))),'%'])
%%

```

```

%%%%%%%%%%%%%% Gait Cycles Comparison
%%%%%%%%%%%%%%
%Defining Step Times
L = find(step ==1);
timeStep = timeVDB(L);
timeStep = timeStep(17:140);
timeStepN = timeStep(1:42);           %Normal Gait Timings
timeStepO = timeStep(43:83);         %Toes-Out Gait
%Timings
timeStepI = timeStep(84:123);        %Toes-In Gait Timings

clear step                            %Saving space.
%%%%%%%%%%%%%% Gait Cycles Plots
%%%%%%%%%%%%%%
%HF
figure(9)
hold on

subplot(1,3,1);
rms1 = gaitgraph(timeStepN,time2,qVDB(:,1),qME2(:,1));
title(['Normal Gait Error: ',num2str(rms1),char(176)], 'FontSize', 12)
ylabel('Hip Flexion in Degrees', 'FontSize', 18)
axis([0 100 -20 45])

subplot(1,3,2);
rms2 = gaitgraph(timeStepO,time2,qVDB(:,1),qME2(:,1));
title(['Toes Out Gait Error: ',num2str(rms2),char(176)], 'FontSize', 12)
xlabel('Gait Cycle (%)', 'FontSize', 18)
axis([0 100 -20 45])

subplot(1,3,3);
rms3 = gaitgraph(timeStepI,time2,qVDB(:,1),qME2(:,1));
title(['Toes In Gait Error: ',num2str(rms3),char(176)], 'FontSize', 12)
axis([0 100 -20 45])

%HA
figure(10)
hold on

subplot(1,3,1);
rms1 = gaitgraph(timeStepN,time2,qVDB(:,2),qME2(:,2));
title(['Normal Gait Error: ',num2str(rms1),char(176)], 'FontSize', 12)
ylabel('Hip Abduction in Degrees', 'FontSize', 18)

```

```

xlabel('Gait Cycle (%)')
axis([0 100 -20 10])

subplot(1,3,2);
rms2 = gaitgraph(timeStepO,time2,qVDB(:,2),qME2(:,2));
title(['Toes Out Gait Error: ',num2str(rms2),char(176)], 'FontSize', 12)
xlabel('Gait Cycle (%)')
axis([0 100 -20 10])

subplot(1,3,3);
rms3 = gaitgraph(timeStepI,time2,qVDB(:,2),qME2(:,2));
title(['Toes In Gait Error: ',num2str(rms3),char(176)], 'FontSize', 12)
xlabel('Gait Cycle (%)')
axis([0 100 -20 10])

%HR
figure(11)
hold on

subplot(1,3,1);
rms1 = gaitgraph(timeStepN,time1,qVDB(:,3),qME2(:,3));
title(['Normal Gait Error: ',num2str(rms1),char(176)], 'FontSize', 12)
ylabel('Hip Rotation in Degrees', 'FontSize', 18)
xlabel('Gait Cycle (%)')
axis([0 100 -50 35])

subplot(1,3,2);
rms2 = gaitgraph(timeStepO,time1,qVDB(:,3),qME2(:,3));
title(['Toes Out Gait Error: ',num2str(rms2),char(176)], 'FontSize', 12)
xlabel('Gait Cycle (%)')
axis([0 100 -50 35])

subplot(1,3,3);
hold on
rms3 = gaitgraph(timeStepI,time1,qVDB(:,3),qME2(:,3));
title(['Toes In Gait Error: ',num2str(rms3),char(176)], 'FontSize', 12)
xlabel('Gait Cycle (%)')
axis([0 100 -50 35])

%KF
figure(12)
hold on

```

```

subplot(1,3,1);
rms1 = gaitgraph(timeStepN,time1,qVDB(:,4),qME2(:,4));
title(['Normal Gait Error: ',num2str(rms1),char(176)], 'FontSize', 12)
ylabel('Knee Flexion in Degrees', 'FontSize', 18)
xlabel('Gait Cycle (%)')
axis([0 100 -70 0])

subplot(1,3,2);
rms2 = gaitgraph(timeStepO,time1,qVDB(:,4),qME2(:,4));
title(['Toes Out Gait Error: ',num2str(rms2),char(176)], 'FontSize', 12)
xlabel('Gait Cycle (%)')
axis([0 100 -70 0])

subplot(1,3,3);
rms3 = gaitgraph(timeStepI,time1,qVDB(:,4),qME2(:,4));
title(['Toes In Gait Error: ',num2str(rms3),char(176)], 'FontSize', 12)
xlabel('Gait Cycle (%)')
axis([0 100 -70 0])
%%
%%%%%%%%%%%%%% Normal Gait Cycles Plot
%%%%%%%%%%%%%%
figure(100)
hold on

subplot(1,4,1);
rms1 = gaitgraph(timeStepN,time1,qVDB(:,1),qME2(:,1));
title(['Gait Error: ',num2str(rms1),char(176)], 'FontSize', 12)
ylabel('Hip Flexion in Degrees', 'FontSize', 18)
xlabel('Gait Cycle (%)', 'FontSize', 18)
axis([0 100 -70 20])

subplot(1,4,2);
rms1 = gaitgraph(timeStepN,time1,qVDB(:,2),qME2(:,2));
title(['Gait Error: ',num2str(rms1),char(176)], 'FontSize', 12)
ylabel('Hip Abduction in Degrees', 'FontSize', 18)
xlabel('Gait Cycle (%)', 'FontSize', 18)
axis([0 100 -70 20])

subplot(1,4,3);
rms1 = gaitgraph(timeStepN,time1,qVDB(:,3),qME2(:,3));
title(['Gait Error: ',num2str(rms1),char(176)], 'FontSize', 12)
ylabel('Hip Rotation in Degrees', 'FontSize', 18)
xlabel('Gait Cycle (%)', 'FontSize', 18)

```

```
axis([0 100 -70 20])

subplot(1,4,4);
rms1 = gaitgraph(timeStepN,time1,qVDB(:,4),qME2(:,4));
title(['Gait Error: ',num2str(rms1),char(176)], 'FontSize', 12)
ylabel('Knee Flexion in Degrees', 'FontSize', 18)
xlabel('Gait Cycle (%)', 'FontSize', 18)
axis([0 100 -70 20])
legend('Visual Mocap','ReCap')
```

APPENDIX E
(MatLab Program CaliCurve.mat)

```
function CaliCurve(b,q1,q2,x,y)

T(1) = min(q2);
T(2) = max(q2);
hold on
plot(q1,q2,'go')
plot(T,T,'k')
axis equal square

if x == 1 && y == 0
    xlabel('Degrees (Strain)')
elseif x == 0 && y == 1
    ylabel('Degrees (Visual)')
elseif x == 1 && y == 1
    xlabel('Degrees (Strain)')
    ylabel('Degrees (Visual)')
end

if strcmp(b,'HF')||strcmp(b,'Hf')||strcmp(b,'hf')||strcmp(b,'hF')
    title('Hip Flexion')
elseif strcmp(b,'HA')||strcmp(b,'Ha')||strcmp(b,'ha')||strcmp(b,'hA')
    title('Hip Abduction')
elseif strcmp(b,'HR')||strcmp(b,'Hr')||strcmp(b,'hr')||strcmp(b,'hR')
    title('Hip Rotation')
elseif strcmp(b,'KF')||strcmp(b,'Kf')||strcmp(b,'kf')||strcmp(b,'kF')
    title('Knee Flexion')
end
```

APPENDIX F
(MatLab Program gaitgraph.mat)

```
function [rms] = gaitgraph(timeStep,time,dataVDB,dataME)

du = 0;
p = 0;
hold on

for j = 1:length(timeStep)-1
    l = time > timeStep(j) & time < timeStep(j+1);
    l = find(l == 1);
    timeCycle = (time(l)-timeStep(j))/(timeStep(j+1)-timeStep(j))*100;
    x = dataVDB(l);
    xx = dataME(l);
    plot(timeCycle,x,'ko--')
    plot(timeCycle,xx,'r*--')
    do = (xx - x).^2;
    du = du + sum(do);
    p = p + length(do);
end

rms = (du/p)^.5;
```

APPENDIX G

(IRB-Approved Test Protocol Document)



Washkewicz College
of Engineering

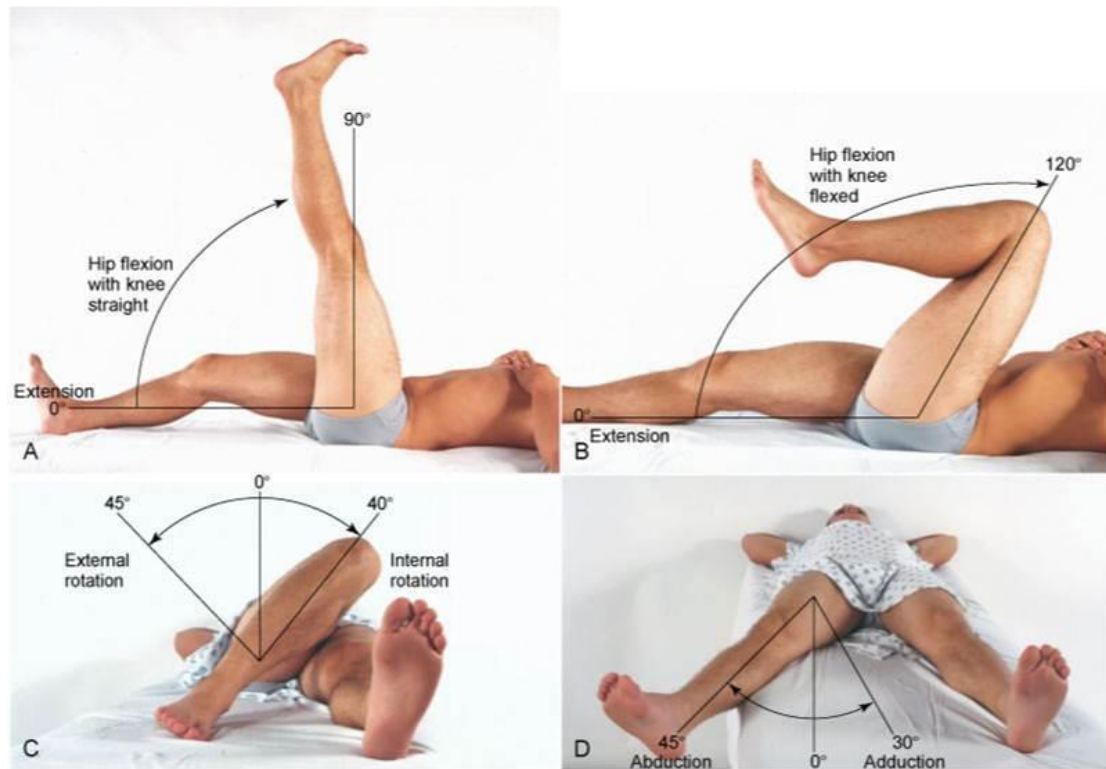
CHRISTOPHER SCHROECK

*Bachelor of Science in Mechanical Engineering
Cleveland State University, May 2017*

ReCAP PROTOCOL

FLEXION & ROTATION CALIBRATION TEST

- 1) Participant is sized [S/M/L] and given corresponding prototype to put on.
- 2) Sensors are attached to prototype around the 3 DoF of the hip & 1 DoF of the knee and given initial tension.
- 3) Participant allows the instructor to move their leg (passively) through the following RoM tests (x2 each):



Copyright © 2012, 2008, 2004, 2000, 1996, 1992 by Saunders, an imprint of Elsevier Inc. All rights reserved.

Due to prototype limitations, “Hip flexion with knee flexed” range will be shortened to maintain tension throughout the test as situationally appropriate

4) Participant performs the double leg squat with feet at various distances:

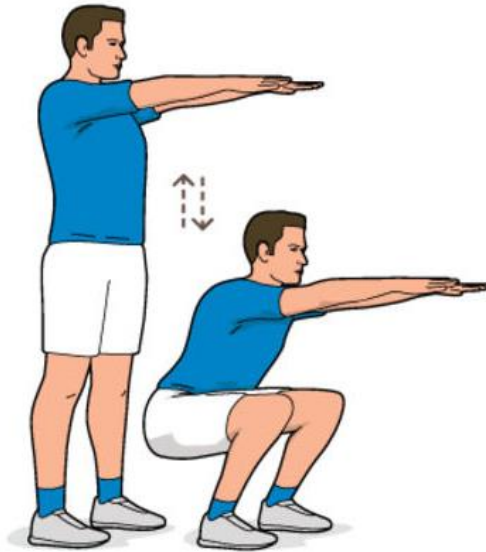


Image from FourFourTwo.com

- a. Feet together (toes forward)
 - b. Feet together (toes apart)
 - c. Feet shoulder width apart (toes forward)
 - d. Feet shoulder width apart (toes apart)
- 5) Participant then walks for 1 minute on the treadmill x3
- a. Normal walk (feet forward)
 - b. Duck walk (feet pointed outward)
 - c. Pigeon toed (feet pointed inward)
- 6) Participant repeats step 3 to test system stability (only x1 each)

APPENDIX H
(Permission from Katherine Florek)



Chris Schroeck <chrishrek@gmail.com>

Calibration Comparison Graph Use Permission

Katherine Florek <katherineflorek@gmail.com>
To: Chris Schroeck <chrishrek@gmail.com>

Mon, Apr 29, 2019 at 6:55 PM

Hi Chris,

You have my permission to reuse the calibration comparison graphs I created for our senior design project in your thesis.

Best regards,
Kate

On Apr 29, 2019, at 5:13 PM, Chris Schroeck <chrishrek@gmail.com> wrote:

Hello Kate,

Can I reused the calibration comparison graphs you generated for our senior design project in my thesis?

Sincerely,

Chris



Virus-free. www.avast.com